

UNIVERSITÀ DI PISA

Scuola di Dottorato in Ingegneria “Leonardo da Vinci”



Corso di Dottorato di Ricerca in
INGEGNERIA DELL'INFORMAZIONE

Tesi di Dottorato di Ricerca

**ANALYSIS, MODELLING, AND SIMULATION
OF AN INTEGRATED MULTISENSOR
SYSTEM FOR MARITIME BORDER
CONTROL**

Autore:

Sofia Giompapa _____

Relatori:

Prof. Fulvio Gini _____

Dr. Alfonso Farina _____

Prof. Lucio Verrazzani _____

Prof. Marco Luise _____

Anno 2008

To my family

Acknowledgments

I would like to express my sincere gratitude to Prof. Fulvio Gini and Dr. Alfonso Farina for their precious suggestions and for the great work environment that they have created during the development of this research project.

I also would like to acknowledge Prof. Lucio Verrazzani, Prof. Marco Luise and Dr. Maria Sabrina Greco.

I thank Dr. Antonio Graziano and Dr. Riccardo Di Stefano, from SELEX – Sistemi Integrati, Roma, Italy, for their help and for their comments since the beginning of this activity. I am grateful to Dr. Rodolfo Croci, SELEX – Sistemi Integrati, for his contribution in the algorithm for the analytical computation of the confusion matrix and in Appendix A.

I am also grateful to: Dr. Ennio Giaccari and Dr. Fulvio Marozz, Finmeccanica - SESM, Roma, Italy; Dr. Paolo Marrucci, from Galileo Avionica, Pomezia, Italy, for his suggestions about some typical parameters of a visible camera and an infrared camera; Dr. Fabian D. Lapierre, from the Royal Military Academy, Brussels, Belgium, for kindly providing the temperature file exploited for the simulation of the infrared images; Dr. Ugo D'Elia and Dr. Maria Grazia Del Gaudio, from MBDA, Roma, Italy, and Dr. Francesco Prodi, SELEX – Sistemi Integrati, for kindly providing the simulated electro-magnetic images used in this work.

I thank Dr. Gerard T. Capraro, from Capraro Technologies Inc., Utica, NY, and Dr. Michael C. Wicks, from U.S. Air Force Research Laboratory, Rome, NY, for their comments and encouragement.

Thank you so much.

Disclaimer: All the material provided in this dissertation is unclassified and the described system is hypothetical and not related to any real operational scenario.

Abstract

In this dissertation a notional multi-sensor system acting in a maritime border control scenario for Homeland Security (HS) is analyzed, modelled, and simulated. The functions performed by the system are the detection, tracking, identification and classification of naval targets that enter a sea region, the evaluation of their threat level and the selection of a suitable reaction to them. The emulated system is composed of two platforms carrying multiple sensors: a land based platform, located on the coast, and an air platform, moving on an elliptic trajectory in front of the coast. The land based platform is equipped with a Vessel Traffic Service (VTS) radar, an infrared camera (IR) and a station belonging to an Automatic Identification System (AIS). The air platform carries an Airborne Early Warning Radar (AEWR) that can operate on a spotlight Synthetic Aperture Radar (SAR) mode, a video camera, and a second IR camera. A Command and Control (C^2) centre, located on the coast, coordinates the surveillance operation. In the maritime scenario four classes of naval targets are considered: high speed dinghy, immigrant boat, fishing boat, and oil tanker. A classification algorithm is also proposed which exploits an analytical approach based on the confusion matrix (CM) of the imaging sensors that belong to the system. The performance of the integrated system is evaluated in terms of its *Measures of Effectiveness* (MoE), which are the system metrics on the detection, classification, threat level evaluation, and selection of the intervention. These metrics are evaluated considering both the cases where an ideal error free classification process and a non-ideal classification process are performed.

Contents

List of Figures.....	xi
List of Tables.....	xiii
List of Acronyms, Operators, and Symbols	xv
Chapter 1 - Introduction	1
1.1 Motivations.....	1
1.2 Main factors and contributions	3
1.3 Outlines.....	5
Chapter 2 - The system architecture	7
2.1 System overview.....	7
2.2 The scenario and the environmental conditions.....	10
2.3 The sensors of the integrated system	13
2.3.1 The Vessel Traffic Service radar.....	13
2.3.2 The Automatic Identification System	16
2.3.3 The Airborne Early Warning Radar	18
2.3.3.1 <i>The spotlight SAR mode</i>	21
2.3.4 The video camera	25
2.3.5 The infrared camera	29
2.4 The Command and Control centre.....	33
2.5 The end to end simulator	33
Chapter 3 - The classification process.....	35
3.1 Introduction	35
3.2 The classification algorithm	37
3.3 Construction of a multisensor image database.....	41
3.3.1 The video camera database	44
3.3.2 The infrared camera database.....	48
3.3.3 The spotlight SAR database.....	53
3.4 The fusion of the decision on the target class	59
3.5 Performance of the fusion process.....	68
3.5.1 Numerical example	71
Chapter 4 - The Command and Control centre.....	75
4.1 Introduction	75
4.2 Track association and fusion	76
4.3 The threat evaluation logic	78
4.4 The selection of the intervention	82
Chapter 5 - Performance analysis.....	87
5.1 Measures of Effectiveness	87
5.2 Simulation results	90
5.2.1 <i>Ideal</i> classification process	92
5.2.2 <i>Non ideal</i> classification process	98

Chapter 6 - Conclusions	103
Appendix A - Analytical computation of the confusion matrix	107
References	117
List of Publications.....	123

List of Figures

Figure 2.1 – System architecture	8
Figure 2.2 – Scenario	10
Figure 2.3 – VTS detection probability: a) sea state 0; b) sea state 4	15
Figure 2.4 – Allocation of time slots in the AIS	16
Figure 2.5 – AEWDR detection probability: a) sea state 0; b) sea state 4	21
Figure 2.6 – Spotlight SAR geometry.....	22
Figure 2.7 – Video camera model.....	28
Figure 2.8 – Minimum Resolvable Temperature Difference	30
Figure 2.9 – IR camera model	31
Figure 2.10 – Flow chart of the MatLab [®] end to end simulator.....	34
Figure 3.1 – Classification based on the elements of the CM.....	39
Figure 3.2 – Computation of the CM.....	41
Figure 3.3 – CAD models.....	42
Figure 3.4 – CAD decomposition into polygonal facets.....	43
Figure 3.5 – Translation and rotation of the geographical system on the target	44
Figure 3.6 – Azimuth and elevation required for the CAD projection	46
Figure 3.7 – Construction of the video camera database	47
Figure 3.8 – Example of simulated images for the video camera	48
Figure 3.9 – View angles (a) and range values (b) considered in the IR database construction.....	49
Figure 3.10 – Association intervals for the view angle.....	50
Figure 3.11 – Construction of the IR camera database	50
Figure 3.12 – Example of simulated images for the IR camera for the 5 view angles.....	51
Figure 3.13 – Example of simulated IR images for all the classes considered	53
Figure 3.14 – Construction of the spotlight SAR database.....	56
Figure 3.15 – SAR geometry	56
Figure 3.16 – Example of simulated images for the spotlight SAR.....	59
Figure 3.17 – Fusion of the decisions on target class	61
Figure 3.18 – Example of pmf for the sequence $d^{[8]}=(1,2,4)$ when H_1 is true.....	67
Figure 3.19 – Probability of correct classification equal to the factor Q	74
Figure 4.1 – Tracker architecture.....	76
Figure 4.2 – Example of intervention on a TL2 tack with resource B	84
Figure 5.1 – MoE on the detection ($\mathbf{n}_{\text{evaluated}}$) for <i>Case A</i>	93
Figure 5.2 – Motion of the air platform (P_2) on the elliptic trajectory	93
Figure 5.3 – MoE during the threat evaluation logic for <i>Case A</i>	94
Figure 5.4 – MoE during the intervention for <i>Case A</i>	97
Figure 5.5 – Evolution of the scenario during a single Monte Carlo trial.....	98
Figure 5.6 – MoE during the threat evaluation: a) <i>Case A</i> ; b) <i>Case B</i>	99

Figure 5.7 – MoE during the threat evaluation: a) *Case C*; b) *Case D* 101

Figure A.1 – Approximation for the conditional error probability 113

List of Tables

Table 2.1 – Target parameters	11
Table 2.2 – Beaufort scale	12
Table 2.3 – VTS radar typical parameters	14
Table 2.4 – AEW radar typical parameters.....	19
Table 2.5 – Geometric parameters of the air platform trajectory.....	20
Table 2.6 – Video camera Fields of View (FOV).....	25
Table 2.7 – Typical parameters for the video camera.....	28
Table 2.8 – Typical parameters for the IR camera.....	31
Table 2.9 – Meteorological vectors for the IR camera	32
Table 3.1 – Predicted RCS of the targets.....	55
Table 3.2 – Dimensions of the simulated EM images	55
Table 3.3 – Observable sequences.....	63
Table 3.4 – Fusion table for MV rule	64
Table 3.5 – Fusion table for ML rule.....	68
Table 3.6 – CM of the video camera, $C^{(1)}$	72
Table 3.7 – CM of the IR camera, $C^{(2)}$	72
Table 3.8 – CM of the spotlight SAR, $C^{(3)}$	72
Table 3.9 – Fused CM by using the MV rule, F_{MV}	73
Table 3.10 – Fused CM by using the ML rule, F_{ML}	73
Table 3.11 – Performance of the CMs.....	74
Table 4.1 – Tolerance thresholds.....	79
Table 4.2 – Threat evaluation logic for the dinghy.....	80
Table 4.3 - Threat evaluation logic for the immigrant boat.....	80
Table 4.4 - Threat evaluation logic for the fishing boat.....	80
Table 4.5 - Threat evaluation logic for the oil tanker	81
Table 4.6 - Threat evaluation logic for class “ <i>unknown</i> ”.....	81
Table 4.7 – Selection of the intervention	82
Table 4.8 – Parameters of the resources	83
Table 5.1 – Parameters of the targets for the fixed simulation scenario	91
Table 5.2 – System response time during the threat evaluation process.....	95
Table 5.3 – MoE during the intervention for <i>Case A</i>	96

List of Acronyms, Operators, and Symbols

Acronyms

AEWR	Airborne Early Warning Radar
AIS	Automatic Identification System
ATC	Automatic Target Classification
C ²	Command and Control
CAD	Computer Aided Design
CM	Confusion Matrix
DM	Decision Making
EM	Electro-Magnetic
EO	Electro-Optic
FD	False Declaration
FOV	Field Of View
GPS	Global Positioning System
HS	Homeland Security
IMO	International Maritime Organization
IR	Infrared
ISAR	Inverse Synthetic Aperture Radar
IT	Information Technology
LOS	Line Of Sight
LOWTRAN	LOW resolution TRANsmission model
LRIT	Long Range Identification and Tracking
MA	Missed Assessment
ML	Maximum Likelihood

MoE	Measures Of Effectiveness
MRC	Minimum Resolvable Contrast
MRTD	Minimum Resolvable Temperature Difference
MTF	Modulation Transfer Function
MV	Majority Voting
NEIL	Noise Equivalent Illuminance
NETD	Noise Equivalent Temperature Difference
OL	Off Limit
pmf	Probability Mass Function
PRF	Pulse Repetition Frequency
RCS	Radar Cross Section
RS	Response Selection
SA	Situation Assessment
SAR	Synthetic Aperture Radar
SNR	Signal to Noise Ratio
SOTDMA	Self Organizing Time Division Multiple Access
SS	Sea State
TAMORA	TARget MOdelling for Radar Applications
TIR	Thermal Infrared
TL	Threat Level
VHF	Very High Frequencies
VTS	Vessel Traffic Service
WZ	Warning Zone
2D	Two Dimensional
3D	Three Dimensional

Operators

$tr(\cdot)$	Trace of a matrix
-------------	-------------------

Symbols

$\mathbf{C}^{(k)}$	Confusion Matrix of the k -th sensor
$c_{ij}^{(k)}$	Element ij of the confusion matrix $\mathbf{C}^{(k)}$
D_{CR}	Target critical dimension
ΔL	Luminance difference between the target and the background in an EO image
ΔT	Temperature difference between the target and the background in an IR image
$\Delta\tau_{TL2}$	Delay in the evaluation of all the threat targets that enter the scene
$f_{\#}$	f number (ratio between the depth of focus and the lens diameter)
FAR	External area in the sea scenario
f_{max}	Maximum spatial frequency
F_n	Receiver noise factor
F_p	Pattern propagation factor
f_s	Spatial frequency
F_S	Scale factor taking into account for the predicted RCS of the target in the SAR images
G	Antenna gain
h_T	Height of the radar tower
H	Horizontal plane
H_i	i -th hypothesis
η_1	Ratio between the number of interventions performed and the number of real threat targets detected by the system
η_2	Ratio between the number of interventions performed and the number of tracks evaluated as threat by the system
η_3	Ratio between the number of interventions performed and the number of real threat targets that enter the scene
η_{TL2}	Percentage of correct intervention with respect to the total number of interventions
η_{TL0}	Percentage of incorrect intervention with respect to the total number of interventions
$\eta_{OL/WZ/FAR}$	Number of interventions performed respectively in the regions OL, WZ and FAR, with respect to the total number of interventions

ICSTL	Air mass factor
IN	Direction of a target that approaches the coast line
φ_{az}	Azimuth beamwidth
φ_{el}	Elevation beamwidth
k	Boltzmann constant ($1.38 \cdot 10^{-23} \text{ J}^\circ\text{K}$)
k_a	Earth radius (6378.137 km)
λ	Wavelength of the transmitted pulse
L_α	Loss due to the atmosphere attenuation
L_t	Loss due to the transmission line
M	Number of target classes
N_a	Number of pulses integrated in azimuth
N_A	Number of resources of type A (helicopters)
N_B	Number of resources of type B (patrol boats)
N_C	Number of resolvable cycles for the recognition
N_H	Number of pixels on the horizontal plane
N_{pixels}	Number of pixels
N_V	Number of pixels on the vertical plane
OUT	Direction of a target that moves opposite to the coast line
P_{CC}	Probability of correct classification
$P_{CC H_i}$	Probability of correct classification given the hypothesis H_i
P_{ERR}	Classification error probability
$P_{ERR H_i}$	Classification error probability given the hypothesis H_i
P_D	Probability of detection
P_{FA}	Probability of false alarm
$P_{FD TL0}$	Probability of false declaration given a neutral target
$P_{FD TL2}$	Probability of false declaration given a threat target
P_{MA}	Probability of missed assessment
P_{rec}	Probability of recognition
q	Size of scattering particles
Q	Quality factor of the classification process

R	Reflectivity of the EO sensor
ρ_b	Reflection coefficient of the background
R_{\max}	Maximum range of the radar
ρ_t	Reflection coefficient of the target
S	Sensitivity of the EO sensor
σ_{atm}	Atmosphere extinction coefficient
σ_ρ	Resolution in range of the radar
σ_θ	Resolution in azimuth of the radar
τ	Width of the transmitted pulse
T_a	Antenna temperature
T_{appr}	Approaching time of the target to the coast
τ_{atm}	Atmosphere transmittivity
$T_{\text{availableA/B}}$	Time available for the reaction for resource type A/B
T_d	Radar dwell time
T_{dep}	Departure time of the resource
T_e	Effective input noise temperature of the receiver
T_{insp}	Inspection time of the resource
TL0	Threat Level 0 (neutral target)
$TL0_{\text{remaining}}$	Average number of TL0 targets waiting for an assessment after that the observation time of the scene is elapsed
TL1	Threat Level 1 (suspect target)
TL2	Threat Level 2 (threat target)
$TL2_{\text{remaining}}$	Average number of TL2 targets waiting for an assessment after that the observation time of the scene is elapsed
T_r	Noise temperature of the transmission line
$T_{\text{reactA/B}}$	Reaction time of the resource type A/B
T_{RT}	Round trip time of the resource
T_s	System equivalent temperature
T_{scan}	Radar scan time
$T_{\text{unavailable}}$	Time during which the resource is unavailable
T_0	Environment temperature
V	Visibility of the sensor
V_A	Speed of resource type A
V_B	Speed of resource type B

Chapter 1

Introduction

1.1 Motivations

In the last few years Homeland Security (HS) has become a very important concern for many governments, which have to protect their nations and their critical infrastructures, and thus it is gaining a considerable interest in the research community. From a scientific point of view, it is a difficult task to provide a definition of this topic and to exactly draw up its boundaries. In fact, when we talk about the security and the surveillance of a country, several problems and aspects must be considered. In particular, the following factors play a crucial role and define the complexity level of the considered application field: the number of potential threats can be high and uncertain; the surveillance operation occurs during peace conditions, so that many environmental elements can make confusion and cause distraction; the threat detection and identification can be made more complicated by the use of camouflaging techniques; the monitored area is typically wide and it requires a large and heterogeneous sensor network; the surveillance operation is strongly related to the operational scenario, so that it is not possible to define a unique approach to solve the problem.

Due to the confluence of all these factors, the context and the background of nowadays military operations and of the emerging civil requirements are considerably different from the past: in the new operational scenarios the threat

does not operate in a dense warfare environment and it can no more be identified with the number of targets, but it takes the form of a hidden and an unexpected threat, that can be a single dangerous target often acting during peace condition. This consideration is forcing the national military community to revisit the widely developed military techniques towards a different direction, where a single target represent the threat that must be detected, recognized and prevented. While a wide scientific literature is available dealing with the classical military techniques, only recently some emerging research activities are oriented to investigate different approaches to deal with this new type of threat.

Information Technology (IT) can provide an important support to HS in preventing, detecting, and early warning of intentional disasters. Technologies for identification and authentication, border security, and controlled access to critical infrastructures are significant steps to prevent unexpected attacks. Both future military operations and civil needs require innovative powerful sensors and sensor configurations that are able to dynamically change their behaviour to overcome with the changing priorities and requirements of the mission [59]. This implies the use of complex sensor networks, integrated information techniques, effective decision aids, robust command and control systems for early threat detection and for rapid response and recovery efforts ([1],[11],[50],[56]). Even though the link between Information Technology and Homeland Security is relatively recent and many technical aspects are yet undetermined, sensor integration and collaboration is a widely applied technique aimed to aggregate data from multiple sources, to yield timely information on potential threats and to improve the accuracy in monitoring events ([43],[60]). A large number of sensors based on dissimilar phenomenology have already been developed to support surveillance operations. Furthermore, the development of more efficient fusion strategies and the improvement in the design of advanced sensors, equipped with quick microprocessor to perform distributed data processing and computation, can provide a significant aid to HS and can reduce the computational load of the surveillance operations. Sensor integration has been widely addressed in the

literature ([4],[8],[9],[15],[16],[20],[46]), but it is still a challenging issue and it requires deeper studies in order to solve the problems related to the difference in the nature of the sensors integrated together, in their internal characteristics and in the type of information provided.

In this dissertation a notional integrated multi-sensor system acting in a maritime border control scenario for HS is analyzed, modelled, and simulated. The mission of this system is the detection, the tracking, the identification, the classification of multiple naval targets, their threat level evaluation and the selection of an intervention on them. The system is composed of two platforms carrying multiple sensors: a land based platform, containing a Vessel traffic Service (VTS) radar, an infrared camera (IR) and a station belonging to an Automatic Identification System (AIS); an airborne platform, moving along an elliptic patrol in front of a coastal region and carrying an Airborne Early Warning Radar (AEWR) and three imaging sensors, that are a video camera, a second IR camera and a spotlight Synthetic Aperture Radar (SAR). A Command and Control (C^2) centre coordinates the surveillance operations. The system uses the kinematical parameters provided by the two radars, the identification information provided the AIS station, and the class information provided by the imaging sensors in order to classify the detected target, to evaluate if it represents a potential threat and to select a suitable intervention on it. The performance of this system has been evaluated in terms of *Measures of Effectiveness* (MoE), which are the system metrics during the detection, classification, threat level evaluation, and selection of the intervention. These metrics have been evaluated considering both the cases where an ideal error free classification process and a non-ideal classification process are performed.

1.2 Main factors and contributions

As stated before, surveillance for HS is an extensive application field and the performance of this operation is strongly related to the operative background. A

first step that can help to define and to analyze a system acting in the field of HS is to exactly define the scenario where the system acts.

In this context the main contributions of this work are the following:

- A complex multi-sensor system is defined, including a large sensor network aimed at monitoring a wide sea area. The sensors considered in the network present technological limitations complementary to each other and their integration represents the possibility to compensate for these limitations [28].
- The scenario where the system acts is completely characterized, including the geographical area considered, the environmental conditions, the target features and the proprieties of the sensors in the network [28].
- An *end-to-end* simulator that emulates this system is implemented, using the MatLab[®] software. In this simulator we consider the whole complex multi-sensor system, including the scenario, the environment, and the phenomenology of each sensor. The targets are model using their kinematical parameters and their geometrical features, and the signal processing for the sensors is taken into account ([26],[28]).
- A classification algorithm for the imaging sensors belonging to the system is developed. This algorithm exploits the knowledge of the confusion matrix (CM), analytically evaluated for each imaging sensor, and it allows us to easily include the target classification process inside the software simulation of the complex multi-sensor system. The algorithm is general and it also applies to imaging sensors different from those considered in this work [27]. We also consider and solve the problem of the fusion of the class information provided by the different imaging sensors.

Considering the confluence of these contributions, this work provides a significant example of the methodology for analyzing a complex application field such as HS and a concrete tool for the qualitative evaluation of the performance of all the processes and functions involved in this mission.

1.3 Outlines

This dissertation is organized as follows. **Chapter 2** describes the architecture of the integrated multi-sensor system: details are provided for each sensor of both the land based and the air platforms. **Chapter 3** describes the classification algorithm developed to insert the classification process into the study of the complex system and it presents the construction of a multi-sensor image database for the three imaging sensors considered inside the system. The fusion of the class information coming from dissimilar sensors is also described and examples of results concerning the fusion process are shown. **Chapter 4** describes the operations performed inside the C^2 centre. The performance analysis of the overall system is presented in **Chapter 5**. Finally, conclusions and directions for future works are reported in **Chapter 6**.

Chapter 2

The system architecture

2.1 System overview

In this section we provide an overview of the complete system architecture and of its functions. The notional surveillance system analyzed in this work is composed of two platforms carrying multiple sensors: a land based platform, located on the coast, and an airborne platform, moving along an elliptic trajectory in front of the coast line. The land platform is equipped with a Vessel Traffic Service (VTS) radar, an infrared camera (IR), and a station belonging to an Automatic Identification System (AIS), which provides an information on the target cooperativeness. The air platform carries an Airborne Early Warning Radar (AEWR), which can operate in a spotlight SAR mode, a video camera and a second IR camera. The mission of the system is the detection, tracking, identification, and classification of multiple targets that enter a sea region, the assessment of their threat level, and the selection of a suitable intervention on them. The monitored area is divided into three regions: an off-limit region, in front of the coast, a warning zone and an external area. The threat evaluation and the selection of the intervention are performed by a Command and Control (C^2) centre that coordinates all the operations of the multi-sensor system. The system architecture is shown in Figure 2.1.

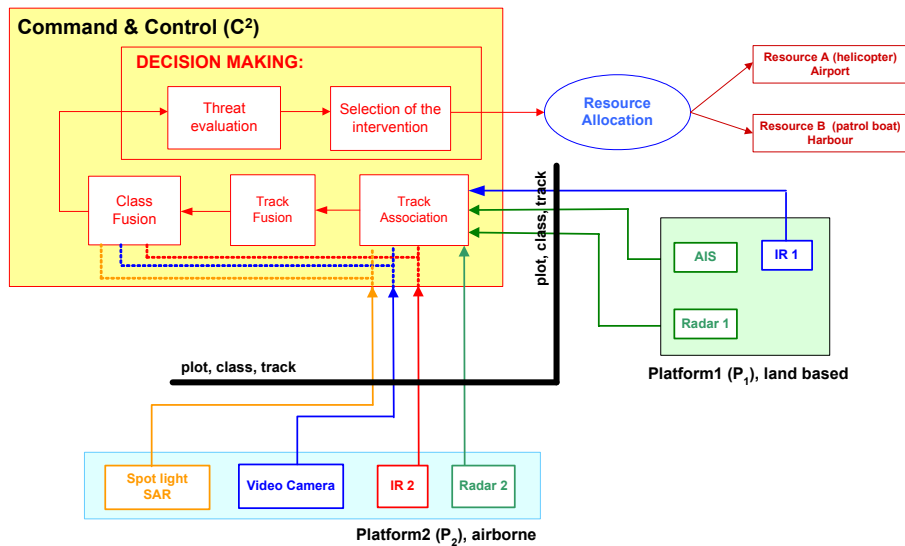


Figure 2.1 – System architecture

The system uses the kinematical parameters provided by the two radars, the identification information provided by the AIS station, and the class information provided by the imaging sensors to classify the target, to evaluate if it represents a threat and to select a suitable intervention on it. In particular, the imaging sensors provide information on the target class, based on a processing of the target image. Their performance is expressed by means of the confusion matrix, which is analytically computed for each sensor as a function of the following parameters: the sensor signal-to-noise ratio (SNR), the sensor resolution, a database of reference images, and the cross-correlation between these reference images. As described in Chapter 3, this approach corresponds to a high level of abstraction and it allows us to simplify the analysis of the complex classification process related to a sensor and to insert it in the study of the multi-sensor system. In order to simplify the notation, in the rest of this work we will refer to the confusion matrix analytically computed for each imaging sensor as the *sensor confusion matrix* (CM).

The detection and the tracking of the targets are performed independently by the two radars. When these processes are completed, the C² centre performs the

association and the fusion of the tracks, the fusion of the class information, and finally the track processing, that consists in the evaluation of the target parameters required to assess the threat level. More specifically, the following parameters are computed:

- the target estimated trajectory;
- the expected intersection point between the target trajectory and the boundary of the off-limit region;
- the target direction with respect to the coast;
- the target distance from the coast;
- the potential point where the target is expected to approach the coast and the estimated approaching time.

After this processing the threat level of the target is assessed. First of all the target is identified as cooperative or non-cooperative, on the basis of the information provided by the AIS, if it is available. The non-cooperative targets are subject to the threat level evaluation. The threat evaluation logic is based on a deterministic comparison between the target kinematical parameters and some tolerance threshold on the speed, on the distance between the target and the coast, and on the direction. A different logic is used for each target class. According to the evaluation logic a *Threat Level* (TL) is assigned to the non-cooperative targets in the set $\{TL0, TL1, TL2\}$, where TL0 indicates a neutral target, TL1 a suspect target, and TL2 a threat target.

After the threat evaluation process, the C^2 centre selects an appropriate reaction to the target. The neutral targets do not require any intervention and their parameter are no more stored in the C^2 centre. For the targets that are evaluated as suspect the decision on the intervention is delayed, in order to acquire more information on their nature during the following observation time. An intervention is only selected for the targets assessed as threat and it consists in the allocation of a system resource to inspect the nature of the target. Two types of resources are considered here: a helicopter and a patrol boat; both the resources are used only for the target inspection and they do not carry any sensor on board. The system performance is

evaluated in terms of MoE, which include metrics on the detection capability of the integrated system, on the classification, on the threat evaluation, and on the intervention.

2.2 The scenario and the environmental conditions

The scenario is composed of the geographical area considered, the environmental conditions (the sea state and the atmosphere model), the position of the sensors in this area, the multiple naval targets that enter the scene, and the resources of the system. The sea area considered in this work is a portion of the Sicilian coast in front of the Channel of Sicily. The choice of this particular geographical area has been performed only to provide an example for the scenario.

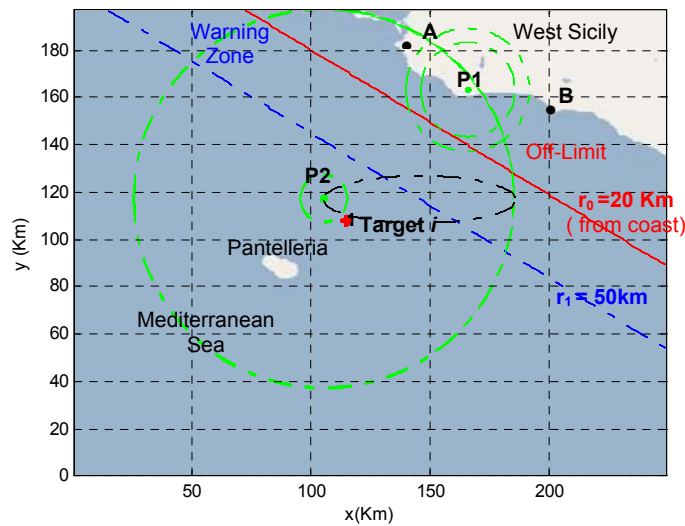


Figure 2.2 – Scenario

The scenario is shown in Figure 2.2. The sea area considered is divided into three regions:

- the *off-limit region* (OL), that is the area included between the coast line and the bound line r_0 , that is 20 Km far from the coast;

- the *warning zone* (WZ), that is the area included between 20 Km and 50 Km from the coast (between lines r_0 and r_1 in the figure);
- the *external area* (FAR), that is the wide sea area contiguous to the warning zone.

The point P_1 in Figure 2.2 represents the position of the land based platform, and the point P_2 is the position of the air platform that moves on an elliptic trajectory centred on the boundary between the warning zone and the external area. The resources of the system are located on the points A and B: the point A, corresponding to Trapani airport, is the departure base of the helicopters (resource A) and the point B, corresponding to Sciacca harbour, is the departure base of the patrol boats (resource B).

Four classes of naval targets have been considered inside this area:

- *Class 1*: high speed dinghy;
- *Class 2*: immigrant boat;
- *Class 3*: fishing boat;
- *Class 4*: oil tanker.

The parameters of each target are generated according to its class, as reported in Table 2.1 In particular, the velocity of the target is assumed to be constant and it is generated as a random variable uniformly distributed in the intervals reported in the third column of the table. The last column represents the estimated radar cross section (RCS) for each target class.

Table 2.1 – Target parameters

Class	Size	Speed	Cooperativeness	RCS
Dinghy (1)	(10 x 4.6 x 3) m	0 ÷ 60 Nodes ¹	N	3 m ²
Immigrant boat (2)	(15 x 4.7 x 5.3) m	0 ÷ 24 Nodes	N	10 m ²
Fishing boat (3)	(16 x 5.3 x 7) m	0 ÷ 12 Nodes	Y/N	100 m ²
Oil tanker (4)	(100 x 33.5 x 37.6) m	0 ÷ 20 Nodes	Y/N	1000 m ²

¹ 1 Node = 1.852 Km/h.

In this scenario two possible values for the sea state (SS) have been considered, equal to 0 and 4 in the Beaufort scale. This scale classifies the sea state according to the wave height and to the wind speed and assigns it a numerical value in the interval 0÷12 [45]. The complete scale is reported in Table 2.2.

Table 2.2 – Beaufort scale

Beaufort number	Description	Wind speed		Wave height	
		knots	Km/h	m	ft
0	Calm	0	0	0	0
1	Light air	1-3	1-6	0.1	0.33
2	Light breeze	4-6	7-11	0.2	0.66
3	Gentle breeze	7-10	12-19	0.6	2
4	Moderate breeze	11-15	20-29	1	3.3
5	Fresh breeze	16-21	30-39	2	6.6
6	Strong breeze	22-27	40-50	3	9.9
7	Moderate gale	28-33	51-62	4	13.1
8	Fresh gale	34-40	63-75	5.5	18
9	Strong gale	41-47	76-87	7	23
10	Storm	48-55	88-102	9	29.5
11	Violent storm	56-63	103-119	11.5	37.7
12	Hurricane	64-80	120	>14	>46

The value 0 represents the state of calm and flat sea, while the value 4 represents the state of moderate breeze, with wind speed lower than 29 Km/h and small waves (maximum height equal to 1 meter).

The atmosphere conditions influence the performance of the sensors involved in the surveillance operation. The atmosphere model assumed in this work takes into account for the effects of the sea state, for the temperature, for the visibility and for the relative humidity. This model is based on the Lambert absorption law [53]:

$$\tau_{\text{ATM}}(R, V, \lambda) = e^{-\sigma_{\text{ATM}}(V, \lambda) \cdot R} \quad (2.1)$$

where τ_{ATM} is the atmosphere transmittivity, V is the sensor visibility, λ is the sensor wavelength, R is the distance between the sensor and the target, and σ_{ATM} is the atmosphere extinction coefficient. The transmittivity depends on the deepness of the crossed atmosphere layer, and thus it depends on the sensor height, on the distance between the sensor and the ship, and on the view angle. The evaluation of the atmosphere extinction coefficient for each sensor of the system is reported in the next sections.

2.3 The sensors of the integrated system

In this section we provide a description of the model of the each sensor belonging to the system: the VTS radar, the AIS station, and the IR camera for the land based platform; the AEW radar, the video camera, the second IR camera for the air platform. The spotlight SAR is an operative mode of the AEW radar. The model for the IR cameras contained in the two platforms is the same.

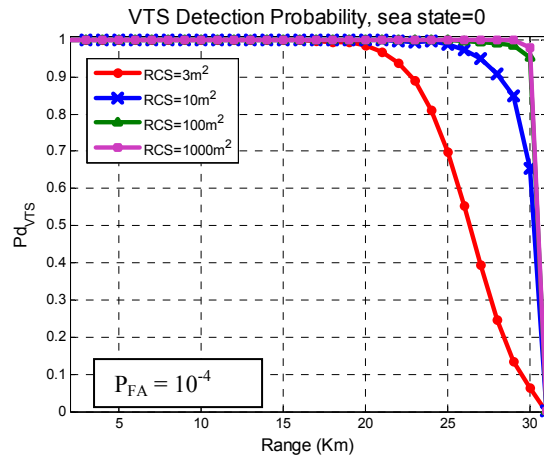
2.3.1 The Vessel Traffic Service radar

The land based radar is located on the south west coast of Sicily and it is a Vessel Traffic Service (VTS) like radar. The VTS is a radar typically used to monitor the maritime traffic and for the surveillance of small, medium and large harbors ([39],[63]). They usually operate in the S and X bands [35] and their coverage range can go from 10 Km to 38 Km, dependent on the target RCS. The parameters of the VTS radar used in our system are reported in Table 2.3.

Table 2.3 – VTS radar typical parameters

Parameter	Value
Range resolution	$\sigma_\rho = 7.5$ m
Azimuth resolution	$\sigma_\theta = 0.37^\circ$
Scan time	$T_{\text{scan}} = 2.3$ s
Tower height	$h_T = 40$ m
Maximum range	$R_{\text{max}} \cong 30$ Km
False alarm probability	$P_{\text{FA}} = 10^{-4}$

The detection probability curves as a function of the range are shown in Figure 2.3 a) and b), respectively for sea state values equal to 0 and 4 in the Beaufort scale. These curves are referred to a false alarm probability equal to 10^{-4} .



a)

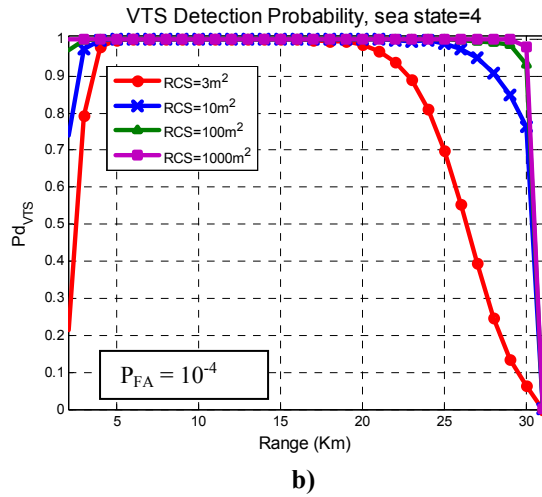


Figure 2.3 – VTS detection probability: a) sea state 0; b) sea state 4

These curves have been analytically evaluated by solving the radar equation for different values of the target RCS and also taking into account for the clutter, for the multipath and for the atmosphere attenuation. The maximum range reported in Table 2.3 is consistent with the radar horizon formula [52], that provide the maximum theoretical radar visibility as a function of the height of the radar tower:

$$d = \sqrt{2 \cdot k_a \cdot h_t}, \text{ where } k_a \text{ is the earth radius.}$$

In the integrated system analyzed in this work, the land based radar provides the target kinematical parameters, which are the coordinates, the speed, and the direction. It is assumed the track initialization takes place when the detection has occurred for three radar scans over a window of five scans. We also have assumed that the tracking is performed with respect to an inertial reference system, whose centre is located in the point $\mathbf{O} \equiv (0;0)$ of Figure 2.2. In the reminder of this dissertation we will refer to this system as the geographical system.

2.3.2 The Automatic Identification System

The Automatic Identification System (AIS) is a broadcast communication system that operates in the VHF marine band. It was introduced around 1980 as an aid tool for the observation of the traffic around the ships and in the harbors.

The system allows the exchange of information between the AIS stations and a transponder on board of the ship. This information usually concerns the ship identity, the position, the speed, the size, and the route. The AIS uses a Self Organizing TDMA technique (SOTDMA) with a transmission speed equal to 9.6 Kbps: every time minute is divided into 2250 time slots of 26.6 ms. One ship in the system usually allocates one time slot in order to transmit the information about its position and its identity [31]. The allocation of the time slots is described in Figure 2.4.

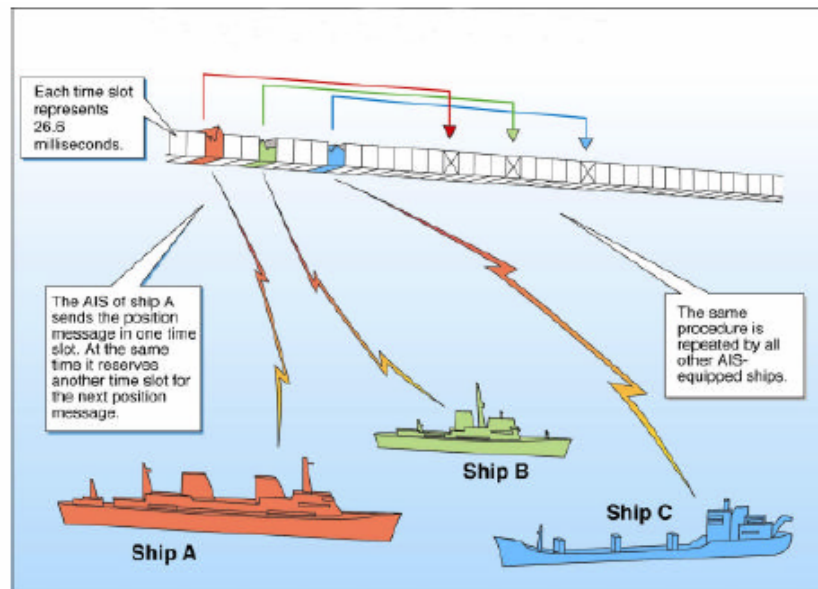


Figure 2.4 – Allocation of time slots in the AIS

Even though the main purpose of the system is the identification of the ship, the aid to the tracking operations and the exchange of information aimed to avoid the collision between the ships, when other time slots are available the system can also

be used to transmit additional information, such as the type of shipment onboard, an assistance request, etc. More specifically, the system provides for 22 encoded binary messages also used for management communications (*acknowledgement, interrogation, etc.*) ([33],[37]).

The ship transponders are synchronized to the Global Positioning System (GPS) clock. These transponders transmit broadcast messages using two channels in the VHF marine band (161.975MHz, 162.025MHz). The coverage of the VHF band for maritime communications is typically around 20 Km, even though the coverage area of the device is established by the competent authority [32]. Since the AIS works in the VHF radio band, it is able to run communications in the line of sight (LOS). When the number of AIS stations in the LOS of a receiver station exceeds the system capability in terms of available time slots, the SOTDMA algorithm automatically breaks off the communications of the farther stations in favour of the closer stations [31]. The result is a progressive reduction in the size of the radio cell and thus in the coverage. When the traffic intensity is very high this can cause a block of the system. In such cases the performance could be derived by modelling the system as a Markov chain and by evaluating the block probability [23]. The critical factors related to the use of the AIS are:

- The functioning of the system depends on the presence of the GPS signal, thus the precision in the timing information depends on the GPS precision. Considering the practical experience, the risk of absence of the GPS signal is extremely low.
- The problem related to the traffic intensity and to the unavailability of time slots. However this problem can be reduced by increasing the number of stations and repeaters into the system.
- The sensitivity of the overall performance to the position of the GPS antenna: this factor can considerably influence the information about the position of a large ship and thus it can increase the probability of collision with other ships.
- The potential errors in the installation of the AIS transponder onboard the ship [36].

- The effects due to the synchronization jitter, i.e. the time between nominal slot start as determined by the UTC synchronisation source and the effective start of the transmission from the AIS station. The synchronization jitter must not be higher than $\pm 104 \mu\text{s}$ using UTC direct synchronisation and $\pm 312 \mu\text{s}$ using UTC indirect synchronisation [34].
- The possible errors related to the human operator, e.g. in the communication of the ship identity [31].

In this work the AIS station is only used to identify the target as a *cooperative* or a *non-cooperative* one. It is assumed that the coverage of the AIS station is 10% higher than the VTS coverage; anyway the analysis performed in this work is parametric. In some cases, practical experiences show a much higher coverage by the AIS versus a VTS radar. Since we consider simulation scenarios characterized by the presence of no more than 20 targets during an observation time of one hour, we have assumed an ideal behaviour for the AIS station and we have not considered the block probability of the system due to the traffic intensity.

There is an invitation of the International Maritime Organization (IMO) that asks to use a Long Range Identification and Tracking (LRIT) system onboard the new constructed ships, starting from January 2008. The new system is based on the same principle of the AIS, but it exploits satellite communications instead of the VHF channels [62].

2.3.3 The Airborne Early Warning Radar

The airborne radar moves on an elliptic trajectory between the warning zone and the external area and it is a coherent Airborne Early Warning Radar (AEWR). The parameters of the radar used inside the system are listed in Table 2.4.

Table 2.4 – AEW radar typical parameters

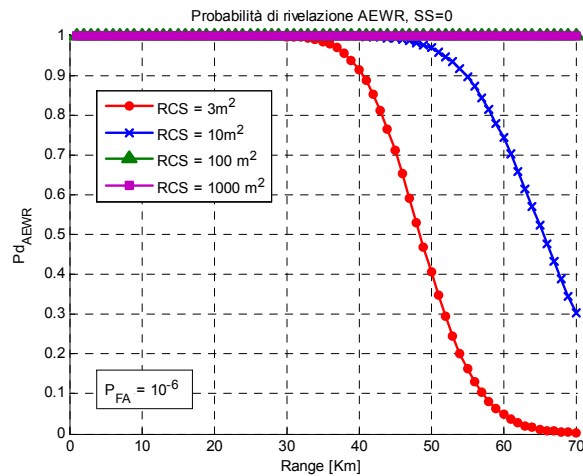
Parameter	Value
Range resolution	$\sigma_p = 2.4$ m
Azimuth resolution	$\sigma_\theta = 0.25^\circ$
Elevation beamwidth	$\varphi_{el} = 6^\circ$
Azimuth beamwidth	$\varphi_{az} = 2.5^\circ$
Grazing angle	3.7°
Scan time	$T_{scan} = 1$ s
Flight quote	$h_T = 914.4$ m
Maximum range	$R_{max} \cong 70\div 80$ Km
Platform speed	90 m/s
Central frequency	$f_0 = 9.6$ GHz
PRF	625 Hz
Signal bandwidth	$B = 150$ MHz
Pulse width	$\tau = 20\mu\text{s}$ (16 ns for the compressed pulse)
Transmitted power	$P_T = 3$ W
Polarization	H
False alarm probability	$P_{FA} = 10^{-6}$

The elliptic trajectory of the air platform is shown in Figure 2.2. The geometric parameters of the ellipse are reported in Table 2.5. The coordinates of the ellipse centre $(X_{Oe}; Y_{Oe})$ are referred to the inertial reference system centred in the point $\mathbf{O} \equiv (0; 0)$ of Figure 2.2.

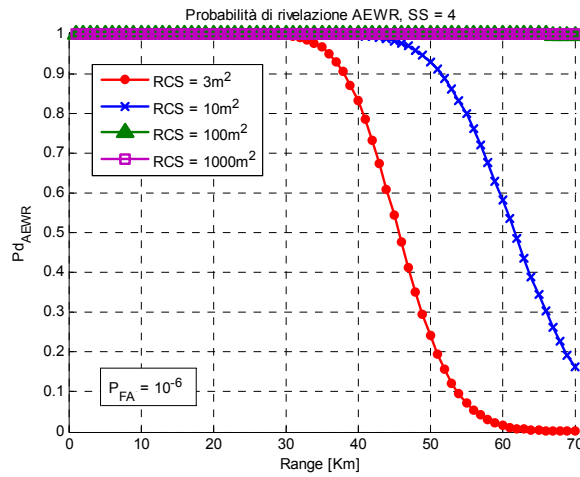
Table 2.5 – Geometric parameters of the air platform trajectory

Parameter	Value
Platform speed	$v_{p2} = 90 \text{ m/s}$
Ellipse centre	$(X_{Oc}, Y_{Oc}) \equiv (146000 \text{ m}; 116932 \text{ m})$
Major semi-axis	$a = 40500 \text{ m}$
Minor semi-axis	$b = 10000 \text{ m}$
Starting point of the trajectory	$(x_0; y_0) \equiv (X_{Oc} - a; Y_{Oc})$
Ellipse length	$L = \pi \left[3(a+b) - \sqrt{(3a+b) \cdot (a+3b)} \right]$
Orbit period	$T_{p2} = L/v_{p2}$
Rotation frequency	$2\pi/T_{p2}$

The detection probabilities of the AEW radar acting in a coherent mode are shown in Figure 2.5 a) and b) respectively for sea state values equal to 0 and 4 of the Beaufort scale. These curves refer to a false alarm probability equal to 10^{-6} .



a)



b)

Figure 2.5 – AEW detection probability: a) sea state 0; b) sea state 4

The AEW radar performs the detection and the tracking independently of the land based radar, providing the kinematical parameters of the target. Also in this case, it is assumed that the track initialization occurs when the detection has occurred for three radar scans over a window of five consecutive scans and that the tracking operation is performed with respect to the geographical system.

2.3.3.1 The spotlight SAR mode

The spotlight SAR ([7],[22]) is an operative mode of the airborne radar. The spotlight SAR geometry exploits the movement of the radar, i.e. the airborne radar in the case considered here. During the platform motion, the beam of the radar antenna always covers the same portion of sea (or of surface, in a more general case).

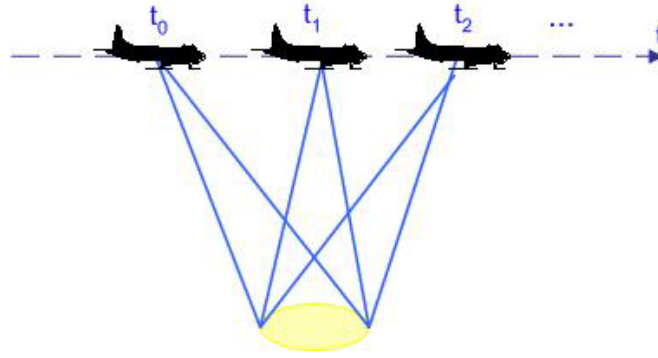


Figure 2.6 – Spotlight SAR geometry

We derive the expression of the signal to noise ratio (SNR) as a function of the radar parameters for the spotlight SAR geometry, by considering the radar equation. The parameters of the radar are described in Table 2.4. From the definition of SNR, we have:

$$\text{SNR}' = \frac{P'_r}{P'_n} \quad (2.2)$$

where we have not considered the number of pulses integrated along the azimuth direction. In Equation (2.2), P'_r represents the signal received power and P'_n is the noise power. The received power can be computed from the radar equation as:

$$P'_r = \frac{P_T \cdot G^2 \cdot \lambda^2 \cdot RCS \cdot F_p^4}{(4\pi)^3 \cdot R^4 \cdot L_t \cdot L_\alpha} \quad (2.3)$$

where P_T is the average transmitted power, G is the antenna gain, λ is the wavelength, RCS is the target radar cross section, and R is the distance between the target and the radar. The factor F_p represents the pattern propagation factor that takes into account the multipath effects, L_t is the transmission line loss and L_α is the atmosphere attenuation [5]. In this analysis we will neglect the multipath and we will assume $F_p=1$. Thus the received power is:

$$P'_r = \frac{P_T G^2 \lambda^2 RCS}{(4\pi)^3 R^4 L_t L_\alpha} \quad (2.4)$$

The thermal noise is assumed to be a white stationary Gaussian process, whose power is:

$$P'_n = kT_s B \quad (2.5)$$

Where k is the Boltzmann constant $k=1.38 \cdot 10^{-23} \text{J/}^\circ\text{K}$, T_s is the system equivalent temperature, and B is the noise bandwidth. For simplicity the noise band is assumed to be equal to the band of the chirp B_s [44]. The system equivalent temperature can be computed as [51]:

$$T_s = T_a + T_r + L_r T_e \quad (2.6)$$

where T_a is the antenna noise temperature. Since the antenna beam is directed towards the sea, T_a is assumed to be equal to the temperature of water; T_r is the transmission line noise temperature, L_r is the loss factor due to the receiving transmission line and T_e is the effective input noise temperature of the receiver, that can be computed as:

$$T_e = T_0 (F_n - 1) \quad (2.7)$$

where T_0 is, by convention, 290 K and F_n is the linear value of the receiver noise factor. In this analysis, we assume $T_a = 290 \text{ K}$, we neglect the term T_r with respect to the others and we assume $L_r = 1$ and $F_n = 3 \text{ dB} = 1.99$. The resulting system temperature is approximately $T_s = 579 \text{ K}$.

The signal to noise ratio is then:

$$SNR' = \frac{P_T G^2 \lambda^2 RCS}{(4\pi)^3 R^4 L_t L_a k T_s B} = \frac{P_T G^2 \lambda^2 RCS \tau}{(4\pi)^3 R^4 L_t L_a k T_s} \quad (2.8)$$

that represents the signal to noise ratio at the output of the matched filter. In the second part of Equation (2.8) we have considered the inverse of the chirp band equal to the pulse width. The parameters in the expression of SNR' are:

- P_T , the transmitted power: $P_T = 3 \text{ W}$, from Table 2.4.
- G , the antenna gain: for a pencil-beam antenna, when only the beamwidths in the principal planes are known, can be approximated as [51]:

$$G = \frac{40000}{\varphi_{az} \cdot \varphi_{el}} \quad (2.9)$$

where φ_{AZ} and φ_{EL} are the azimuth and the elevation half-power beamwidth in degree, available from Table 2.4. This approximation states that a 1 degree pencil-beam antenna has a gain of 46 dB.

- λ , wavelength of the transmitted signal:

$$\lambda = \frac{c}{f_0} \quad (2.10)$$

with $c=3.10^8$ m/s the light speed, and $f_0=9.6$ GHz the central frequency (X-band).

- τ , the length of the pulse.
- R , the distance between the target and the radar.
- L_t , transmission line loss. An indicative value of this parameter for the considered system, based on the experience, is 1.5 dB.
- L_α , atmosphere attenuation. It can be computed from the transmittance law as:

$$L_\alpha = e^{-\gamma \cdot R} \quad (2.11)$$

where R is the distance between the target and the sensor in Km and γ is the atmosphere attenuation coefficient. This coefficient is 0.024 dB/Km for the X band [5].

- T_s , the system equivalent temperature evaluated from (2.6).
- RCS , the radar cross section of the target.

By considering the number of pulses integrated in azimuth, the expression of the signal to noise ratio becomes:

$$SNR = N_a \cdot SNR' = \frac{P_t G^2 \lambda^2 RCS \tau N_a}{(4\pi)^3 R^4 L_t L_\alpha K T_s} \quad (2.12)$$

where N_a is:

$$N_a = PRF \cdot T_d \quad (2.13)$$

and T_d is the dwell time.

2.3.4 The video camera

The video camera is a standard monochromatic TV camera. The fields of view (FOV) for the camera are listed in Table 2.6.

Table 2.6 – Video camera Fields of View (FOV)

Field of view (FOV)	Horizontal (H)	Vertical (V)
FOV 1	0.6°	0.45°
FOV 2	0.3°	0.22°
FOV 3	0.2°	0.15°
FOV 4	0.1°	0.07°

The model of the video camera assumes that the detection is performed by the radar belonging to the platform where the camera is located, while the acquisition and the recognition of the image is performed according to the Johnson criterion ([6],[49],[57]), with a recognition probability P_{rec} . This probability is calculated as follows:

1. The original luminance difference between the target and the image background is:

$$\Delta L_0 = \frac{E}{\pi}(\rho_t - \rho_b) \text{ [Lux]} \quad (2.14)$$

where E is the scene luminance, ρ_t is the target reflection coefficient and ρ_b is the background reflection coefficient. Under the assumption of direct sunlight the scene luminance is $E = 1.3 \cdot 10^{-5}$ Lux.

2. The luminance difference at the input of the sensor, considering the atmosphere attenuation, is:

$$\Delta L = \Delta L_0 \cdot e^{-\sigma_{ATM}R} \text{ [Lux]} \quad (2.15)$$

where σ_{ATM} is the atmosphere extinction coefficient of Equation (2.1).

3. A Minimum Resolvable Contrast (MRC) curve is constructed as follows:

$$\text{MRC}(f_s) = \frac{\text{NEIL}}{\text{MTF}_{\text{sys}}(f_s)} \quad (2.16)$$

The numerator is the Noise Equivalent ILuminance (NEIL) of the sensor, defined as follows:

$$\text{NEIL} = \frac{S \cdot R}{\text{SNR} \cdot (2f_{\#})^2} \quad (2.17)$$

where S is the camera sensitivity, i.e. the luminance level (Lux) incident on the camera display² that produce a video signal equal to the saturation value, i.e. 700 mV for the monochromatic camera considered here. The parameter R is the display reflectivity³ and it is provided by the constructor, and $f_{\#}$ (*f number*) is the ratio between the depth of focus and the lens diameter (f/D); SNR represents the signal-to-noise ratio measured at the output of the sensor, when a luminance difference value that generate a video signal equal to the saturation level is considered. The denominator of Equation (2.17) is the Modulation Transfer Function [53] (MTF) of the system composed by the atmosphere, the sensor and the display. It takes into account of the MTF of the single sensor and also of the effect vibrations in the platform where the sensor is located:

$$\text{MTF}_{\text{sys}}(f_s) = \begin{cases} 1 - \bar{k} \cdot f_s & 0 \leq f_s \leq \bar{f}_s \\ 0 & f_s > \bar{f}_s \end{cases} \quad (2.18)$$

Where f_s is the spatial frequency and the factors \bar{k} and \bar{f}_s are constants dependent on the FOV and provided by the constructor.

4. The MRC curve is scaled in order to obtain the curve representing the luminance difference between the target and the background ΔL as a function of the spatial frequency (f_s) for a fixed distance from the sensor (\bar{R}), by means of the *camera equation*:

² The camera display is supposed to be a lambertian diffuser.

³ The reflectivity is an adimensional parameter, representing the energy associated to the propagation of an electromagnetic wave, when it is reflected on the separation interface between two different media.

$$\text{MRC}(\bar{R}, f_s) = \frac{\pi}{(2f_{\#})^2} \cdot \Delta L(\bar{R}, f_s) \quad (2.19)$$

$$\Delta L(\bar{R}, f_s) = \frac{(2f_{\#})^2}{\pi} \cdot \text{MRC}(\bar{R}, f_s) \quad (2.20)$$

5. The maximum resolvable spatial frequency required for the recognition is then evaluated from the $\Delta L(\bar{R}, f_s)$ curve, by using the difference luminance value ΔL computed at point 2:

$$f_{\max} = f^{-1}(\Delta L) \quad (2.21)$$

6. The number of resolvable cycles N_C across the target critical dimension needed for the recognition is evaluated as follows [49]:

$$N_C = f_{\max} \cdot \frac{D_{CR}}{\bar{R}} \quad (2.22)$$

where the ratio between the target critical dimension and the range (D_{CR}/\bar{R}) represents the target angular dimension.

7. The value of the recognition probability is finally derived as a function of the number of cycles, $P_{rec} = f(N_C)$, by means of an interpolation of a set of empirically generated curves provided by the producer.

Typical parameters for a standard monochromatic TV camera are reported in Table 2.7.

Table 2.7 – Typical parameters for the video camera

Parameter	Value			
S , Sensitivity [Lux]	FOV 1	FOV 2	FOV 3	FOV 4
	798	3192	8003	22743
$NEIL$ @50dB [mLux]	FOV 1	FOV 2	FOV 3	FOV 4
	51	204	511.9	1453.9
R , Reflectivity (adimensional)	0.9			
$f_{\#}$, f number (f/D)	3.33			
Number of pixels, vertical (V) x horizontal (H)	576 (V) x 768 (H)			
\bar{k} (adimensional)	FOV 1	FOV 2	FOV 3	FOV 4
	0.045	0.023	0.0166	0.0126
\bar{f}_s [cycles/mrad]	FOV 1	FOV 2	FOV 3	FOV 4
	22	43	60	79

The model of the video camera described is shown in Figure 2.7. The atmosphere effect is considered by means of the Lambert absorption law of Equation (2.1).

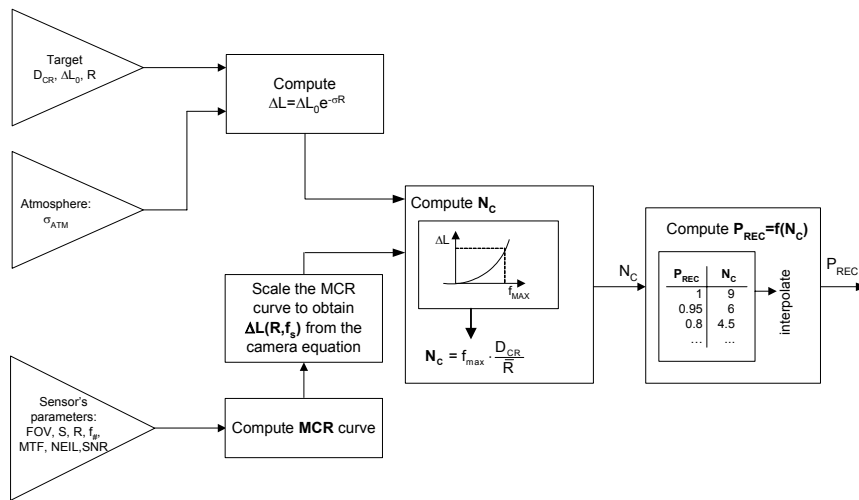


Figure 2.7 – Video camera model

The atmosphere extinction coefficient is evaluated, for fixed values of the visibility V and of the wavelength λ , as [40]:

$$\sigma_{\text{ATM}}(V, \lambda) = \frac{3.912}{V} \cdot \left(\frac{\lambda}{550\text{nm}} \right)^{-q} \quad (2.23)$$

where q is the size distribution of the scattering particles:

$$q = \begin{cases} 1.6 & \text{for high visibility } (V > 50 \text{ km}) \\ 1.3 & \text{for average visibility } (6 \text{ km} < V < 50 \text{ km}) \\ 0.16V + 0.34 & \text{for haze visibility } (1 \text{ km} < V < 6 \text{ km}) \\ V - 0.5 & \text{for mist visibility } (0.5 \text{ km} < V < 1 \text{ km}) \\ 0 & \text{for fog visibility } (V < 0.5 \text{ km}) \end{cases} \quad (2.24)$$

A visibility $V=23 \text{ Km}$ and a wavelength $\lambda=0.55 \mu\text{m}$ (in the middle of the visible window) have been assumed for the video camera, thus the resulting value for q is 1.3.

The noise features of the video camera are expressed in terms of Noise Equivalent Luminance (NEIL) introduced in Equation (2.17). This parameter represents the output luminance of the sensor produced by a signal whose amplitude is equal to the noise *effective* value. Considering this definition and Equation (2.17), the SNR at the output of the sensor for a target characterized by a luminance difference with the background equal to ΔL can be expressed as:

$$\text{SNR} = \frac{\Delta L}{\text{NEIL} \cdot (2f_{\#})^2} \quad (2.25)$$

2.3.5 The infrared camera

The infrared camera used in the integrated system is a standard IR camera. The recognition process is based on the Johnson criterion, as in the case of the video camera, but the temperature difference between the target and the image background is considered instead of the luminance difference:

1. The original temperature difference between the target and the image background is ΔT_0 . The temperature difference at the input of the sensor, considering the atmosphere attenuation, is:

$$\Delta T = \Delta T_0 \cdot e^{-\sigma_{\text{ATM}} R} \quad (2.26)$$

2. The maximum resolvable spatial frequency required for the recognition is evaluated from a Minimum Resolvable Difference Temperature (MRTD) curve, provided by the constructor and shown in Figure 2.8.

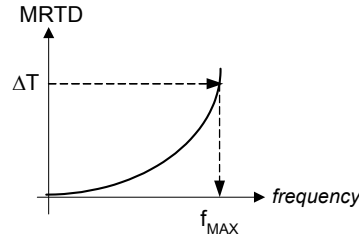


Figure 2.8 – Minimum Resolvable Temperature Difference

3. The number of resolvable cycles across the target critical dimension needed for the recognition, N_C , is evaluated for a fixed value of the range \bar{R} :

$$N_C = f_{\text{max}} \cdot \frac{D_{\text{CR}}}{\bar{R}} \quad (2.27)$$

where D_{CR} is the critical dimension of the target and the ratio D_{CR}/\bar{R} represents the target angular dimension.

4. The value of the recognition probability is derived as a function of the number of cycles, $P_{\text{rec}} = f(N_C)$, by means of an interpolation of a set of empirically generated curves provided by the producer.

The typical parameters for a standard IR camera are reported in Table 2.8. The model of the IR model is described in Figure 2.9

Table 2.8 – Typical parameters for the IR camera

Parameter	Value
<i>NETD</i> [m°K]	20
<i>Number of pixels</i> vertical (V) x horizontal (H)	576 (V) x 768 (H)
<i>Maximum range</i> [Km]	20

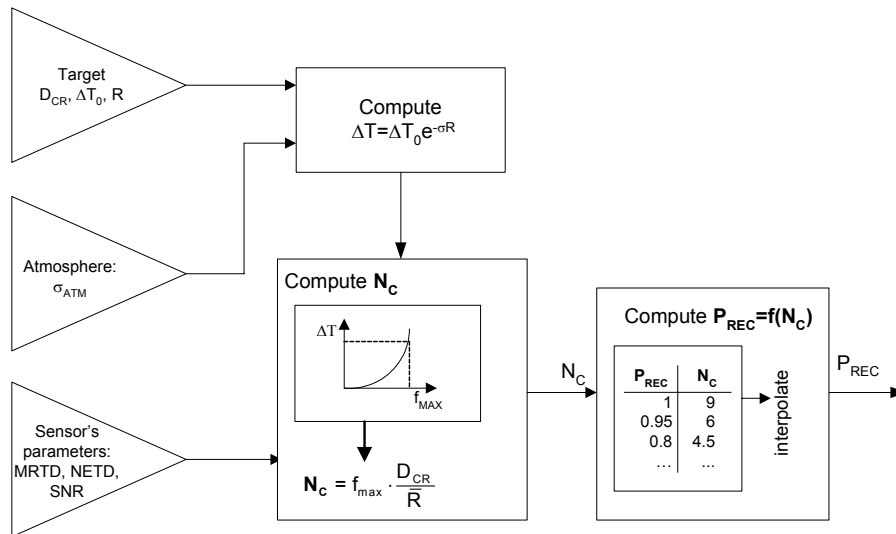


Figure 2.9 – IR camera model

Also in this case, the atmosphere effect is considered by means of the Lambert absorption law of Equation (2.1). The atmosphere extinction coefficient σ_{ATM} has been evaluated using the software LOWTRAN (LOW resolution TRANsmission model) [48], under the following assumptions:

- Temperature: $T = 30^\circ$;
- Visibility: $V = 23$ Km;

- Relative humidity: 43%;
- Sea state: SS = 0 and 4.

Table 2.9 – Meteorological vectors for the IR camera

Weather Vectors			
#	Parameter	Vector 1	Vector 2
1	Temperature	30 °C	30 °C
2	Visibility	23 km	23 km
3	Relative humidity	43 %	43 %
4	Sea state	0	4
5	Atmosphere extinction coefficient σ_{ATM}	0.201 km ⁻¹	0.208 km ⁻¹

Table 2.9 describes the resulting weather vectors. This model also assumes:

- Frequency band: 7.5÷10.5 μm , i.e. the band of the thermal infrared (TIR);
- Air mass factor: ICSTL = 8.

The last parameter (ICSTL) is only used in the Navy Aerosol Model [30] and it depends on the amount of aerosol contained in the atmosphere because of the coastal influence. Dependent on the available data, there are three methods to evaluate it [48] :

1. $\text{ICSTL} = \text{INT}(9 \cdot e^{-t/4} + 1)$, where t is the number of days the air has been blowing over the sea;
2. $\text{ICSTL} = \text{INT}(Rn/4) + 1$, where Rn is concentration of the radon 222⁴ in the atmosphere, expressed in picocuriers/m³.
3. the ICSTL can be chosen in the interval [1÷10], as an estimate of the effect of the continental mass considering that is: ICSTL=1 for open ocean and ICSTL=10 for sea near to the coast.

⁴ Randon 222 is a noble gas coming from radium decay.

For the three sea regions of the scenario described in Figure 2.2, we can assume an average value of the ICSTL equal to 8, i.e. the value exploited for the computation of the meteorological vectors of Table 2.9.

The noise features of the IR camera are expressed in terms of its Noise Equivalent Temperature Difference (NETD), i.e. the temperature difference that produces a SNR to one at the output of the detector [14]. From this definition, the SNR at the output of the detector for a target characterized by a temperature difference ΔT can be evaluated as:

$$\text{SNR} = \frac{\Delta T}{\text{NETD}} \quad (2.28)$$

2.4 The Command and Control centre

After that the detection, the tracking, the identification, and the classification of the targets that enter the scene are performed by the sensors of the two platforms, the initialized tracks are sent to the C² centre. Here the tracks coming from the two radars are associated and fused, their threat level is evaluated, and a suitable intervention is selected on each assessed target. The functions performed by the C² centre are described in Chapter 4.

2.5 The end to end simulator

The end to end simulator emulates the functions of the integrated multi-sensor system described above and it evaluated its performance by a Monte Carlo simulation. It has been completely developed using the software MatLab[®]. The flow chart of the simulator is reported in Figure 2.10. For each Monte Carlo trial a fixed observation time for the scenario is considered. This observation time is divided into a number of time slots and for each time slot all the functions of the system are reiterated. The structure and the parameters of the simulation are described in Chapter 5.

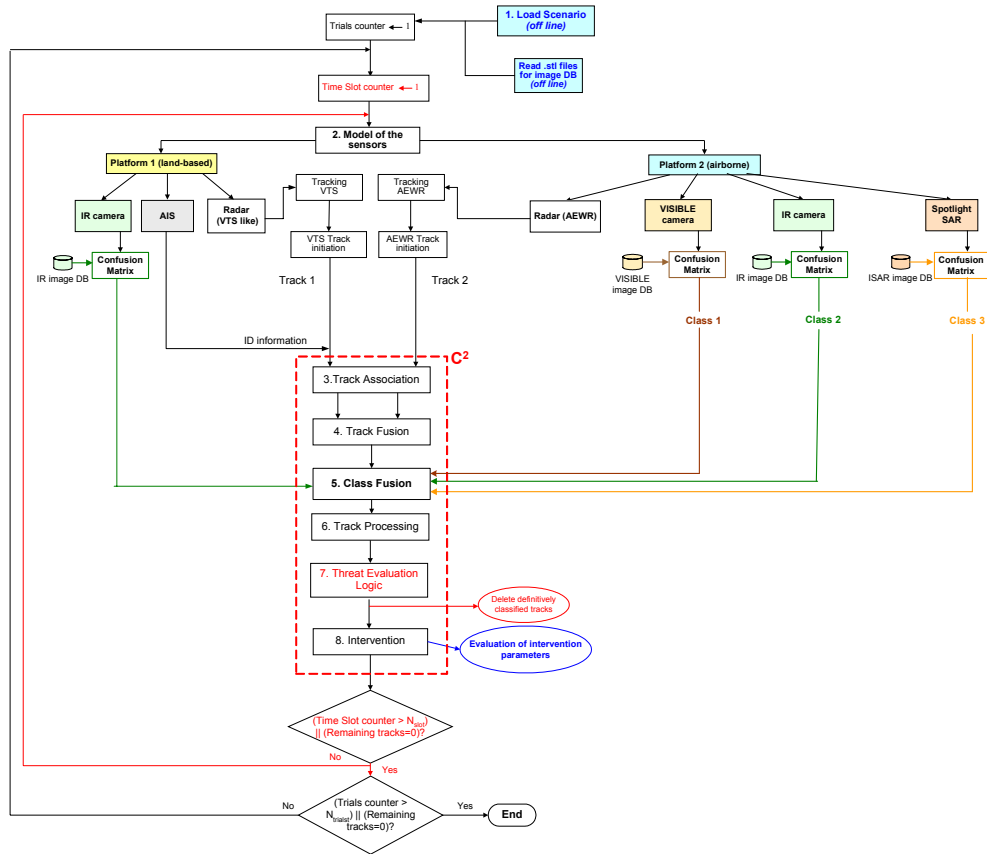


Figure 2.10 – Flow chart of the MatLab[®] end to end simulator

Chapter 3

The classification process

3.1 Introduction

The ability to quickly and reliably recognize non cooperative targets is of primary importance for surveillance operations in HS applications. The development of efficient fusion strategies and the improvements in the design of more reliable sensors has increased the research interest in the classification techniques. In particular, automatic surveillance systems based on imaging sensors are gaining significant interest, as proved by recent research works ([10],[21],[54]) addressed to improve the quality of image-based surveillance systems. The classification techniques can include both approaches based on the human interpretation of the data provided by a sensor system or automatic methods ([12],[24]). The Automatic Target Classification (ATC) techniques can use data coming from sensors of different nature, such as infrared, electro-optic cameras and radar systems. In ATC the classification task can be accomplished using several approaches. A model based technique uses a model of the target, obtained for example by a Computer Aided Design (CAD) model or an Electro-Magnetic (EM) simulation [2], to compare the simulated models with the signature of the target under test. The computational load of this methodology can be very high, especially when more than one sensor is used. Another methodology can consist of collecting many real versions of the target signature and of comparing them with the signature of the current target under test, but in this case a very large database

is required and if the target changes in some way the classification process may be unsuccessful.

In this work we develop a classification algorithm, which uses a different approach, where the information on the target class is provided by the three imaging sensors belonging to the system and it is expressed by means of a confusion matrix (CM). This approach allows us to overcome with the difficulties related to the high computational load of the methodologies described above and to easily insert the classification task in the analysis of the integrated system. The CM is analytically computed for each imaging sensor and it models the performance of the sensor during the classification process. The entries of this matrix are the conditional error probabilities in the classification and the conditional correct classification probabilities. These probabilities amount to the target class likelihood functions and are used to make the decision on the target class by each sensor. Then a final decision on the class is made, using a suitable fusion rule in order to combine the decisions coming from the three sensors. The overall performance of the classification process is evaluated by means of the “*fused*” confusion matrix, i.e. the CM pertinent to the final decision on the target class. The ultimate purpose of this fusion process is to combine the outputs of the three imaging sensors in order to obtain an accurate and reliable estimate of the target class. This information on the class is then used by the C^2 centre during the threat level evaluation, as described in Chapter 4.

In [13], different levels of abstraction in the fusion of data coming from different imaging sensors are described: the signal-level fusion is the combination of signals from different sensors, performed before the production of images; the pixel-level fusion consists of merging different digital images; the feature-level fusion extracts specific features from different image and combines them. The approach developed in this work, using the CM to model the classification capability of the imaging sensor, refers to a higher level of abstraction. A similar approach is also used in [3], but there the classification process is used to support the data association and improve the tracking, especially in presence of association

uncertainty in kinematic measurements. In literature many applications are proposed where radar images are combined with images of different kind of sensors ([13],[15],[18],[55]) or where heterogeneous data set coming from dissimilar imaging sensors are effectively combined at an information fusion level [29]. The main contribution of the proposed classification algorithm is the development of a methodology that allows us to incorporate the classification task in the study of a complex multisensor system, such as the one analyzed in this work, and to use it as a support during other surveillance operations, without increasing the computational complexity of the overall system.

3.2 The classification algorithm

The generic entry of the CM of a classifier is the probability that a target belonging to the class i is misclassified as belonging to class j :

$$c_{ij}^{(k)} = \Pr\{\text{the } k\text{-th sensor decides for } H_j \text{ when } H_i \text{ is true}\} = \Pr\{\hat{d}_k = j \mid H_i\} \quad (3.1)$$

where H_i represents the hypothesis that the target belongs to class i and $\{\hat{d}_k = j\}$ represents the event $\{\text{the } k\text{-th sensor decides for } H_j\}$. Thus each row of the CM represents the class of the target and the class likelihood function for the sensor output j is the j -th column of \mathbf{C} [3]. The off-diagonal elements of the CM represent the conditional error probability during the classification and the diagonal elements are the conditional correct classification probabilities for a given sensor, under the hypothesis H_i :

$$\begin{aligned} P_{CC|H_i}^{(k)} &= \Pr\{\text{correct classification for the } k\text{-th sensor} \mid H_i\} \\ &= \Pr\{\text{the } k\text{-th sensor decides for } H_i \text{ when } H_i \text{ is true}\} \end{aligned} \quad (3.2)$$

Then the correct classification probability is:

$$P_{CC} = \sum_{i=1}^M P_{CC|H_i}^{(k)} \cdot \Pr\{H_i\} \quad (3.3)$$

where the term $P_{CC|H_i}^{(k)}$ is the conditional correct classification probability given by the diagonal element $c_{ii}^{(k)}$ of the confusion matrix, $\Pr\{H_i\}$ is the probability of the i -th hypothesis, and M is the number of hypotheses, i.e. $M = 4$ in the case of four classes considered here. The error probability conditioned to the i -th class, for the k -th sensor, is:

$$P_{ERR|H_i}^{(k)} = \sum_{i=1, i \neq j}^M c_{ij}^{(k)} \quad (3.4)$$

The entries of the CM are used to model the performance of each sensor during the classification and to make the decision on the target class. This means that a target detected by the system is declared as belonging to class j with a probability equal to $c_{ij}^{(k)}$, which is used by the sensor as a threshold for the decision on the class. In order to associate a class to an incoming target, a random variable uniformly distributed in the interval $[0,1]$ is generated and it is compared with the threshold given by the entries of the sensor CM. This is done to simulate the classification event without generating the data. The classification process based on the elements of the CM is shown in Figure 3.1. This implies to assume equal a priori probabilities for the hypotheses.

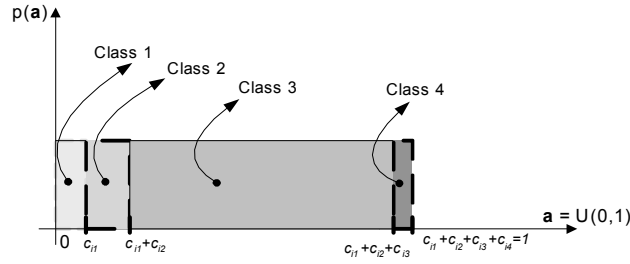


Figure 3.1 – Classification based on the elements of the CM

In the classification approach described in this work, the entries of the CM are computed in an approximated closed-form by means of an analytical evaluation, whose details are described in Appendix A. The parameters required for the analytical evaluation for each sensor are: (i) the signal-to-noise ratio (SNR) at the output of the sensor; (ii) the sensor resolution; (iii) a set of reference images stored in a database; (iv) the cross-correlation between the images of the database. The CM can be expressed as the following function:

$$\mathbf{C} = [\mathbf{c}_{ij}] = f(\text{SNR}, N_H, N_V, M) \quad (3.5)$$

where SNR is the signal-to-noise ratio, N_H and N_V represent the sensor resolution in terms of number of pixels on the horizontal and vertical planes respectively, and M is the dimension of the reference database. As described in Appendix A, the computation of the entries of the CM in the i -th row is derived from the computation of the classification error probability for the i -th class. The error probability is computed in an incremental way, by defining the elementary error event in the space composed by all the possible hypotheses $\{H_1, \dots, H_M\}$ and by adding the contribution of this event to the overall error probability. The partial contributions for the i -th class are assigned to the off-diagonal elements $c_{ij}^{(k)}$. The diagonal elements can be computed as:

$$c_{ii}^{(k)} = 1 - P_{ERR|H_i}^{(k)} = 1 - \sum_{i=1, i \neq j}^M c_{ij}^{(k)} \quad (3.6)$$

The simplified assumptions are:

- The detection of the target is performed by the radar, i.e. the VTS radar or the AEW radar in the system considered in this work.
- The recognition process always occurs, independently of the classification.
- The image database for each sensor is exhaustive, i.e. the possibility that the image of the target under test is not contained in the database is not considered.
- The reference images of each database do not contain any source of noise, but this is added during the analytical computation of the CM.
- The noise added over each image is additive Gaussian and independent from pixel to pixel.

In the case considered here, the dimension of the reference database is equal to the number of classes considered ($M = 4$), since the hypothesis of exhaustive database is made. The images of each reference database are simulated images obtained from a Computer Aided Design (CAD) model of the four ships considered. The construction of the reference database for the three imaging sensors considered in the system is described in Section 3.3.

The computation of the CM is schematically represented in Figure 3.2.

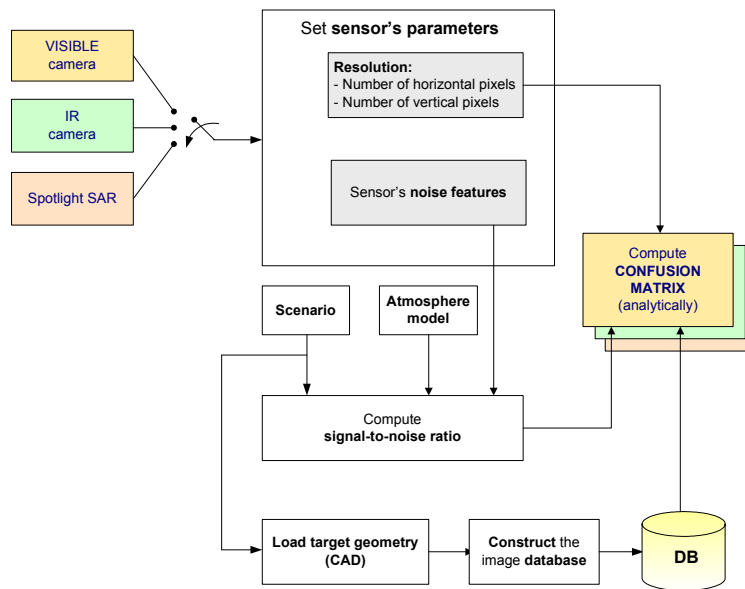


Figure 3.2 – Computation of the CM

The algorithm described is general and it also applies to imaging sensors different from those considered in this work.

3.3 Construction of a multisensor image database

The analytical computation of the CM requires the construction of a database of reference images. This database has been constructed using a three-dimensional (3D) Computer Aided Design (CAD) model of the naval targets considered in the scenario. The same CAD models have been exploited for the construction of the reference database for the video camera, for the IR camera, and for the spotlight SAR. The models are shown in Figure 3.3 for: a) dinghy; b) motor boat; c) fishing boat; d) oil tanker; e) dinghy with people on board; f) fishing boat with people on board.

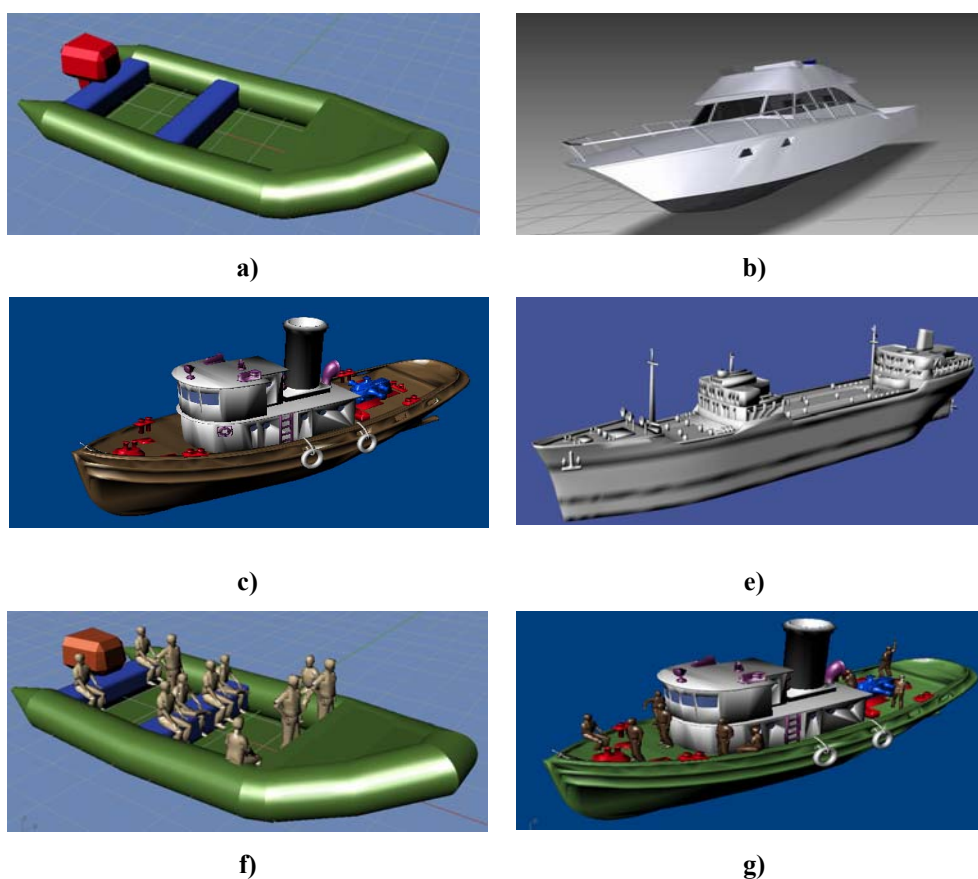


Figure 3.3 – CAD models

The model of the motor boat of Figure 3.3 b) has been exploited to represent the immigrant boat. The size of the naval targets reported in Figure 3.3 is:

- Dinghy: (10 x 4.6 x 3) m;
- Motor boat: (15 x 4.7 x 5.3) m;
- Fishing boat: (16 x 5.3 x 7) m;
- Oil tanker: (100 x 33.5 x 37.6) m.

For the video camera the image generation is simply obtained by the projection of the 3D CAD on the camera focal plane. For the IR camera, the images are simulated using a specific simulation software, the Open-source Software for Modelling and Simulation of Infrared Signatures (OSMOSIS) [41], developed at

the Military Royal Academy of Brussels. For the spotlight SAR the CADs have been processed by a software for the simulation of electro-magnetic (EM) images. In all the cases, the original CADs have been previously decomposed into polygonal facets, as shown in Figure 3.4 for: a) dinghy; b) motor boat; c) fishing boat; d) oil tanker; e) dinghy with people on board; f) fishing boat with people on board.

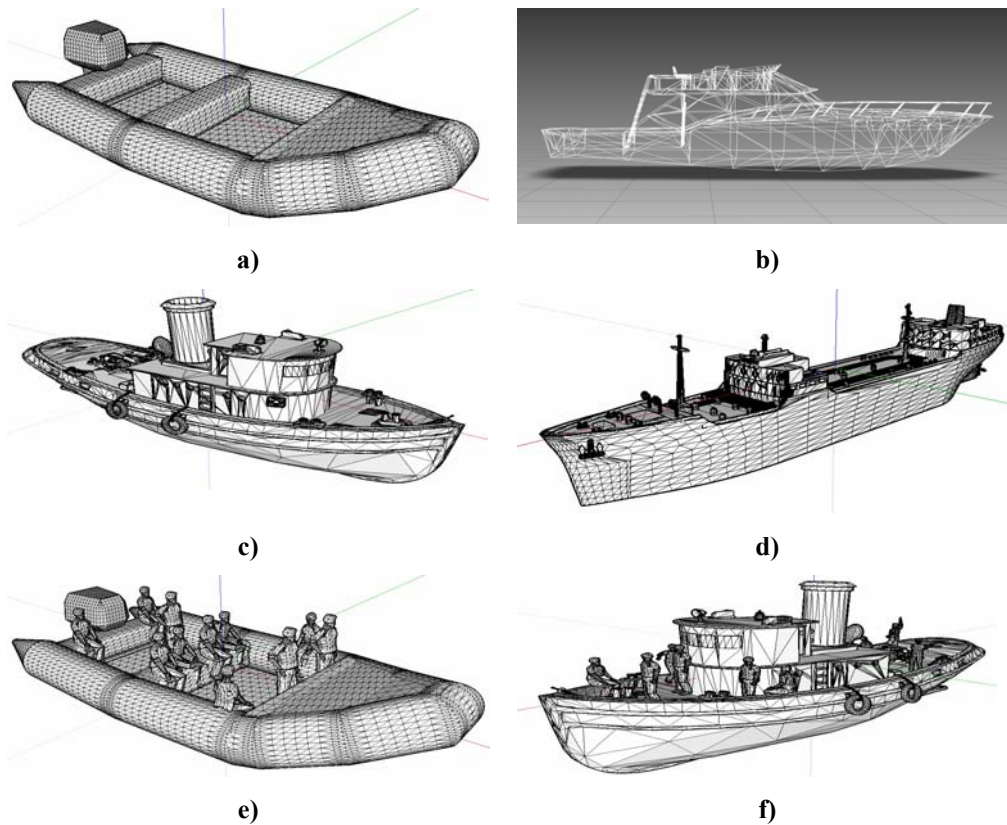


Figure 3.4 – CAD decomposition into polygonal facets

The approach utilized in this work exploits the knowledge of the CM, computed by means of a reference database of simulated images, and thus it represents a trade-off between a completely model based technique and a completely analytical technique.

3.3.1 The video camera database

For the generation of the simulated video images, the original 3D CAD of the ship is projected on the camera focal plane, taking into account for its orientation and its distance from the sensor. The result of this projection is a two-dimensional (2D) black and white image of the ship considered. The MatLab[®] function that makes the projection operates according to the following steps:

1. The origin of the geographical reference system is shifted on the target position $T \equiv (X_T, Y_T, Z_T)$ and it is rotated so that the x axis is parallel to the target direction.
2. In the resulting target centred system, the azimuth and the elevation of the line between the camera and the target are computed and they are used as input to the MatLab[®] tool that projects the 3D object on the camera focal plane⁵.

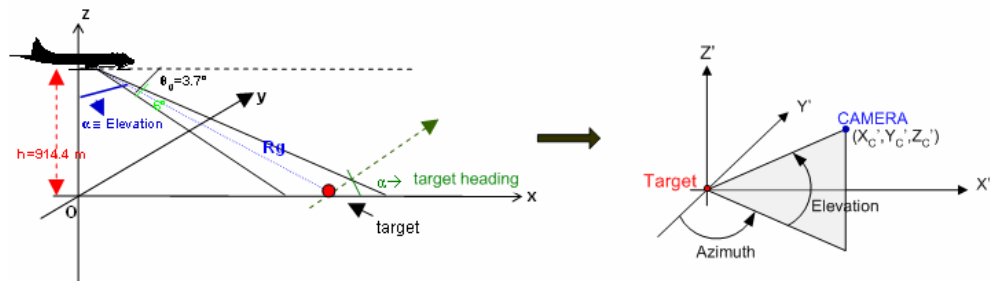


Figure 3.5 – Translation and rotation of the geographical system on the target

The operations described at step 1 are shown in Figure 3.5, where we indicated as:

$$\mathbf{X} = \begin{pmatrix} x \\ y \\ z \\ 1 \end{pmatrix} \quad (3.7)$$

the coordinates of a generic point in the original geographical reference system;

⁵ The operations described at step 1 and 2 are only performed to consider the same reference system of the MatLab[®] function “viewmtx”, used for the CAD projection.

$$\mathbf{X}_T = \begin{pmatrix} X_T \\ Y_T \\ Z_T \\ 1 \end{pmatrix} \quad (3.8)$$

the coordinates of the target in the original reference system;

$$\mathbf{X}' = \begin{pmatrix} X' \\ Y' \\ Z' \\ 1 \end{pmatrix} \quad (3.9)$$

the coordinates of a generic point in the new reference system centred on the target;

$$\mathbf{X}'_C = \begin{pmatrix} X'_C \\ Y'_C \\ Z'_C \\ 1 \end{pmatrix} \quad (3.10)$$

the coordinates of the camera in the new reference system. The translation and rotation are obtained by the following homogeneous transformation:

$$\begin{pmatrix} x \\ y \\ z \\ 1 \end{pmatrix} = \begin{pmatrix} X_T \\ Y_T \\ Z_T \\ 1 \end{pmatrix} + \mathbf{R}_Z \cdot \begin{pmatrix} x' \\ y' \\ z' \\ 1 \end{pmatrix} \rightarrow \mathbf{X} = \mathbf{X}_T + \mathbf{R}_Z \cdot \mathbf{X}' \quad (3.11)$$

$$\mathbf{X} = \mathbf{X}_T + \mathbf{R}_Z \cdot \mathbf{X}' \rightarrow \mathbf{X}' = \mathbf{R}_Z^{-1} \cdot (\mathbf{X} - \mathbf{X}_T) \quad (3.12)$$

$$\mathbf{X}' = \mathbf{R}_Z^{-1} \cdot (\mathbf{X} - \mathbf{X}_T) \rightarrow \mathbf{X}' = \mathbf{R}_Z^{-1} \cdot \mathbf{T}^{-1} \cdot \mathbf{X}$$

where:

$$\mathbf{R} = \begin{bmatrix} \cos(\alpha) & -\sin(\alpha) & 0 & 0 \\ \sin(\alpha) & \cos(\alpha) & 0 & 0 \\ 0 & 0 & 1 & 0 \\ 0 & 0 & 0 & 1 \end{bmatrix}, \quad \mathbf{T} = \begin{bmatrix} 1 & 0 & 0 & X_T \\ 0 & 1 & 0 & Y_T \\ 0 & 0 & 1 & Z_T \\ 0 & 0 & 0 & 1 \end{bmatrix} \quad (3.13)$$

α is the rotation angle, i.e. the angle between the target direction and the x axis of the original reference system, by considering a counter-clockwise rotation from the x axis to the target speed vector. This angle is indicated as *target heading* in Figure

3.5. Note that the fourth component in the vectors (3.7) - (3.11) does not correspond to any physical coordinate, but it has been included only to obtain a homogeneous transformation in the system (3.12) and to easily handle the inversion of the matrices \mathbf{R} and \mathbf{T} in the software. After the change of coordinates, the azimuth and the elevation to be provided to the MatLab[®] projecting function are computed as shown in Figure 3.6.

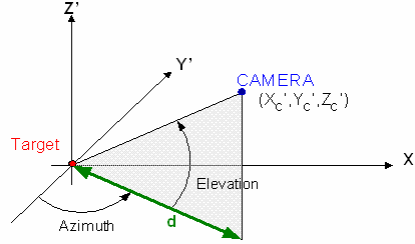


Figure 3.6 – Azimuth and elevation required for the CAD projection

The azimuth is:

$$az = \begin{cases} \pi & \text{if } (x' = 0) \ \& \ (y' > 0) \\ 0 & \text{if } (x' = 0) \ \& \ (y' < 0) \\ \pi/2 & \text{if } (x' > 0) \ \& \ (y' = 0) \\ 3\pi/2 & \text{if } (x' < 0) \ \& \ (y' = 0) \\ \pi/2 + \cos^{-1}(X'_c/d) & \text{if } (x' > 0) \ \& \ (y' > 0) \\ \cos^{-1}(-Y'_c/d) & \text{if } (x' > 0) \ \& \ (y' < 0) \\ 3\pi/2 + \cos^{-1}(X'_c/d) & \text{if } (x' < 0) \ \& \ (y' < 0) \\ \pi + \cos^{-1}(Y'_c/d) & \text{if } (x' < 0) \ \& \ (y' > 0) \end{cases} \quad (3.14)$$

and the elevation is:

$$el = \tan^{-1}\left(\frac{Z'_c}{d}\right) = \tan^{-1}\left(\frac{Z'_c}{\sqrt{X'^2_c + Y'^2_c}}\right) \quad (3.15)$$

After the projection, an image resize is performed in order to match the size of the final image with the resolution of the camera, in term of number of pixels on the

horizontal and vertical planes. The flow chart of the video camera database construction is described in Figure 3.7.

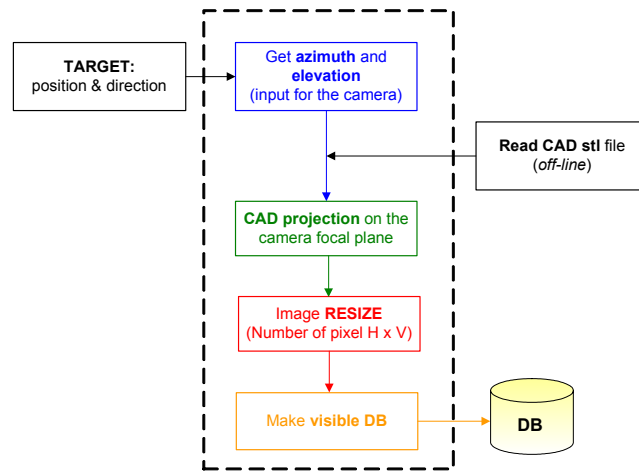


Figure 3.7 – Construction of the video camera database

As an example, Figure 3.8 shows the images derived from the CADs of Figure 3.3 for: a) dinghy; b) motor boat; c) fishing boat; d) oil tanker; e) dinghy with people; f) fishing boat with people. The view angle is equal to 45° , the distance between the target and the camera is 5 Km, the camera FOV is 0.6° in the horizontal direction (H) and 0.45° in the vertical direction (V), and the resolution in terms of pixels is 768 (H) by 576 (V).



a)



b)

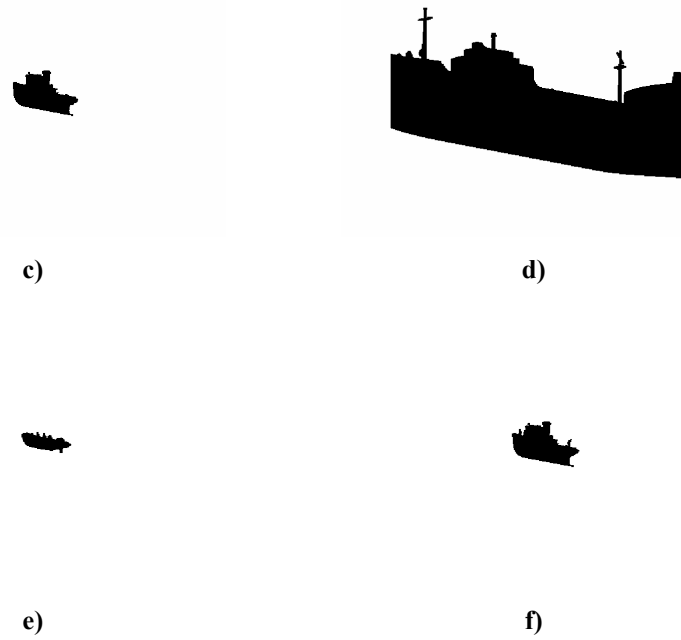


Figure 3.8 – Example of simulated images for the video camera

Figure 3.8 shows that all the targets are clearly recognizable, even though the distance is long (5 Km). This is due to the fact that we have obtained the images by means of a simple projection that takes into account for the target view angle and range, and for its azimuth and elevation with respect to the camera. The resulting images are ideal, since no attenuation, blurring, sea clutter or other distortion effects are considered [23]. Also note that the images are not affected by noise, since this is added during the analytical computation of the CM.

3.3.2 The infrared camera database

The IR images are simulated using the software “Open-source Software for Modelling and Simulation of Infrared Signatures” (OSMOSIS) [41], completely developed at the Belgian Royal Military Academy. This software integrates the dependence of the emissivity upon the surface temperature, the wavelength, and

the elevation angle ([17],[42]). The geometrical features and the temperature features of the target are then merged using the free software GMSH [61]. In the case of the IR database it is not possible to handle the view angle and the range of the target with continuity, since these parameters are manually set in the GMSH software. For this reason we operate a sort of “quantization” of the IR image database by considering only five values of distance between the target and the sensor and only five view angles, as shown in Figure 3.9 a and b. It is assumed that the geometry of the ship is symmetric.

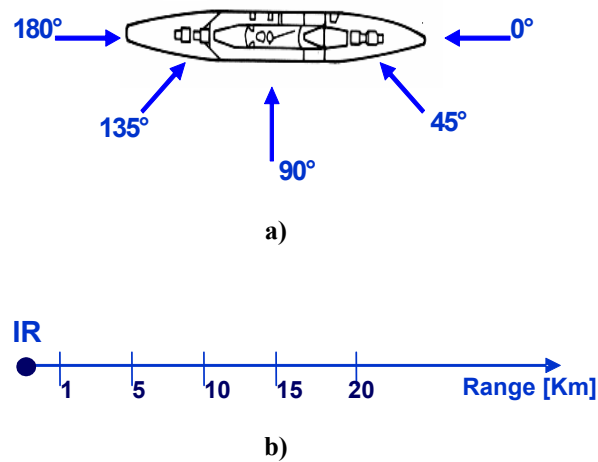


Figure 3.9 – View angles (a) and range values (b) considered in the IR database construction

The association between the incoming target and the simulated image is made by evaluating the effective view angle of the target under test and by choosing the reference database containing the simulated images characterized by the view angle closer to the real target view angle. The same is done for the distance between the target and the camera. The association intervals for the view angles are shown in Figure 3.10.

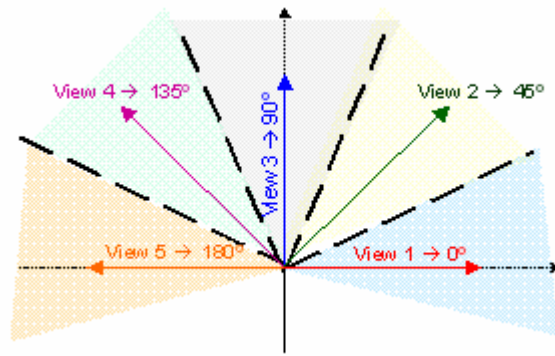


Figure 3.10 – Association intervals for the view angle

The flow chart of the operations applied for the construction of the IR image database is shown in Figure 3.11.

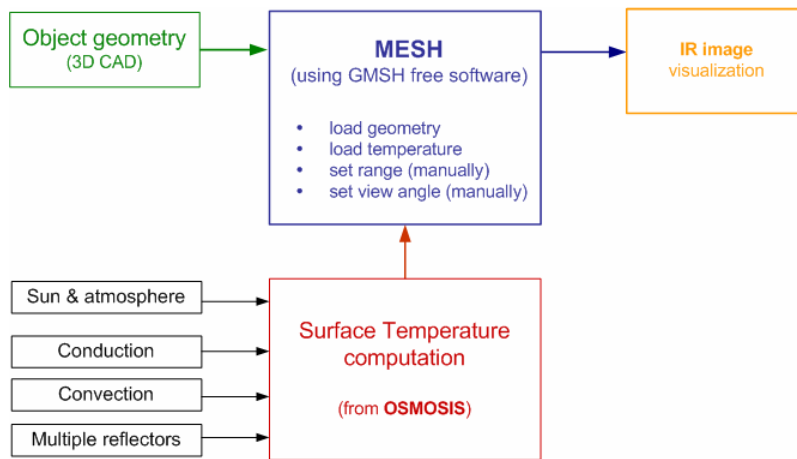


Figure 3.11 – Construction of the IR camera database

Figure 3.12 shows an example of the IR simulated images obtained for the dinghy and for the five view angles considered. The range is 1 Km and the original CAD is that of Figure 3.3a. The camera FOV is 2.50° in the horizontal direction (H) and

1.67° in the vertical direction (V), and the resolution in terms of pixels is 768 (H) by 576 (V). The temperature information is contained in the gray scale of the images. The view angles reported in Figure 3.12 are: a) 0°; b) 45°; c) 90°; d) 135°; e) 180°.

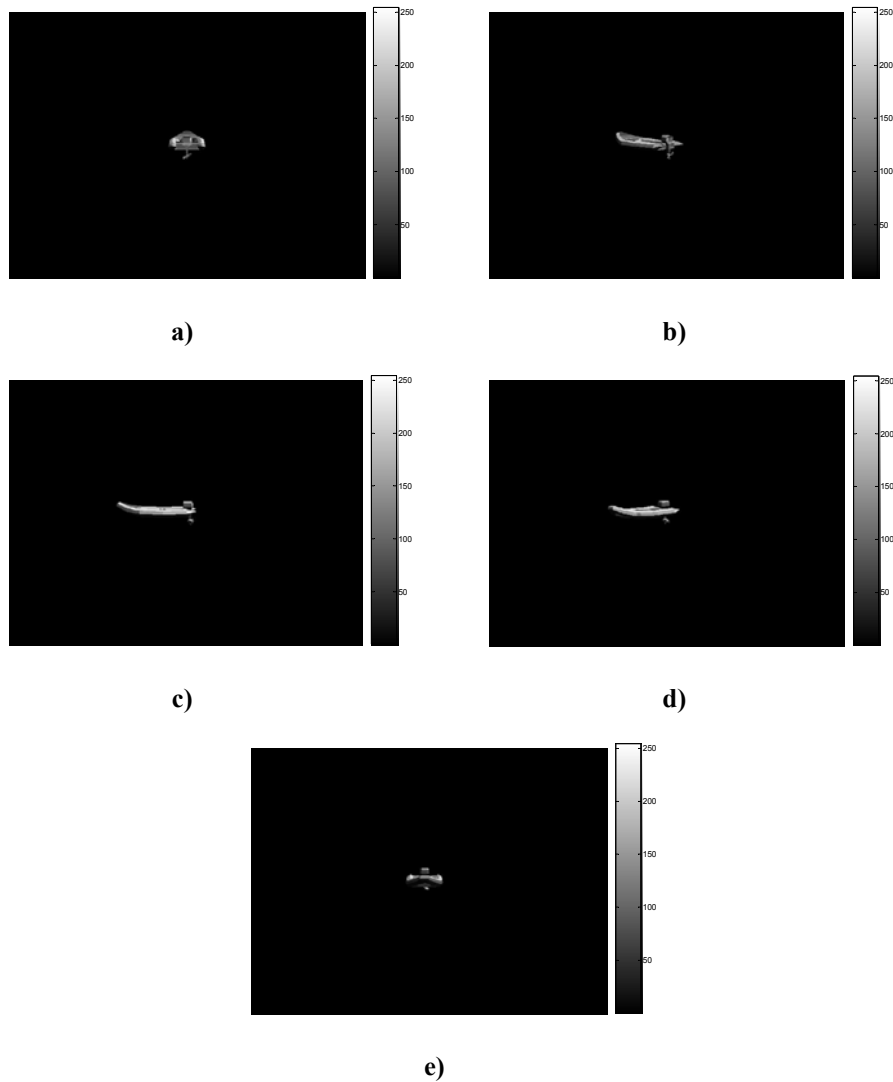


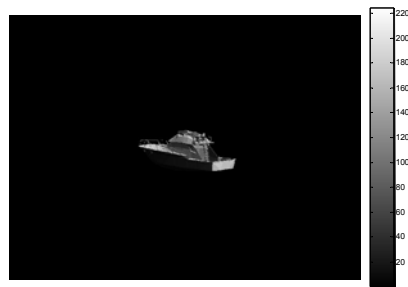
Figure 3.12 – Example of simulated images for the IR camera for the 5 view angles⁶

⁶ Images by courtesy of Dr. F. D. Lapierre, Military Royal Academy, Brussels, Belgium.

Finally, Figure 3.13 shows an example of the IR images for all the classes considered. The images are derived from the CADs of Figure 3.3 for: a) dinghy; b) motor boat; c) fishing boat; d) oil tanker; e) dinghy with people; f) fishing boat with people. The range is 1 Km and the view angle is 45° . The FOV and the resolution of the camera are the same of Figure 3.12. Also in the IR case, the images are not affected by noise.



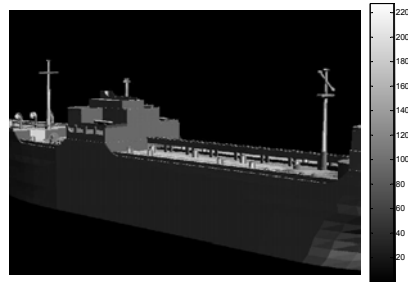
a)



b)



c)



d)

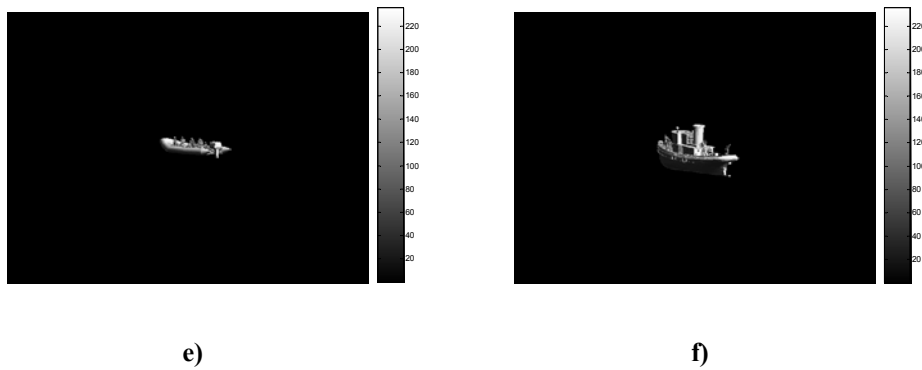


Figure 3.13 – Example of simulated IR images for all the classes considered

3.3.3 The spotlight SAR database

The simulation of the EM images of the spotlight SAR is based on the software “Target MOdelling for Radar Application” (TAMORA). The following assumptions are made:

- The images do not contain background, but only the contribution of the ship geometry is considered.
- The image simulation does not consider the environmental conditions, such as the sea clutter, the multipath, or the atmosphere effect.
- The images do not contain any source of noise.

Also in this case, as for the IR database construction, it is not possible to handle the target view angle with continuity, since this parameter is manually set in the TAMORA software. For this reason we perform an analogous quantization of the SAR database, by considering only the five view angles of Figure 3.9a. The association between the incoming target and the simulated image is the same of Figure 3.10. The construction of the simulated EM images is based on the following steps:

1. The prediction of the echoes coming from the target is performed, by using the geometrical features contained in the 3D CAD. During this operation a

sequence of 81 transmitted frequencies is considered, starting from a frequency value equal to 9400 MHz and increasing it with a step of 5 MHz. In addition, the target is rotated with respect to a fixed view angle (i.e. one of the five view angles considered) by using a rotation angle equal to 0.03° for all the classes, except that for the oil tanker, for which the rotation angle is 0.006° . The rotation of the target is performed in order to simulate the cross range resolution of the spotlight SAR. Then the TAMORA software is used to construct a two-dimensional (2D) complex hologram for each target. In particular, 20 complex holograms are evaluated for the four classes and for the 5 view angles considered.

2. The simulated image of the ship is then reconstructed by means of a 2D Inverse Discrete Fast Fourier Transform (IDFFT) of the hologram obtained during the previous step, performed on the space and frequency domains.

The result of the 2D IDFFT is represented by matrices whose elements are intensities proportional to the RCS of the target. After that the IDFFT is performed these matrices are scaled such that the total RCS of each simulated image is equal to the predicted RCS of the target, which is a function of the frequency and of the view angle. The scale factor F_s is evaluated by assuming that the sum of all the intensity contributions in the image is equal to the target predicted RCS:

$$F_s \sum_{i=1}^{N_{pixels}=N_H \times N_V} p_{lin}(i) = RCS_{predicted} \quad (3.16)$$

$$F_s = \frac{RCS_{predicted}}{\sum_{i=1}^{N_{pixels}=N_H \times N_V} p_{lin}(i)} \quad (3.17)$$

where $p_{lin}(i)$ is the linear value of the pixel square intensity, $RCS_{predicted}$ is the predicted RCS of the target, evaluated during the EM simulations performed with

the software TAMORA, and reported in Table 3.1 for each class and for each view angle. The number of pixels, N_{pixels} , is reported in Table 3.2 for each class.

Table 3.1 – Predicted RCS of the targets

	View 1	View 2	View 3	View 4	View 5
Dinghy	15 dBm ²	5 dBm ²	-10 dBm ²	6 dBm ²	2 dBm ²
Dinghy (with people on board)	15 dBm ²	5 dBm ²	-8 dBm ²	6 dBm ²	-8 dBm ²
Motor boat	15 dBm ²	8 dBm ²	12 dBm ²	6 dBm ²	10 dBm ²
Fishing boat	20 dBm ²	0 dBm ²	20 dBm ²	5 dBm ²	8 dBm ²
Fishing boat (with people on board)	20 dBm ²	1 dBm ²	22 dBm ²	6 dBm ²	5 dBm ²
Oil tanker	32 dBm ²	8 dBm ²	28 dBm ²	12 dBm ²	30 dBm ²

Table 3.2 – Dimensions of the simulated EM images

	Number of pixels (H) x (V)	Size of the pixel [m²]
Dinghy	80 x 80	0.25
Motor boat	100 x 100	0.25
Fishing boat	80 x 80	0.25
Oil tanker	300 x 300	0.4

The operations performed for the generation of the EM simulated images are summarized in Figure 3.14.

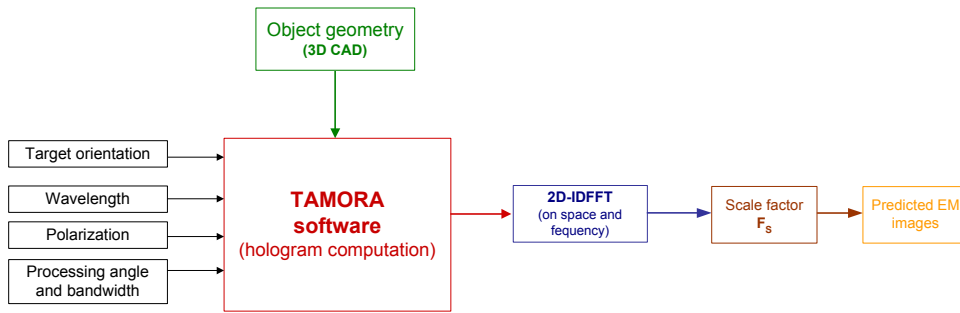


Figure 3.14 – Construction of the spotlight SAR database

As concerns the dependence of the images on the distance between the target and the sensor, for the spotlight SAR we have assumed that the radar resolution is invariant with respect to the range, which is true when the relative motion between the target and the platform is perfectly compensated. This can be proved separately for the SAR and for the spotlight SAR, whose geometry is equivalent to the inverse SAR (ISAR).

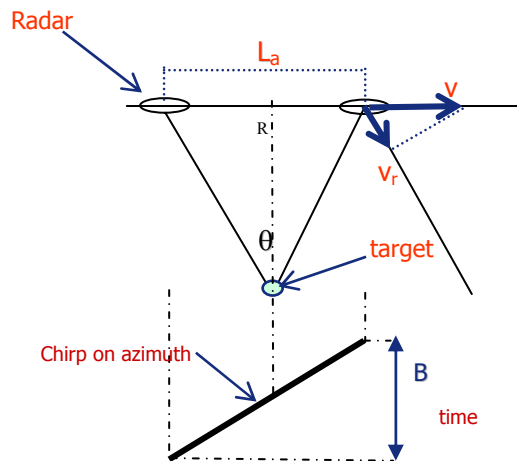


Figure 3.15 – SAR geometry

In Figure 3.15, v is the speed of the sensor platform, θ is the width of the beam on the azimuth and B is the band of the chirp along the azimuth. From the geometry represented in the figure, the band of the chirp can be computed as follows:

$$v_r = v \sin\left(\frac{\theta}{2}\right) \quad (3.18)$$

$$f_{\text{DMAX}} = \frac{2v_r}{\lambda} = \frac{2v}{\lambda} \sin\left(\frac{\theta}{2}\right) \quad (3.19)$$

and

$$B = 2f_{\text{DMAX}} = 4 \frac{v}{\lambda} \sin\left(\frac{\theta}{2}\right) \quad (3.20)$$

The time resolution is:

$$r_t = \frac{1}{B} \cong \frac{\lambda}{2v\theta} \quad (3.21)$$

and the spatial resolution is (for the spotlight SAR):

$$r_x = r_t v = \frac{\lambda}{2\theta} \quad (3.22)$$

Then the spatial resolution depends on the wavelength λ and on the beamwidth θ . In particular, it does not depend on the distance: if the distance changes, the band of the chirp is the same and thus the time resolution and the spatial resolution also remain the same. In the case of the spotlight SAR, such as in the case of the ISAR [58], the cross range resolution is given by Equation (3.22), where θ is the processing angle, i.e. the rotation angle of the target during the dwell time. In fact, after the compensation of the translational motion, both the geometries of the spotlight SAR and the ISAR can be considered as the rotation around a fixed point. If ω indicates the rotation speed of the target, the radial speed of a point whose cross range coordinate is x can be evaluated as:

$$v_r = \omega x \quad (3.23)$$

and by considering the differential with respect to x :

$$dv_r = \omega dx \quad (3.24)$$

By multiplying both sides of Equation (3.24) by the observation time T_0 , we obtain:

$$T_0 \cdot dv_r = T_0 \cdot \omega \cdot dx = \theta \cdot dx \quad (3.25)$$

since $\omega T_0 = \theta$ is the processing angle of the target. From Equation (3.19), we have:

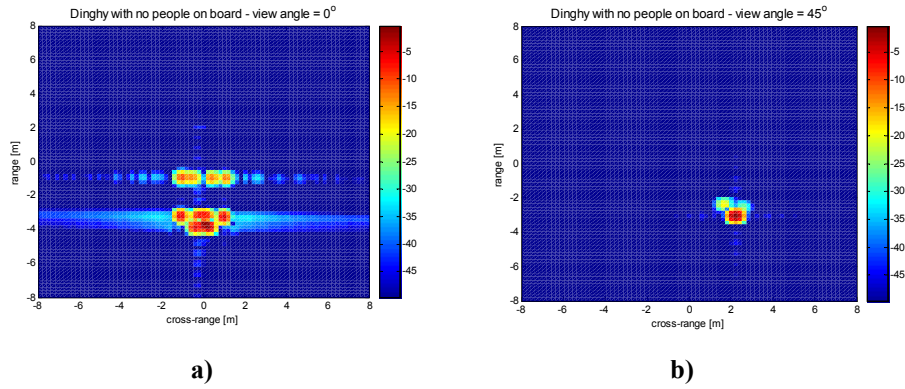
$$dv_r = \frac{\lambda}{2} df_D \quad (3.26)$$

where df_D is the variation of the Doppler frequency. By replacing Equation (3.26) into Equation (3.25), we obtain:

$$\theta \cdot dx = T_0 \cdot dv_r = \lambda \frac{T_0 df_D}{2} \quad (3.27)$$

And considering that the product $T_0 df_D$ is equal to 1, we derive that the cross range resolution is equal to that of Equation (3.22).

As an example, Figure 3.16 shows the EM simulated images obtained according to the procedure described in Figure 3.14, for the dinghy. Also in this case the original CAD is that of Figure 3.3 a. The view angles are: a) 0° ; b) 45° ; c) 90° ; d) 135° ; e) 180° .



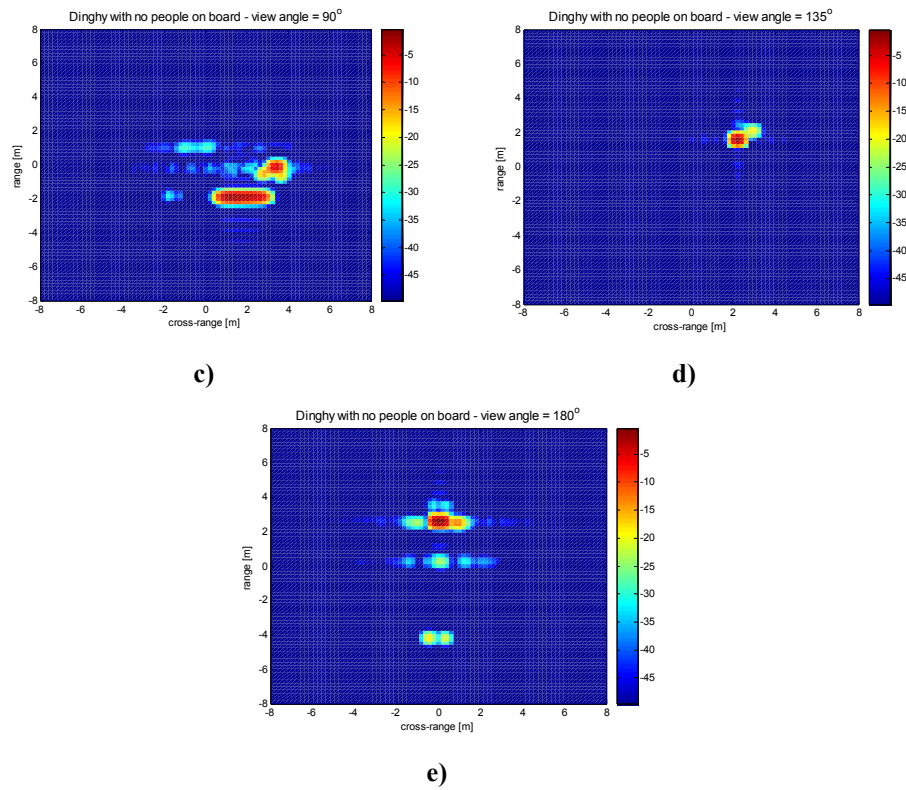


Figure 3.16 – Example of simulated images for the spotlight SAR⁷

3.4 The fusion of the decision on the target class

After that the decision on the target class is made by each imaging sensor, according to the algorithm described in Section 3.2, the fusion of the decisions is performed. The information on the class is generally not very reliable for long distance from the air platform, when only the spotlight SAR is active, and it becomes more reliable when the target is closer to the platform, when also the video camera and IR camera are active. The purpose of the fusion operation is to process the outputs of the three imaging sensors in order to obtain an accurate and reliable estimate of the target class. As stated before, the performance of each

⁷ Images by courtesy of Dr. U. D’Elia and Dr. M. G. Del Gaudio, MBDA, Rome, Italy.

imaging sensor during the classification process is modelled by means of its confusion matrix $\mathbf{C}^{(k)} = [\mathbf{c}_{ij}^{(k)}]$. The CMs of the three imaging sensors considered in this work are $\mathbf{C}^{(1)} = [\mathbf{c}_{ij}^{(1)}]$ for the video camera, $\mathbf{C}^{(2)} = [\mathbf{c}_{ij}^{(2)}]$ for the IR camera and $\mathbf{C}^{(3)} = [\mathbf{c}_{ij}^{(3)}]$ for the spotlight SAR. According to the definition given in Equation (3.1), the generic entry of the matrix $\mathbf{C}^{(1)}$ is the following probability:

$$\mathbf{c}_{ij}^{(1)} = \Pr\{\text{video camera decides for } H_j \text{ when } H_i \text{ is true}\} = \Pr\{d_1 = j | H_i\} \quad (3.28)$$

Similarly, the entries of matrices $\mathbf{C}^{(2)}$ and $\mathbf{C}^{(3)}$ are defined as:

$$\mathbf{c}_{ij}^{(2)} = \Pr\{\text{IR camera decides for } H_j \text{ when } H_i \text{ is true}\} = \Pr\{d_2 = j | H_i\} \quad (3.29)$$

and:

$$\mathbf{c}_{ij}^{(3)} = \Pr\{\text{spotlight SAR decides for } H_j \text{ when } H_i \text{ is true}\} = \Pr\{d_3 = j | H_i\} \quad (3.30)$$

Note that is:

- $\{d_1 = j\} \equiv \{\text{Video camera decides for } H_j\}$
- $\{d_2 = j\} \equiv \{\text{IR camera decides for } H_j\}$
- $\{d_3 = j\} \equiv \{\text{Spotlight SAR decides for } H_j\}$

Thus the conditional correct classification probabilities are $\mathbf{c}_{ii}^{(1)} = \Pr\{d_1 = i | H_i\}$ for the video camera; $\mathbf{c}_{ii}^{(2)} = \Pr\{d_2 = i | H_i\}$ for the IR camera and $\mathbf{c}_{ii}^{(3)} = \Pr\{d_3 = i | H_i\}$ for the spotlight SAR. The fusion process is described in Figure 3.17. For each imaging sensor, the CM matrix is analytically computed as described in Appendix A and its entries are used to make a local decision on the class, i.e. d_1 for the video camera, d_2 for the IR camera, and d_3 for the spotlight SAR. Then these local decisions are combined using an appropriate decision rule.

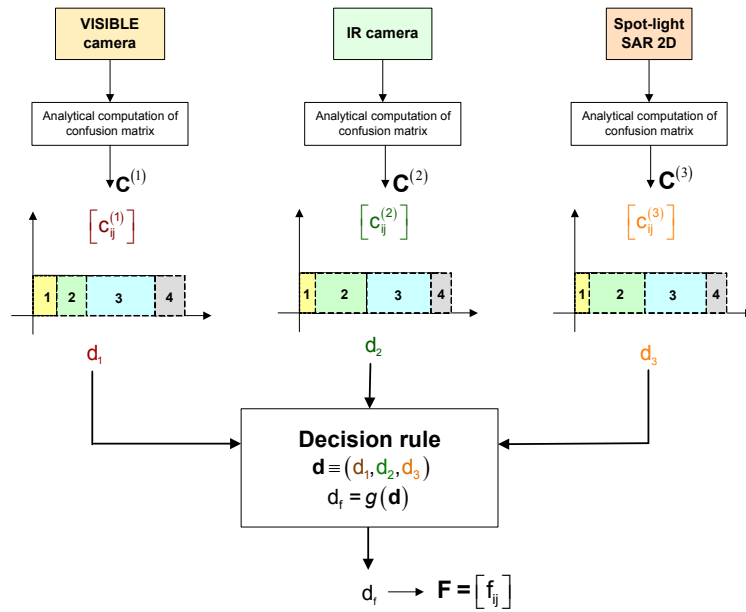


Figure 3.17 – Fusion of the decisions on target class

In our analysis, we have assumed that the decisions coming from the three sensors are aligned in time, i.e. a delay in the fusion process is considered in order to take into account for the sampling rate of the slower sensor. The observed data is a three-dimensional vector $\mathbf{d} = (d_1, d_2, d_3)$ whose elements d_k , for $k = 1, 2, 3$, are discrete random variables (r.v.) that take values in the set $\mathbf{I}_S = \{1, 2, 3, \dots, M\}$, where $M = 4$ is the number of classes considered, and represent the decision on the target class coming from each imaging sensor. Let consider the set $\mathbf{I}_d = \{\mathbf{d}^{[m]}, m = 1 \dots M^K\}$, which is the set of all the observable sequences of $K = 3$ elements that can be constructed with the $M = 4$ elements of the set \mathbf{I}_S . The dimension of \mathbf{I}_d is $M^K = 4^3 = 64$. Our purpose is to map the three-dimensional vectors \mathbf{d} into a scalar value belonging to the set \mathbf{I}_S and representing the final estimated class of the target, i.e. d_f in Figure 3.17. This means to distinguish

between M possible hypotheses $\{H_1, H_2, \dots, H_M\}$. We assume that these hypotheses have the same a priori probability:

$$\Pr\{H_i\} = \frac{1}{M} \quad \text{for } i = 1, \dots, M \quad (3.31)$$

We indicate with $g(\mathbf{d})$ the fusion rule, i.e. the function that maps the observed vector \mathbf{d} into a final decision in favour of one of the M hypotheses:

$$d_f = g(\mathbf{d}) \quad (3.32)$$

where $\{d_f = j\}$ represents the event $\{\text{we decide in favour of } H_j\}$. This approach, based on the fusion of the decisions made by each sensor through the CM entries, allows us to manage the combination of information coming from very dissimilar imaging sensors and to compensate for the sensor parameter differences, such as the fields of view, the resolutions, and the noise features. The overall performance of the fusion process can be expressed by means of a “*fused*” confusion matrix, i.e. the matrix pertinent to the final decision on the target class d_f . Two fusion strategies have been considered in this work: one based on the majority voting decision rule and the other based on the maximum likelihood decision rule.

A. Majority voting decision rule (MV)

The majority voting decision rule consists in choosing for target class that occurs more times in the observed sequence (d_1, d_2, d_3) . In the case of the three-dimensional sequences considered here, the MV rule can be analytically expressed as follows:

$$d_f = q \rightarrow q : \{L_q(d_1, d_2, d_3) \geq 2\} \quad (3.33)$$

where $L_q(d_1, d_2, d_3)$ is the number of times the value q appears in the sequence $\mathbf{d} = (d_1, d_2, d_3)$, i.e. the number of occurrences of the q -th class in the observed sequence. When $L_q(d_1, d_2, d_3) = 1$, i.e. $\{(d_1 \neq d_2) \cap (d_1 \neq d_3) \cap (d_2 \neq d_3)\}$, the MV

rule is not applicable. In these cases, we choose the class for which has decided the “*more reliable sensor*”, i.e. the sensor for which the conditional correct classification probability, given by the diagonal elements of the CM, is higher. For instance, if the sequence $\mathbf{d}^{[8]} = (1, 2, 4)$ is observed, the final class will be $d_f = q$ for which $\Pr\{d_k = q | H_q\}$ is maximum, for $k=1, 2, 3$. In this example we have: $d_1 = 1$, $d_2 = 2$, and $d_3 = 4$; then we consider the diagonal elements $c_{11}^{(1)}$ for the video camera, $c_{22}^{(2)}$ for the IR camera and $c_{44}^{(3)}$ for the spotlight SAR and we decide:

$$d_f = \begin{cases} 1 & \text{if } \max(c_{11}^{(1)}, c_{22}^{(2)}, c_{44}^{(3)}) = c_{11}^{(1)} \\ 2 & \text{if } \max(c_{11}^{(1)}, c_{22}^{(2)}, c_{44}^{(3)}) = c_{22}^{(2)} \\ 4 & \text{if } \max(c_{11}^{(1)}, c_{22}^{(2)}, c_{44}^{(3)}) = c_{44}^{(3)} \end{cases} \quad (3.34)$$

The observable three-dimensional vectors $\mathbf{d}^{[m]}$ are all the possible sequences of $K=3$ objects (d_1, d_2, d_3) that can be made with the $M=4$ elements of the previously defined set \mathbf{I}_d . Table 3.3 shows all the 64 observable sequences.

Table 3.3 – Observable sequences

111	121	131	141
112	122	132	142
113	123	133	143
114	124	134	144
211	221	231	241
212	222	232	242
213	223	233	243
214	224	234	244
311	321	331	341
312	322	332	342
313	323	333	343
314	324	334	344
411	421	431	441
412	422	432	442
413	423	433	443
414	424	434	444

According to the decision rule described by (3.33), we can derive a fusion table for MV decision rule, as shown in Table 3.4.

Table 3.4 – Fusion table for MV rule

	d	# occurrences of 1	# occurrences of 2	# occurrences of 3	# occurrences of 4	d_f
d^[1]	111	3	0	0	0	1
d^[2]	112	2	1	0	0	1
d^[3]	113	2	0	1	0	1
d^[4]	114	2	0	0	1	1
⋮	⋮	⋮	⋮	⋮	⋮	⋮
d^[8]	124	1	1	0	1	(*)
⋮	⋮	⋮	⋮	⋮	⋮	⋮
d^[64]	444	0	0	0	3	4

The last column of the table contains the final decision on the target class made according to the MV rule. Using this table, we can evaluate the fused matrix **F**, after the fusion of the information on the target class:

$$\mathbf{F} = [f_{ij}] \quad (3.35)$$

The entries of this matrix are:

$$f_{ij} = \Pr\{d_f = j | H_i\} = \sum_{m \in D_j} \Pr(\mathbf{d} = \mathbf{d}^{[m]} | H_i) \quad (3.36)$$

where D_j is the decision zone of H_j , i.e. the set of m 's for which we decide in favour of H_j . It is defined as:

$$D_j = \{m : g(\mathbf{d}^{[m]}) = j\} \quad (3.37)$$

* Choose class coming from the more reliable sensor.

The elements of the sum $\Pr(\mathbf{d} = \mathbf{d}^{[m]} | H_i)$ can be computed as:

$$\Pr(\mathbf{d} = \mathbf{d}^{[m]} | H_i) = \Pr(d_1 = d_1^{[m]} | H_i) \cdot \Pr(d_2 = d_2^{[m]} | H_i) \cdot \Pr(d_3 = d_3^{[m]} | H_i) \quad (3.38)$$

that represents the product of the entries of the CMs of the three sensors:

$$\Pr(\mathbf{d} | H_i) = \Pr\{d_1 = j, d_2 = k, d_3 = n | H_i\} = c_{ij}^{(1)} \cdot c_{ik}^{(2)} \cdot c_{in}^{(3)} \quad (3.39)$$

with $j, k, n, i = 1, \dots, 4$.

B. Maximum likelihood decision rule (ML)

In many applications, the most common approach utilized to distinguish between two or more hypotheses is based on the *Bayes rule*, which assumes a prior knowledge of the probabilities of the hypotheses under test. The Bayes rule is based on the minimization of the expectation of the cost function C_{ij} , defined as the cost assigned to the decision to choose in favour of H_j when H_i is true [38]. The analytical formulation of the Bayesian approach applied to the decision on the target class is:

$$d_f = q: q = \arg \max_j \{ \Pr(H_j | \mathbf{d}) \} \quad \text{for } j = 1, \dots, M \quad (3.40)$$

The rule expressed by (3.40) is called *M-ary maximum a posteriori probability* (MAP) decision rule, since $\Pr(H_j | \mathbf{d})$ is the probability of the hypothesis H_j after the observation of the data \mathbf{d} , thus it is an a posteriori probability. As stated before, this decision rule assumes prior knowledge of the likelihoods of the hypotheses. According to the Bayes theorem, the a posteriori probability $\Pr(H_j | \mathbf{d})$ can be expressed as:

$$\Pr(H_j | \mathbf{d}) = \frac{p(\mathbf{d} | H_j) \cdot \Pr(H_j)}{p(\mathbf{d})} \quad (3.41)$$

where $\Pr(H_j)$ is the prior probability of the j -th hypothesis and $p(\mathbf{d})$ is the probability mass function (pmf) of the discrete data \mathbf{d} . Since $p(\mathbf{d})$ is a positive

function that does not depend on the hypothesis, it does not affect the maximization of $\Pr(H_j | \mathbf{d})$. When the assumption of equal prior probability of the hypotheses can be done, the decision rule of (3.40) can be expressed as:

$$\mathbf{d}_f = q : q = \arg \max_j p(\mathbf{d} | H_j) \text{ for } j, q = 1, \dots, M \text{ and } j \neq q \quad (3.42)$$

This is called *M-ary maximum likelihood* (ML) decision rule, since $p(\mathbf{d} | H_j)$ is the likelihood function of the j -th hypothesis. Note that the decision rule (3.42) provides the minimum error probability only when the prior probabilities $\Pr(H_q)$ for $q = 1, \dots, M$ are all equal.

According to the ML rule, to decide the final class of the target using the observed data sequences \mathbf{d} , we have to choose for the hypothesis H_q that maximizes the following probability mass functions:

$$p(\mathbf{d} = \mathbf{d}^{[m]} | H_q), \text{ for } m = 1, \dots, M^K \text{ and for } q = 1, \dots, M \quad (3.43)$$

where:

$$p(\mathbf{d} = \mathbf{d}^{[m]} | H_q) = p(d_1 = d_1^{[m]} | H_q) \cdot p(d_2 = d_2^{[m]} | H_q) \cdot p(d_3 = d_3^{[m]} | H_q) \quad (3.44)$$

The elements of the product in (3.44) are the entries of the confusion matrices $\mathbf{C}^{(1)}$, $\mathbf{C}^{(2)}$, and $\mathbf{C}^{(3)}$, respectively. The joint conditional probability mass function of \mathbf{d} can be expressed as follows:

$$p(\mathbf{d} | H_q) = \Pr\{d_1 = i, d_2 = j, d_3 = n | H_q\} = c_{qi}^{(1)} \cdot c_{qj}^{(2)} \cdot c_{qn}^{(3)} \quad (3.45)$$

This is shown in Figure 3.18 for the sequence $\mathbf{d}^{[8]} = (1, 2, 4)$.

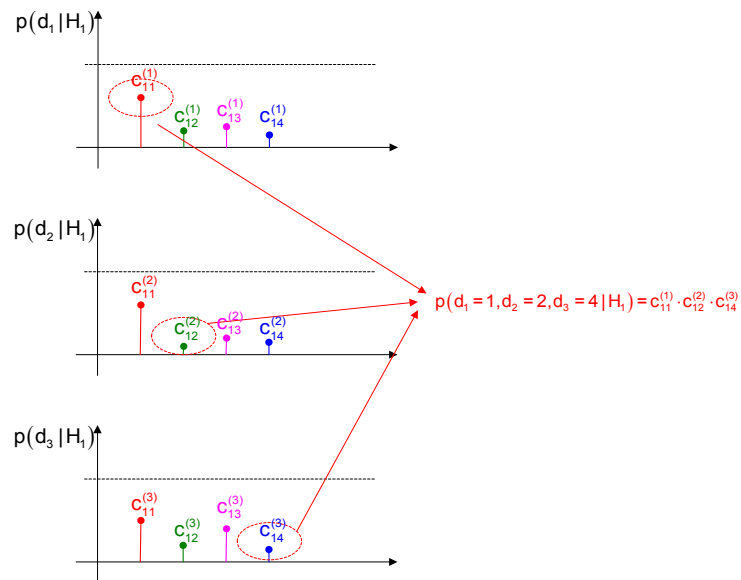


Figure 3.18 – Example of pmf for the sequence $d^{|81|}=(1,2,4)$ when H_1 is true

According to the ML decision rule describe above, we can derive a fusion table for all the observable sequences, as shown in Table 3.5. The last column of the table contains the final decision on the target class made according to (3.42). Similarly to the case of the MV rule, from this table we can obtain the fused confusion matrix $\mathbf{F} = [f_{ij}]$, by using Equations (3.36) and (3.37).

Table 3.5 – Fusion table for ML rule

	d	$p(\mathbf{d} H_1)$	$p(\mathbf{d} H_2)$	$p(\mathbf{d} H_3)$	$p(\mathbf{d} H_4)$	d_f
$\mathbf{d}^{[1]}$	[111]	$c_{11}^{(1)} \cdot c_{11}^{(2)} \cdot c_{11}^{(3)}$	$c_{21}^{(1)} \cdot c_{21}^{(2)} \cdot c_{21}^{(3)}$	$c_{31}^{(1)} \cdot c_{31}^{(2)} \cdot c_{31}^{(3)}$	$c_{41}^{(1)} \cdot c_{41}^{(2)} \cdot c_{41}^{(3)}$	1
$\mathbf{d}^{[2]}$	[112]	$c_{11}^{(1)} \cdot c_{11}^{(2)} \cdot c_{12}^{(3)}$	$c_{21}^{(1)} \cdot c_{21}^{(2)} \cdot c_{22}^{(3)}$	$c_{31}^{(1)} \cdot c_{31}^{(2)} \cdot c_{32}^{(3)}$	$c_{41}^{(1)} \cdot c_{41}^{(2)} \cdot c_{42}^{(3)}$	1
$\mathbf{d}^{[3]}$	[113]	$c_{11}^{(1)} \cdot c_{11}^{(2)} \cdot c_{13}^{(3)}$	$c_{21}^{(1)} \cdot c_{21}^{(2)} \cdot c_{23}^{(3)}$	$c_{31}^{(1)} \cdot c_{31}^{(2)} \cdot c_{33}^{(3)}$	$c_{41}^{(1)} \cdot c_{41}^{(2)} \cdot c_{43}^{(3)}$	1
$\mathbf{d}^{[5]}$	\vdots	\vdots	\vdots	\vdots	\vdots	\vdots
\vdots	\vdots	\vdots	\vdots	\vdots	\vdots	\vdots
$\mathbf{d}^{[8]}$	[124]	$c_{11}^{(1)} \cdot c_{12}^{(2)} \cdot c_{14}^{(3)}$	$c_{21}^{(1)} \cdot c_{22}^{(2)} \cdot c_{24}^{(3)}$	$c_{31}^{(1)} \cdot c_{32}^{(2)} \cdot c_{34}^{(3)}$	$c_{41}^{(1)} \cdot c_{42}^{(2)} \cdot c_{44}^{(3)}$	\vdots
\vdots	\vdots	\vdots	\vdots	\vdots	\vdots	\vdots
$\mathbf{d}^{[64]}$	[444]	$c_{14}^{(1)} \cdot c_{14}^{(2)} \cdot c_{14}^{(3)}$	$c_{24}^{(1)} \cdot c_{24}^{(2)} \cdot c_{24}^{(3)}$	$c_{34}^{(1)} \cdot c_{34}^{(2)} \cdot c_{34}^{(3)}$	$c_{44}^{(1)} \cdot c_{44}^{(2)} \cdot c_{44}^{(3)}$	4

3.5 Performance of the fusion process

The performance of the decision rule can be expressed in terms of closeness of the fused confusion matrix \mathbf{F} to the identity matrix, which represents the ideal case. In fact, an ideal classification process is characterized by probabilities of error (off-diagonal elements of the CM) equal to zero and by probabilities of correct classification (diagonal elements) equal to one:

$$\mathbf{I}_M = \begin{bmatrix} 1 & & & \\ & 1 & & 0 \\ & & \ddots & \\ & 0 & & 1 \\ & & & & 1 \end{bmatrix} \quad (3.46)$$

where the dimension M of the matrix is the number of hypotheses in the classification process ($M = 4$ in the case considered here). The conditional correct classification probabilities for the fused matrix \mathbf{F} can be expressed from its diagonal elements, similarly to those of the CMs of the three sensors, $\mathbf{C}^{(1)}$, $\mathbf{C}^{(2)}$ and $\mathbf{C}^{(3)}$:

$$P_{CC|H_i} = \Pr\{\text{correct classification} \mid H_i\} = f_{ii} \quad (3.47)$$

The probability of correct classification is then:

$$P_{CC} = \sum_{i=1}^M P_{CC|H_i} \cdot \Pr\{H_i\} = \frac{1}{M} \cdot \sum_{i=1}^M P_{CC|H_i} \quad (3.48)$$

where in the last part of the equality, we have used the assumption (3.31) of equal a priori probability for the hypotheses. By replacing equation (3.47) in (3.48), we obtain:

$$P_{CC} = \frac{1}{M} \cdot \sum_{i=1}^M P_{CC|H_i} = \frac{1}{M} \cdot \sum_{i=1}^M f_{ii} = \frac{\text{tr}(\mathbf{F})}{M} \quad (3.49)$$

where we have considered that the sum of the diagonal elements represents the trace of matrix \mathbf{F} . To evaluate the performance of the fused matrix \mathbf{F} , we consider the probability of correct classification expressed in (3.49) and we select as the best performing matrix the one for which the probability of correct classification, and then the ratio $\text{tr}(\mathbf{F})/M$, is the nearest to 1, i.e. its maximum value. This occurs when the trace of matrix \mathbf{F} at the numerator is close to M , which is the trace of the identity matrix. From this point of view the correct classification probability is an index of the closeness of matrix \mathbf{F} to the identity \mathbf{I}_M .

The same performance criterion can also be explained as follows. To evaluate the closeness of the fused matrix \mathbf{F} to the identity, we can define the following quality factor:

$$Q = 1 - \frac{\text{tr}\{\mathbf{I}_M - \mathbf{F}\}}{\text{tr}(\mathbf{I}_M)} = 1 - \frac{\text{tr}(\mathbf{I}_M) - \text{tr}(\mathbf{F})}{\text{tr}(\mathbf{I}_M)} = \frac{\text{tr}(\mathbf{F})}{\text{tr}(\mathbf{I}_M)} = \frac{\text{tr}(\mathbf{F})}{M} \quad (3.50)$$

The parameter Q is included in the interval $[0,1]$ and it is close to 1 when the fused matrix \mathbf{F} is very close to identity and it is close to 0 when \mathbf{F} is significantly different from identity. As we can see by comparing (3.49) and (3.50), the parameter Q is equivalent to the probability of correct classification. Thus, the best fused matrix is the one for which this quality factor is nearest to 1, that is also the maximum value of the correct classification probability. The difference $\text{tr}(\mathbf{I}_M) - \text{tr}(\mathbf{F})$ at the numerator of the first side of Equation (3.50) represents the sum of the off-diagonal elements of \mathbf{F} :

$$\text{tr}(\mathbf{I}_M) - \text{tr}(\mathbf{F}) = M - \text{tr}(\mathbf{F}) = \sum_{\substack{j=1 \\ j \neq i}}^M \sum_{i=1}^M f_{ij} \quad (3.51)$$

This property is due to the fact that the sum of all the elements of the matrix \mathbf{F} is equal to M , as can be demonstrated by using the definition given in (3.36):

$$\sum_{j=1}^M \sum_{i=1}^M f_{ij} = \sum_{j=1}^M \sum_{i=1}^M \Pr\{d_f = j | H_i\} \quad (3.52)$$

By setting the value of j in the previous expression and considering only the sum $\sum_{i=1}^M \Pr\{d_f = j | H_i\}$, i.e. the sum over the columns of \mathbf{F} , from the total probability theorem we obtain:

$$\Pr\{d_f = j\} = \sum_{i=1}^M \Pr\{d_f = j | H_i\} \Pr\{H_i\} \quad (3.53)$$

and by using the assumption of equal probability of the hypotheses Equation (3.53) can be written as:

$$\Pr\{d_f = j\} = \sum_{i=1}^M \Pr\{d_f = j | H_i\} \Pr\{H_i\} = \frac{1}{M} \sum_{i=1}^M \Pr\{d_f = j | H_i\} \quad (3.54)$$

and the sum $\sum_{i=1}^M \Pr\{d_f = j | H_i\}$ becomes:

$$\sum_{i=1}^M \Pr\{d_f = j | H_i\} = M \cdot \Pr\{d_f = j\} \quad (3.55)$$

Then the sum of all the elements of matrix \mathbf{F} defined in (3.52) can be expressed as:

$$\begin{aligned}
\sum_{j=1}^M \sum_{i=1}^M f_{ij} &= \sum_{j=1}^M \left[\sum_{i=1}^M \Pr\{d_f = j | H_i\} \right] = \sum_{j=1}^M M \cdot \Pr\{d_f = j\} = \\
&= M \cdot \sum_{j=1}^M \Pr\{d_f = j\} = M
\end{aligned} \tag{3.56}$$

Since the events $\{d_f = j\}$ for $j=1, \dots, M$ represent the set of all possible decision events, it is:

$$\sum_{j=1}^M \Pr\{d_f = j\} = 1 \tag{3.57}$$

Using these performance criteria, we have found that the best fusion rule between the two described above is the one based on the ML decision rule.

3.5.1 Numerical example

In this section we provide a numerical example concerning the classification process performed by the three imaging sensors, for the four naval targets that we have described in the scenario: dinghy, motor boat, fishing boat, and oil tanker. The databases of simulated images required for the computation of the CM have been constructed as described in Section 3.3 for three imaging sensors. A distance between the target and the sensor equal to 10 Km and a view angle equal to 180° have been considered. The SNR over the single pixel of the reference images has been evaluated by considering the noise features of each imaging sensor, as described in Section 2.3.4 for the video camera, in Section 2.3.5 for the IR camera, and in Section 2.3.3.1 for the spotlight SAR. The effect of the atmosphere has been taken into account by considering the extinction coefficient of Equation (2.23) for the video camera, the coefficient of Table 2.9 for the IR camera, and the factor L_α of Equation (2.11) for the spotlight SAR. In all the cases, the sea state is assumed to be equal to 0. The simulated images of the three sensors are referred to the same geometrical and environmental conditions, but the SNR value can be different from one sensor to the other, due to the different nature of the sensors.

The resulting CMs for the video camera, the IR camera and the spotlight SAR are reported, respectively, in Table 3.6-Table 3.8.

Table 3.6 – CM of the video camera, $C^{(1)}$

output → input ↓	<i>Dinghy</i>	<i>Motor boat</i>	<i>Fishing boat</i>	<i>Oil tanker</i>
<i>Dinghy</i>	0.9209	0.0648	0.0142	0.0000
<i>Motor boat</i>	0.0648	0.8490	0.0862	0.0000
<i>Fishing boat</i>	0.0142	0.0862	0.8996	0.0000
<i>Oil tanker</i>	0.0000	0.0000	0.0000	1.0000

Table 3.7 – CM of the IR camera, $C^{(2)}$

output → input ↓	<i>Dinghy</i>	<i>Motor boat</i>	<i>Fishing boat</i>	<i>Oil tanker</i>
<i>Dinghy</i>	0.8076	0.0289	0.1635	0.0000
<i>Motor boat</i>	0.0289	0.9529	0.0182	0.0000
<i>Fishing boat</i>	0.1635	0.0182	0.8182	0.0000
<i>Oil tanker</i>	0.0000	0.0000	0.0000	1.0000

Table 3.8 – CM of the spotlight SAR, $C^{(3)}$

output → input ↓	<i>Dinghy</i>	<i>Motor boat</i>	<i>Fishing boat</i>	<i>Oil tanker</i>
<i>Dinghy</i>	0.5995	0.2306	0.1698	0.0000
<i>Motor boat</i>	0.2306	0.7167	0.0526	0.0000
<i>Fishing boat</i>	0.1698	0.0526	0.7775	0.0000
<i>Oil tanker</i>	0.0000	0.0000	0.0000	1.0000

These tables show that the less reliable sensor, as concerns the classification of the four targets considered, is the spotlight SAR. The correct classification

probability conditioned to *Class 4* (oil tanker) is always $P_{C|H_4} = 1$, due to the fact that the size of this class of target (100 m) is significantly different from the size of the other targets considered. The fused CMs obtained by the majority voting rule, F_{MV} , and by the maximum likelihood rule, F_{ML} , are shown in Table 3.9 and in Table 3.10.

Table 3.9 – Fused CM by using the MV rule, F_{MV}

output → input ↓	<i>Dinghy</i>	<i>Motor boat</i>	<i>Fishing boat</i>	<i>Oil tanker</i>
<i>Dinghy</i>	0.9455	0.0226	0.0317	0.0000
<i>Motor boat</i>	0.0523	0.9407	0.0069	0.0000
<i>Fishing boat</i>	0.0660	0.0069	0.9269	0.0000
<i>Oil tanker</i>	0.0000	0.0000	0.0000	1.0000

Table 3.10 – Fused CM by using the ML rule, F_{ML}

output → input ↓	<i>Dinghy</i>	<i>Motor boat</i>	<i>Fishing boat</i>	<i>Oil tanker</i>
<i>Dinghy</i>	0.9460	0.0229	0.0309	0.0000
<i>Motor boat</i>	0.0262	0.9597	0.0140	0.0000
<i>Fishing boat</i>	0.0166	0.0097	0.9735	0.0000
<i>Oil tanker</i>	0.0000	0.0000	0.0000	1.0000

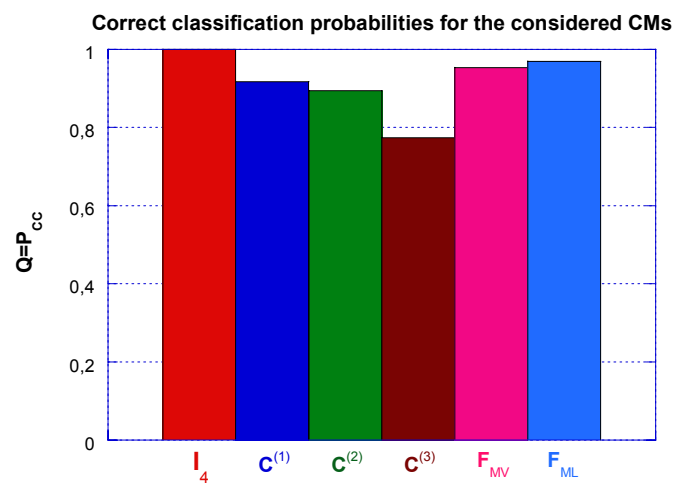
From these tables we can observe that the best performing fused matrix, i.e. the nearest to I_4 , is the one obtained by the ML decision rule, F_{ML} .

The goodness of the CMs in Table 3.6 - Table 3.10 is expressed by means of the probability of correct classification P_{CC} that is equal to the quality factor Q defined in (3.50). As shown in Table 3.11, the value of $P_{CC} \equiv Q$ nearest to 1 is that corresponding to the fused matrix F_{ML} .

Table 3.11 – Performance of the CMs

	A	B	C	F_{MV}	F_{ML}
$Q \equiv P_{cc}$	0.9174	0.8947	0.7734	0.9533	0.9698

The fusion process can provide an improvement in the correct classification probability equal to 3.59% for the MV rule and equal to 5.24% for the ML rule, with respect to the more reliable sensor, i.e. the video camera in the numerical example considered here. The value $P_{cc} \equiv Q$ for all the CMs considered in this numerical example is also graphically shown in Figure 3.19.

**Figure 3.19 – Probability of correct classification equal to the factor Q**

Chapter 4

The Command and Control centre

4.1 Introduction

The surveillance operation performed by the integrated system is coordinated by a Command and Control (C²) centre. The targets detected, identified and classified by the multiple sensors of the system are sent to the C² centre, where the following functions are performed:

- the association and the fusion of the tracks coming from the two radars;
- the processing of the tracks, in order to evaluate the parameters required for the threat evaluation;
- the threat level evaluation of the detected targets;
- the selection of a suitable intervention on the evaluated targets;
- the allocation of a system resource in order to inspect the nature of the targets evaluated as potentially threat.

The decision making (DM) process for the evaluation of the threat level and for the selection of an intervention is composed by two steps: the Situation Assessment (SA) step, during which the threat level of the targets is assessed, and the Response Selection (RS) step, which corresponds to the selection of a suitable intervention on the previously assessed targets and to the allocation of a system resource for the target inspection. The C² centre also performs the fusion of the class information described in Section 3.4, when this is available from the imaging sensors.

4.2 Track association and fusion

As stated before, the land based radar and the airborne radar perform the detection and the tracking of the targets independently. For both the radars it is assumed that the track initialization takes place when the detection has occurred for three radar scans over a window of five scans. It is also assumed that the two radars perform the tracking with respect to the inertial geographical system centred in the point $\mathbf{O} \equiv (0;0)$ of Figure 2.2. This means that the target coordinates are detected by each radar with respect to its own reference system and then they are shifted on the geographical system, before that the tracking is performed. This is schematically represented in Figure 4.1.

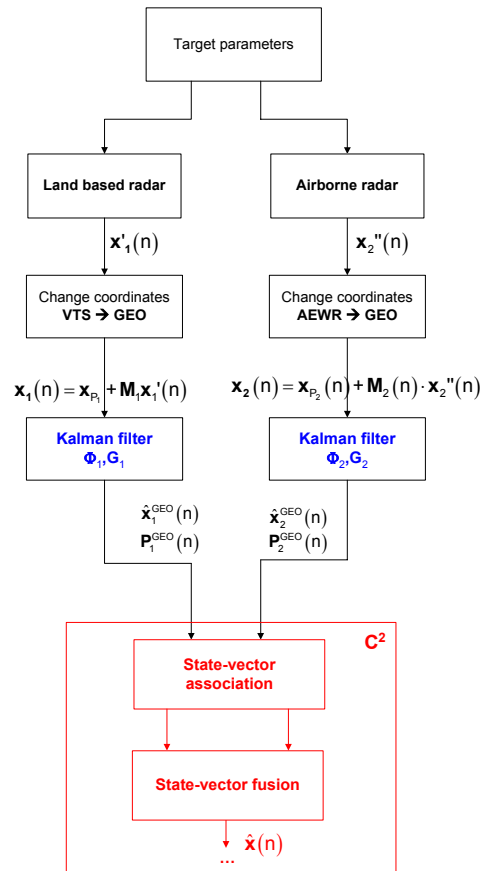


Figure 4.1 – Tracker architecture

To simplify the computational load of the simulator developed in this work, we have not implemented the tracker architecture inside the end to end simulator, but we have taken into account for the tracking process by means of analytical expressions of the measurement errors in the target coordinates. An interesting future development of this work is the inclusion of the tracking architecture inside the simulator and the study of the computational issues related to this operation. The measurement errors on the Cartesian coordinates have been computed as follows [19]:

$$\begin{aligned}\sigma_x^2 &= \sigma_\rho^2 \cos^2 \theta + \rho^2 \sigma_\theta^2 \sin^2 \theta \\ \sigma_y^2 &= \sigma_\rho^2 \sin^2 \theta + \rho^2 \sigma_\theta^2 \cos^2 \theta \\ \sigma_{xy} &= (\sigma_\rho^2 - \rho^2 \sigma_\theta^2) \sin \theta \cos \theta\end{aligned}\quad (4.1)$$

where σ_ρ and σ_θ are the standard deviations of the radar errors on the range and on the azimuth and it is assumed that the radar measurement errors are small compared with the true target coordinates.

When the initialized tracks are sent to the C^2 centre, a test for the *track to track association* is performed before that the tracks are fused together. In our analysis we have assumed that the estimation errors in the state vector from the two radars are independent [4]. The track association is performed on the bases of the estimated coordinates, i.e. the tracks are considered as belonging to the same target when the following conditions are verified:

$$\begin{aligned}\hat{X}_1 - \hat{X}_2 &< 2\sqrt{(\sigma_{x_1}^2 + \sigma_{x_2}^2)} \\ \hat{Y}_1 - \hat{Y}_2 &< 2\sqrt{(\sigma_{y_1}^2 + \sigma_{y_2}^2)}\end{aligned}\quad (4.2)$$

where (\hat{X}_1, \hat{Y}_1) and (\hat{X}_2, \hat{Y}_2) are respectively the target Cartesian coordinates estimated by the VTS radar and by the AEW radar.

After the track association test, the tracks that belong to the same target are combined in order to obtain a more accurate estimate of the state vector. The fusion

equation is obtained by weighting the track coming from each radar proportionally to its accuracy. The fusion equation under the error independence assumption is:

$$\hat{\mathbf{x}} = \mathbf{P}^2 (\mathbf{P}^1 + \mathbf{P}^2)^{-1} \hat{\mathbf{x}}^1 + \mathbf{P}^1 (\mathbf{P}^1 + \mathbf{P}^2)^{-1} \hat{\mathbf{x}}^2 \quad (4.3)$$

where \mathbf{P}^1 and \mathbf{P}^2 are the covariance matrices of the estimation errors respectively for the land based radar and for the airborne radar, $\hat{\mathbf{x}}^1$ and $\hat{\mathbf{x}}^2$ are the estimated state vectors from the two radars, and $\hat{\mathbf{x}}$ is the final state vector after the fusion process. The corresponding fusion equation for the covariance matrix is:

$$\mathbf{P} = \mathbf{P}^1 (\mathbf{P}^1 + \mathbf{P}^2)^{-1} \mathbf{P}^2 \quad (4.4)$$

4.3 The threat evaluation logic

When the track fusion has been performed, the C^2 centre processes the track parameters in order to obtain the information required to evaluate the target threat level. More specifically, the following quantities are estimated:

- the trajectory of the target;
- the coordinates (X_I, Y_I) of the estimated intersection point between the target trajectory and the bound of the off-limit region;
- the coordinates (X_C, Y_C) of the expected impact point between the target and the coast line;
- the distance between the target and the coast line;
- the direction of the target with respect to the coast;
- the target approaching time to the coast.

After the track processing, a decision making process occurs in order to evaluate the threat level of each track. The threat evaluation logic is based on a deterministic comparison between the target parameters and some allowed values, defined by tolerance thresholds that depend on the operational scenario and on the information available on the target. In the scenario considered in this work, the tolerance

thresholds are expressed in terms of the maximum allowed target speed, the minimum distance allowed between the target position and the coast line, the target direction with respect to the coast. These thresholds are described in Table 4.1.

Table 4.1 – Tolerance thresholds

Speed (V)	LOW ($V < 12$ Nodes) MEDIUM ($12 \leq V \leq 40$ Nodes) HIGH ($V > 40$ Nodes)
Distance	FAR (out of the Warning Zone) WZ (inside the Warning Zone) OFF (inside the Off – Limit region)
Direction	IN : approaching the coast OUT : otherwise

First, the target is identified as *cooperative* or *non-cooperative* on the base of the information provide by the AIS station, if available. The non-cooperative targets are further evaluated in order to define their Threat Level ($TL_i, i = 0, 1, 2$):

- TL0: neutral target;
- TL1: suspect target;
- TL2: threat target.

The evaluation logic also takes into account for the class information derived from one or more imaging sensors. This logic is shown in Tables 4.2 - 4.5 for the four classes of targets. In the tables “IN” indicates a target approaching the coast and “OUT” indicates a target whose direction is opposite to the coast. In Table 4.6 the case of class “*unknown*” has been considered, i.e. when the target class has not been detected by the imaging sensors.

Table 4.2 – Threat evaluation logic for the dinghy

Class	Speed	Distance from the coast	Direction	TL
Dinghy (1)	LOW	FAR	IN	TL ₁
	LOW	FAR	OUT	TL ₀
	LOW	WZ	IN	TL ₁
	LOW	WZ	OUT	TL ₀
	LOW	OFF	IN	TL ₂
	LOW	OFF	OUT	TL ₁
	MEDIUM	FAR	IN	TL ₁
	MEDIUM	FAR	OUT	TL ₀
	MEDIUM	WZ	IN	TL ₂
	MEDIUM	WZ	OUT	TL ₁
	MEDIUM	OFF	IN	TL ₂
	MEDIUM	OFF	OUT	TL ₁
	HIGH	FAR	IN	TL ₂
	HIGH	FAR	OUT	TL ₁
	HIGH	WZ	IN	TL ₂
	HIGH	WZ	OUT	TL ₁
	HIGH	OFF	IN	TL ₂
HIGH	OFF	OUT	TL ₂	

Table 4.3 – Threat evaluation logic for the immigrant boat

Class	Speed	Distance from the coast	Direction	TL
Immigrant boat (2)	LOW	FAR	IN	TL ₁
	LOW	WZ	IN	TL ₂
	LOW	OFF	IN	TL ₂
	MEDIUM	FAR	IN	TL ₁
	MEDIUM	WZ	IN	TL ₂
	MEDIUM	OFF	IN	TL ₂

Table 4.4 – Threat evaluation logic for the fishing boat

Class	Speed	Distance from the coast	Direction	TL
Fishing boat (3)	LOW	FAR	IN	TL ₁
	LOW	FAR	OUT	TL ₀
	LOW	WZ	IN	TL ₁
	LOW	WZ	OUT	TL ₁
	LOW	OFF	IN	TL ₂
	LOW	OFF	OUT	TL ₂

Table 4.5 – Threat evaluation logic for the oil tanker

Class	Speed	Distance from the coast	Direction	TL
Oil tanker (4)	LOW	FAR	IN	TL ₁
	LOW	FAR	OUT	TL ₀
	LOW	WZ	IN	TL ₁
	LOW	WZ	OUT	TL ₁
	LOW	OFF	IN	TL ₂
	LOW	OFF	OUT	TL ₂
	MEDIUM	FAR	IN	TL ₁
	MEDIUM	FAR	OUT	TL ₀
	MEDIUM	WZ	IN	TL ₁
	MEDIUM	WZ	OUT	TL ₁
	MEDIUM	OFF	IN	TL ₂
	MEDIUM	OFF	OUT	TL ₂

Table 4.6 – Threat evaluation logic for class “unknown”

Class	Speed	Distance from the coast	Direction	TL
Unknown (not detected by the imaging sensors)	LOW	FAR	IN	TL ₁
	LOW	FAR	OUT	TL ₀
	LOW	WZ	IN	TL ₁
	LOW	WZ	OUT	TL ₁
	LOW	OFF	IN	TL ₂
	LOW	OFF	OUT	TL ₂
	MEDIUM	FAR	IN	TL ₁
	MEDIUM	FAR	OUT	TL ₀
	MEDIUM	WZ	IN	TL ₁
	MEDIUM	WZ	OUT	TL ₁
	MEDIUM	OFF	IN	TL ₂
	MEDIUM	OFF	OUT	TL ₂
	HIGH	FAR	IN	TL ₂
	HIGH	FAR	OUT	TL ₁
	HIGH	WZ	IN	TL ₂
	HIGH	WZ	OUT	TL ₁
	HIGH	OFF	IN	TL ₂
	HIGH	OFF	OUT	TL ₂

The basic idea of this logic is to delay the decision when not enough information is available to derive the target nature, in order to acquire more accurate information on the target nature. The tracks that are evaluated in a definitive way as neutral (TL₀) or threat (TL₂) are no more stored in the C² centre and they are removed

from the simulation scenario. Only the tracks that are evaluated as suspect (TL1) are stored in the C² centre to be further evaluated until a definitive decision on their nature can be made and a suitable intervention can be selected.

Note that an immigrant boat can only approach the coast, in order to simulate a realistic scenario. Since the parameters of the target are generated according to the values reported in Table 2.1, only for the dinghy the speed can assume the value “high”.

4.4 The selection of the intervention

After the threat evaluation process, the C² centre selects an appropriate reaction on the target. The intervention is only selected for targets assessed as threat (TL2) and it consists in the allocation of a system resource, in order to inspect the nature of the target. The targets that are evaluated as neutral (TL0) do not require any intervention and their parameters are no more stored in the C² centre. For the targets that are evaluated as suspect the decision on the intervention is delayed, in order to acquire more information on their nature during the following observation time. Table 4.7 shows the selection of the intervention on the evaluated tracks.

Table 4.7 – Selection of the intervention

Track	Intervention
Cooperative track	No intervention
TL ₀ : neutral track	No intervention
TL ₁ : suspect track	Delay the decision
TL ₂ : threat track	Allocate a resource of the system (<i>type A or type B</i>) to inspect the target nature

In the system analyzed in this work, two types of resources are considered for the intervention: a helicopter (type A) and a patrol boat (type B); both the resources are used only for the target inspection and they do not carry any

sensors on board. The choice of the type of resource depends on the time available for the reaction, which is related to the parameters of the operative scenario, such as the target speed, the target approaching time to the coast, or the number of resources available. The parameters of each resource are reported in Table 4.8. The numerical values shown in the table are merely indicative and they must be properly selected for each operational context under investigation.

Table 4.8 – Parameters of the resources

Resource A: helicopter	
Availability	$N_A=3$ helicopters
Speed	$V_A= 300\text{Km/h}$;
Departure base	Airport (Trapani)
Inspection time	300 sec
Departure time	300 sec
Resource B: patrol boat	
Availability	$N_B=7$ patrol boats
Speed	$V_B= 60\text{Km/h}$;
Departure base	Harbor (Sciacca)
Inspection time	300 sec
Departure time	300 sec

The time available for the reaction for the resource B (or A) is evaluated as follows. The reaction time of the resource B (or A) is defined as the time required by the resource to intercept the trajectory of the target. In Figure 4.2 we indicate as $P \equiv (X_p; Y_p) \in r_T$ the potential point where the resource will intercept the target trajectory, which is indicated by the line r_T , and as $T \equiv (X_T; Y_T)$ the current position of the target.

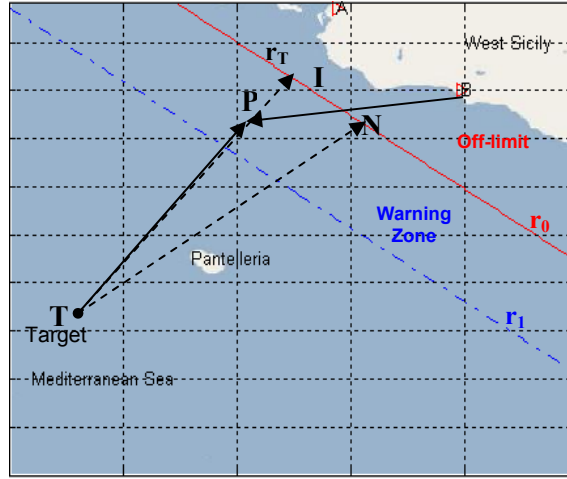


Figure 4.2 – Example of intervention on a TL2 tack with resource B

The time instants:

$$\bar{t}_T = \frac{d_{TP}}{|V|} = \frac{\sqrt{(X_T - X_P)^2 + (Y_T - Y_P)^2}}{|V|} \quad (4.5)$$

$$\bar{t}_R = \frac{d_{BP}}{V_B} = \frac{\sqrt{(X_B - X_P)^2 + (Y_B - Y_P)^2}}{V_B} \quad (4.6)$$

are, respectively, the instant when the target will be in the point **P** and the instant when the resource will be in the same point; V is the speed of the target and V_B is the speed of resource B. The coordinates of point **P** can be evaluated by solving the following system:

$$\begin{cases} \bar{t}_T = \bar{t}_R \\ P \in r_T \rightarrow Y_P = m_T X_P + q_T \end{cases} \quad (4.7)$$

if the solution for the system exists. Thus the reaction time is:

$$T_{reactB} = \bar{t}_R \quad (4.8)$$

and the time available for the reaction is:

$$T_{availableB} = T_{appr} - T_{reactB} \quad (4.9)$$

where T_{appr} is the approaching time of the target to the coast. If the time $T_{availableB}$ is higher than zero and if the number N_B of available patrol boats is not zero, the intervention can be performed with the resource B. Otherwise, the time available for the reaction for the resource A ($T_{availableA}$) is evaluated in the same way of that of resource B, by considering the coordinates $(X_A; Y_A)$ and the speed V_A in Equation (4.6). If $T_{availableA}$ is higher than zero and if the number N_A of available helicopters is not zero, the intervention is performed with resource A; otherwise a missed intervention occurs, i.e. a system error during the resource allocation. In both cases the resource is not allocated when the point **P**, where it could intercept the target, is next to the coast line. When a resource (B or A) is allocated for the inspection of the target, the system evaluates the time during which it is involved with the target inspection and then it is unavailable. This time is equal to the sum of the time that the resource spends to reach the target, to inspect it, and to return to the departure base:

$$T_{unavailable} = T_{dep} + T_{RT} + T_{insp} \quad (4.10)$$

where T_{dep} is the departure time required to the resource, T_{RT} is the round trip time, and T_{insp} is the inspection time. In this way, a resource can be considered again available when the time $T_{unavailable}$ is expired. For simplicity, we have not considered the use of a resource when it has completed the inspection, but it is not yet returned in the departure base.

Chapter 5

Performance analysis

5.1 Measures of Effectiveness

The performance of the overall system is evaluated in terms of measures of effectiveness (MoE). These MoE include metrics on the detection capability of the integrated system, on the threat evaluation, and on the intervention.

The metric concerning the detection is represented by the parameter $\eta_{\text{evaluated}}$, defined as the ratio between the number of targets detected by the integrated system, i.e. by one of the two radars or by both of them, and thus sent to the C^2 centre for the threat evaluation, and the total number of targets that enter the scene. This parameter takes into account that the tracks evaluated in a definitive way as TL0 or TL2 are removed from the simulation scenario, and only the tracks evaluated as TL1 are stored in the C^2 centre for a further evaluation.

The metrics on the threat evaluation process are:

- the probability of false declaration (FD) conditioned to the presence of a neutral target, i.e. $P_{FD|TL_0} = Pr(TL_2 | TL_0)$, that could cause a false intervention during the response selection task;
- the probability of FD conditioned to the presence of a threat target, i.e. $P_{FD|TL_2} = Pr(TL_0 | TL_2)$, that will cause a missed intervention;
- the probability of missed assessment (MA), which is the probability

$P_{MA} = Pr(TL_1 | TL_0, TL_2)$ to declare the target as suspect and then to not be able to evaluated in a definitive way the target during the first assessment operation.

We have also defined some parameters related to the system response time during the threat evaluation process:

- $mean(\Delta\tau_{TL2})$: average value of the delay in the evaluation of all the threat targets that enter the scene, that provides a sign about the average time instant during which all the threat targets have been evaluated and removed from the scene;
- $std(\Delta\tau_{TL2})$: standard deviation of the delay in the evaluation of all the threat targets;
- $TL2_{remaining}$: average number of TL2 targets waiting for an assessment after that the observation time of the scene is elapsed;
- $TL0_{remaining}$: average number of TL0 targets waiting for an assessment after that the observation time of the scene is elapsed.

These parameters provide an indicator of the time required to evaluate all the targets of the simulation scenario during a fixed observation time of the scene.

The metrics on intervention are the following:

- the ratio between the number of interventions performed and the number of real threat targets detected by the system:

$$\eta_1 = \frac{\# \text{ of interventions performed}}{\text{total \# of **real TL2 tracks detected** by the system}} \quad (5.1)$$

- the ratio between the number of interventions performed and the number of tracks evaluated as TL2 by the system:

$$\eta_2 = \frac{\# \text{ of interventions performed}}{\# \text{ of **tracks evaluated as TL2** by the system}} \quad (5.2)$$

- the ratio between the number of interventions performed and the number

of real threat targets that enter the scene:

$$\eta_3 = \frac{\text{\# of interventions performed}}{\text{\# of real TL2 tracks that enter the scene}} \quad (5.3)$$

- the ratio between the number of interventions on TL2 tracks and the total number of intervention performed, i.e. the percentage of correct intervention with respect to the total number of interventions:

$$\eta_{TL2} = \frac{\text{\# of correct interventions (performed on TL2)}}{\text{total \# of interventions performed}} \quad (5.4)$$

- the ratio between the number of interventions on TL0 tracks and the total number of intervention performed, i.e. the percentage of incorrect intervention with respect to the total number of interventions:

$$\eta_{TL0} = \frac{\text{\# of incorrect interventions (performed on TL0)}}{\text{total \# of interventions performed}} \quad (5.5)$$

These metrics also take into account for the number and type of available resources. Finally, we have also defined the parameters η_{OL} , η_{WZ} and η_{FAR} that represent the number of interventions performed respectively in the regions OL, WZ and FAR, with respect to the total number of interventions performed:

$$\eta_{OL} = \frac{\text{\# of interventions performed in the OL region}}{\text{total \# of interventions performed}} \quad (5.6)$$

$$\eta_{WZ} = \frac{\text{\# of interventions performed in the WZ region}}{\text{total \# of interventions performed}} \quad (5.7)$$

$$\eta_{FAR} = \frac{\text{\# of interventions performed in the FAR region}}{\text{total \# of interventions performed}} \quad (5.8)$$

These three parameters indicate the average distance from the coast where the intervention is performed.

5.2 Simulation results

The MoE introduced in the previous section have been evaluated by a Monte Carlo simulation, developed using the software MatLab[®]. The complete flow chart of the simulator has been shown in Figure 2.10. The number of independent Monte Carlo trials is $N_{\text{trials}} = 100$ and the observation time of the scenario for each trial is 1 hour. This observation time is divided into time slots of 60 seconds; during each time slot the operations of the C^2 centre are repeated. The tracks that are definitively evaluated as neutral (TL0) or threat (TL2) are removed from the scenario. The tracks declared as suspect are saved in the C^2 centre to be further evaluated during the subsequent time slots, until the system is able to make a definitive decision about their nature or when the observation time is elapsed.

The simulation scenario is fixed and it is generated outside the simulation cycle. To simulate a realistic scenario, most of the targets are initially located at the boundary between the external area and the warning zone. During the simulation, the trajectory of each target evolves according to a uniform motion, approaching or not the coast on the basis of the direction of their trajectory. Due to this reason most of the targets are located in the coverage area of the air platform. The number of targets considered is also fixed and equal to 20; their parameters are reported in Table 5.1. The table shows:

- the number of the target, from 1 to 20 (*Id*);
- the cooperativeness index of the target (*Coop*): 1 for a cooperative target, 0 for a non-cooperative target;
- the speed of the target (V_i), assumed to be constant;
- the target heading, i.e. the angle included between the x axis of the reference system of Figure 2.2 and the speed vector of the target (*Heading*);
- the initial coordinates of the target (X_0, Y_0)⁸;
- the threat level of the target, defined according to Tables 4.2 - 4.6 (*TL*).

⁸ The altitude of the target is assumed equal to 0 ($Z_0=0$).

Table 5.1 – Parameters of the targets for the fixed simulation scenario

Id	Class	Coop	V_t [m/s]	Heading [°]	X_0 [m]	Y_0 [m]	TL
1	4	0	10.200	221.60	105499.22	149668.95	0
2	1	0	4.000	1.00	41000.00	162000.00	2
3	2	0	3.186	119.50	159000.00	100000.67	2
4	3	0	6.137	170.00	86091.42	158583.58	0
5	4	0	10.200	229.00	172100.74	129000.70	0
6	1	0	9.453	218.46	175289.61	118018.45	0
7	1	0	30.800	174.95	144000.00	132500.00	0
8	3	0	4.344	118.70	112532.65	132095.04	2
9	3	0	5.897	58.60	143950.23	132242.94	2
10	1	0	29.304	349.60	149000.00	119000.00	2
11	1	0	15.167	149.00	147000.00	109000.00	0
12	1	0	29.850	127.03	120046.08	157766.74	2
13	1	0	8.000	136.61	111877.03	131310.58	2
14	2	0	12.000	39.90	163071.42	118000.00	2
15	3	1	5.208	181.01	168715.37	102714.68	Coop
16	3	0	6.137	178.50	148292.45	150689.14	0
17	4	1	7.182	163.08	111878.00	131486.91	Coop
18	3	0	2.400	200.00	160173.94	105310.46	0
19	3	1	6.137	195.00	162765.35	123388.04	Coop
20	3	0	4.138	240.60	161748.77	111848.83	0

The following cases have been considered, as concerns the set of the imaging sensors active inside the system:

- *Case A*: the IR cameras are active on both the land based and the airborne platforms. The classification process is assumed to be ideal and then the CM of the two IR cameras is assumed to be equal to identity. This means that no classification errors are considered during the threat evaluation.
- *Case B*: the IR cameras are active on both the platforms and the error during the classification is considered by means of the CM entries.
- *Case C*: the spotlight SAR is active on the airborne platform and other imaging sensors are not considered inside the system. The classification process is assumed to be ideal, i.e. the spotlight SAR CM is assumed to be equal to the identity (\mathbf{I}_4).
- *Case D*: the spotlight SAR is active on the airborne platform and other imaging sensors are not considered inside the system. The error during the

classification process is considered, thus the spotlight SAR CM is different from the identity.

The CMs of the two IR cameras in *Case B* and of the spotlight SAR in *Case D* are evaluated according to the analytical approach introduced in Chapter 3. The complete analysis of the performance has been performed for the *Case A* and the results are described in Section 5.2.1. The metrics during the threat evaluation process have been also evaluated for the other cases, in order to evaluate a first impact of the classification algorithm described in Chapter 3 on the system performance.

5.2.1 *Ideal classification process*

In this section we provide a complete description of the MoE of the system for the *Case A*, i.e. when the IR cameras are active on both the land based and the airborne platforms and the classification process is assumed to be ideal, i.e. no errors are considered in the classification.

Figure 5.1 shows the metric on the detection, $\eta_{\text{evaluated}}$, defined as the ratio between the number of targets detected by the integrated system, and sent to the C² centre for the evaluation, and the total number of targets that enter the scene during the current slot time. This parameter is represented as a function of the time slot and it takes into account that the track evaluated as TL0 or TL2 are removed from the simulation scenario. The curve refers to the case of sea state equal to zero.

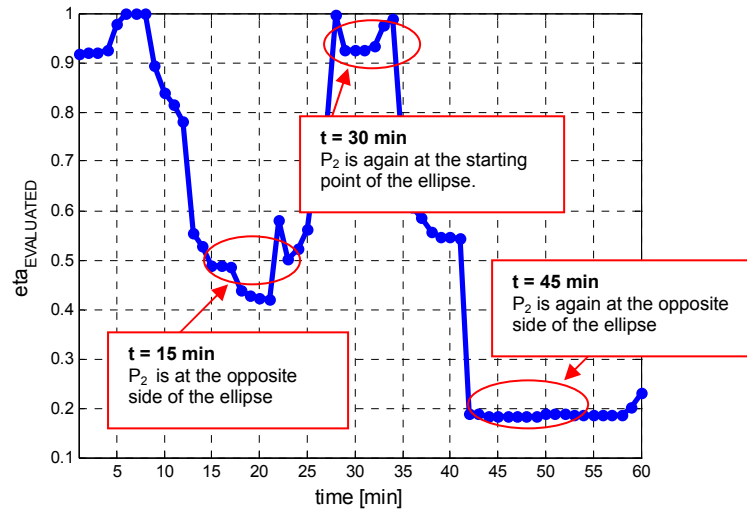


Figure 5.1 – MoE on the detection ($\eta_{\text{evaluated}}$) for Case A

The curve has a pseudo-periodic trend. This is due to the motion of the airborne platform along its elliptic trajectory, as shown in Figure 5.2.

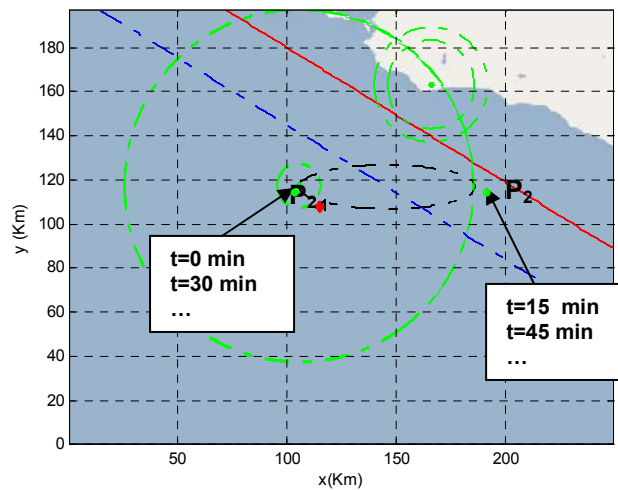


Figure 5.2 – Motion of the air platform (P_2) on the elliptic trajectory

The time that P_2 spends to cover the semi-elliptic path is 15 time slots, i.e. 15 minutes. After this time the number of detected targets decreases because most of them are out of the AEW coverage. During the interval between 15 and 30 minutes the platform covers the lower semi-ellipse and the observed situation is symmetric to that of the interval between 0 and 15 minutes. After 30 minutes P_2 is again at its initial position: the number of detected targets increases and it decreases during the following 15 minutes. After 45 minutes, $\eta_{\text{evaluated}}$ decreases rapidly to zero, since after this amount of time the position of the remaining targets could be changed considerably and they could be out of the AEW coverage area. As stated before, the parameter $\eta_{\text{evaluated}}$ primarily depends on the airborne radar detection capability, since in the considered scenario most of the targets are located on the coverage area of the air platform.

The metrics during the threat evaluation process are reported in Figure 5.3.

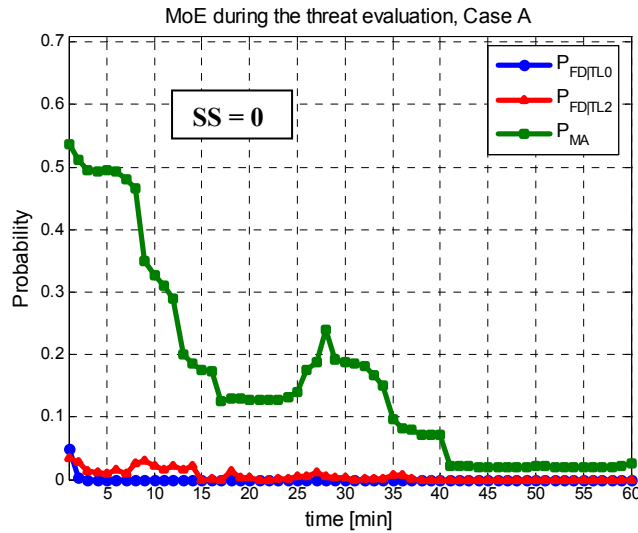


Figure 5.3 – MoE during the threat evaluation logic for Case A

The figure shows the probabilities $P_{FD|TL0}$, $P_{FD|TL2}$ and P_{MA} as functions of the time slot, when the sea state is zero. The false declaration probability conditioned to a

TL0 track, $P_{FD|TL0}$, has been evaluated with respect to the initial number of neutral targets (i.e. 12)⁹; the false declaration probability conditioned to a TL2 track, $P_{FD|TL2}$, has been evaluated with respect to the initial number of threat target (i.e. 8); and, finally, the missed assessment probability, P_{MA} , has been evaluated with respect to the initial number of total targets (i.e. 20). The curves show that P_{MA} is significantly higher than $P_{FD|TL0}$ and $P_{FD|TL2}$: this is due to the fact that usually no enough information is available to make a definitive decision on the target nature, for the simulation scenario considered. The non strictly monotonic decreasing behaviour of P_{MA} is related to the trend of $\eta_{evaluated}$, shown in Figure 5.1: it is possible that one or more targets are not detected, and then evaluated by the C² centre, during one time slot, but they could be detected during the subsequent slots. The parameters related to the system response time during the threat evaluation process are reported in Table 5.2, for two different values of sea state (0 and 4).

Table 5.2 – System response time during the threat evaluation process

	SS=0	SS=4
mean($\Delta\tau_{TL2}$)	15.6100 min	16.3800 min
std($\Delta\tau_{TL2}$)	8.2766	10.3629
TL2_{remaining}	0.1400	0.0400
TL0_{remaining}	0.3800	0.4600

On the average, the system is able to classify all the threat targets after 16 time slots and at the end of the observation time (1 hour) almost all the tracks, both TL0 and TL2, have been evaluated.

The metrics on the intervention are reported in Table 5.3, for the sea state equal to 0 and 4.

⁹ The cooperative targets of the last column in Table 5.1 are considered as neutral.

Table 5.3 – MoE during the intervention for Case A

	SS = 0	SS = 4
η_1	0.6286	0.6361
η_2	1	1
η_3	0.5800	0.5763
η_{TL2}	0.8763	0.8820
η_{TL0}	0.1237	0.1180
η_{OL}	0.4425	0.4450
η_{WZ}	0.5575	0.5550
η_{FAR}	0	0

The values reported in Table 5.2 and in Table 5.3 show that the sea state does not significantly influence the MoE, since the difference between the detection probability of the AEW radar for sea state equal to 0 and for sea state equal to 4 is not significant, as shown in Figure 2.5. The value of parameter η_1 states that the percentage of interventions performed with respect to the total number of threats detected by the system is higher than 62%. The value of η_2 is always equal to 1, showing that the choice of the resource parameters is appropriate for the scenario considered here: the available resources allow the system to inspect all the targets evaluated as threat¹⁰. The parameter η_{TL0} shows that the number of incorrect interventions is low (about 12%). Finally, the parameters η_{OL} and η_{WZ} show that most of the interventions occurs in the warning zone, and then with a sufficient advance in reaction. No intervention occurs in the external area, as stated by the parameter η_{FAR} , which is always equal to zero. Also note that is:

$$\eta_{TL2} + \eta_{TL0} = 1 \quad (5.9)$$

$$\eta_{OL} + \eta_{WZ} + \eta_{FAR} = 1 \quad (5.10)$$

as results from the definitions given in Equations (5.4) - (5.8).

The MoE during the intervention are also graphically shown in Figure 5.4.

¹⁰ Note that in the simulation scenario considered in this work no more than 20 targets enter the monitored area during an observation time of 1 hour. The number of available resources considered in Table 4.8 is adequate for this particular scenario, but it could not be sufficient for scenarios with a higher density of targets.

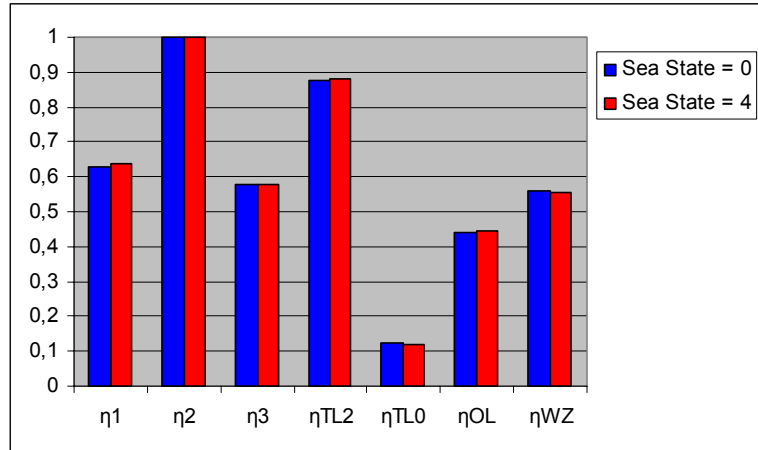


Figure 5.4 – MoE during the intervention for Case A

As an example, Figure 5.5 shows the evolution of the scenario during the observation time (1 hour) for a single Monte Carlo trial. The red arrows in the figure represent the threat target and the green arrows represent the neutral or cooperative target. The circles on each arrow represent the evaluation performed by the system: a green circle refers to a target evaluated as neutral, an orange circle refers to a target evaluated as suspect and, finally, a red circle refers to a target evaluated as threat; when a circle is not overlapped to the arrow, it means that the track has not been detected and evaluated by the system. The figure shows that during the first time slot the system is able to perform an intervention on all the tracks evaluated as TL2. During this time slot an error on the threat evaluation occurs (on the third track) and it causes a missed intervention on a threat target. During the following time slots the system is again able to perform the intervention on the targets evaluated as threat.

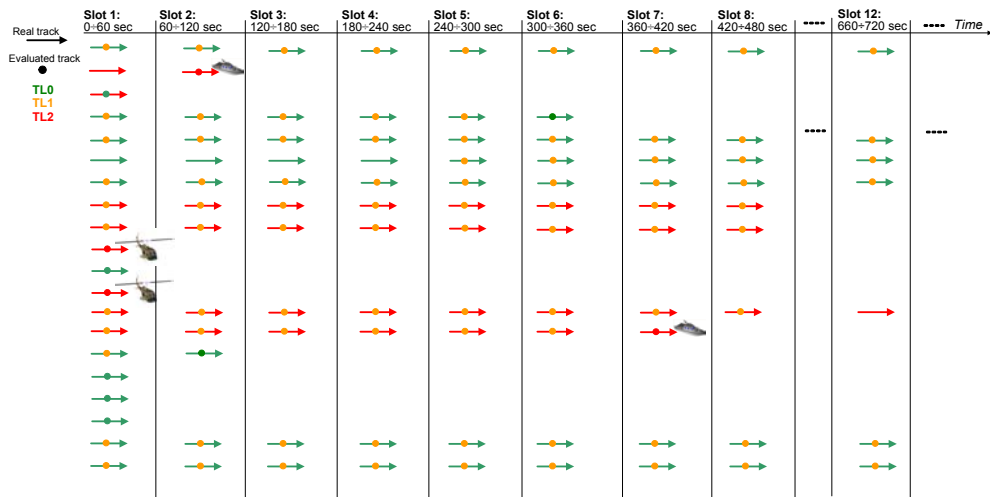


Figure 5.5 – Evolution of the scenario during a single Monte Carlo trial

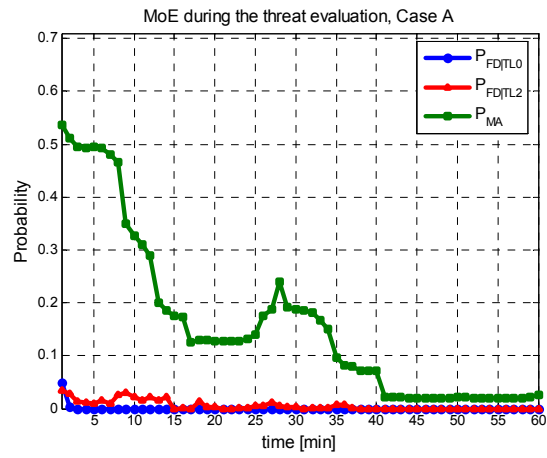
The graph of Figure 5.5 also shows that, after the twelfth time slot, only 7 of the 20 initial tracks require a further evaluation, that are the tracks for which the evaluation process is more uncertain and thus more information is required to make a definitive decision.

5.2.2 Non ideal classification process

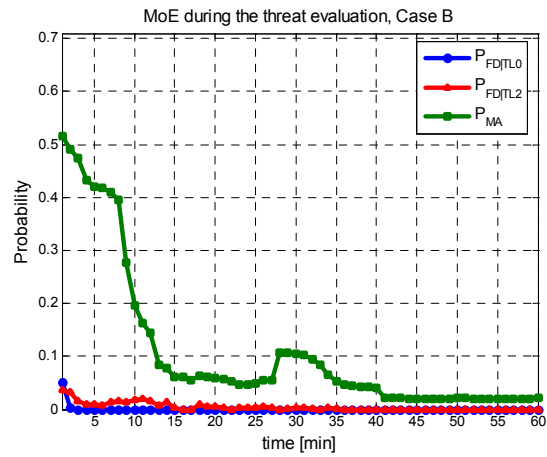
A preliminary evaluation of the impact of the classification process on the system performance has been performed, by comparing the metrics during the threat evaluation process when different suites of imaging sensors are active in the system and considering both an ideal error free classification process and a non-ideal classification process, (*Cases A-D*).

The results concerning the error probabilities during the threat evaluation process for the four cases introduced in Section 5.2 are shown in the following figures. All the cases are referred to a sea state value equal to 0. Figure 5.6 shows the comparison between the error probabilities in *Case A* and *Case B*, when only the IR cameras are active on both the land based and the air platform, respectively for a

correct classification probability equal to 1 ($P_{CC}=1$) and different from 1 ($P_{CC} \neq 1$).



a)

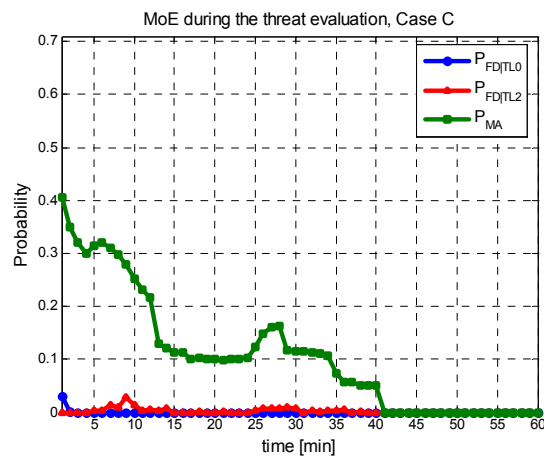


b)

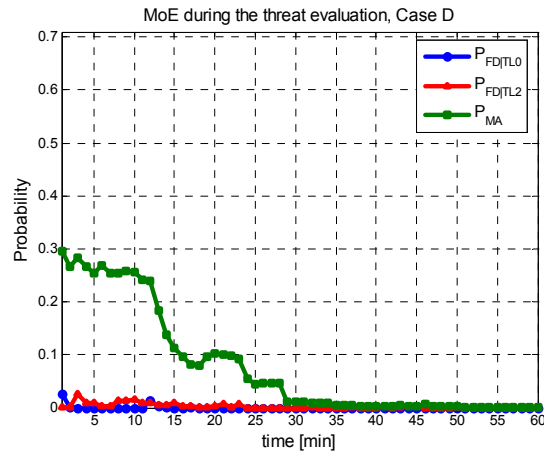
Figure 5.6 – MoE during the threat evaluation: a) Case A; b) Case B

The error probabilities for the *Case A* have been already shown in the previous section. They are reported again in Figure 5.6 in order to analyze the effect of the classification process when the same set of imaging sensors is active inside the

integrated system. The comparison between Figure 5.6 a) and b) shows that the effect of a non ideal classification process ($P_{CC} \neq 1$) on the defined probabilities is not significant. This is basically due to the simulation scenario considered: when only the IR cameras are active, for most of the time the system evaluates the tracks under the condition of *unknown* class, i.e. not detected by the active imaging sensors, since the maximum range of the IR is about 20 Km (dependent on the RCS of the target). An interesting future development of this work could be the analysis of different simulation scenarios, where the targets are located on the coverage area of all the imaging sensors, to better evaluate the effect of the classification task on the overall performance of the integrated system. Figure 5.7 shows the comparison between the error probabilities during the threat evaluation in *Case C* and *Case D*, when only the spotlight SAR is active in the air platform, respectively for a correct classification probability equal to 1 ($P_{CC} = 1$) and different from 1 ($P_{CC} \neq 1$).



a)



b)

Figure 5.7 – MoE during the threat evaluation: a) Case C; b) Case D

Also in the cases reported in Figure 5.7, the effect of the error in the classification process is not significant. On the other hand, by comparing Figure 5.6 with Figure 5.7, we can observe a reduction in the probability of missed assessment, P_{MA} , when the spotlight SAR is active instead of the IR camera. This is due to the fact that the coverage area of the spotlight SAR is significantly higher than the coverage area of the IR camera. As a result, in cases A/B the threat evaluation is usually performed without knowledge of the class information and the C^2 centre usually delays the decision and evaluates the target as suspect; in cases C/D the class information is usually detected by the spotlight SAR and then, more frequently, a definitive evaluation is made. The non strictly monotonic decreasing behaviour of the probabilities shown in Figures 5.6 – 5.7 is once again due to the trend of the parameter $\eta_{\text{evaluated}}$.

Chapter 6

Conclusions

In this dissertation the analysis, modelling, and simulation of a notional multi-sensor system acting in a maritime border control scenario for Homeland Security (HS) has been described. The functions performed by the system are the detection, tracking, identification and classification of naval targets that enter a sea region, the evaluation of their threat level and the selection of a suitable reaction to them. The emulated system is composed of two platforms carrying multiple sensors: a land based platform, equipped with a Vessel Traffic Service (VTS) radar, a station belonging to an Automatic Identification System (AIS), and an IR camera; an airborne platform, carrying an Airborne Early Warning Radar (AEWR) that can operate on a spotlight SAR mode, a video camera, and a second IR camera. A Command and Control (C²) centre, located on the coast, coordinates the surveillance operation. In the maritime scenario four classes of naval targets have been considered: high speed dinghy, immigrant boat, fishing boat, and oil tanker. The imaging sensors provide an information on the target class and their performance is evaluated by means of their confusion matrix (CM), analytically computed as a function of: the signal-to-noise ratio at the input of the sensor, the sensor resolution, a database of reference images, and the cross-correlation between the reference images. The entries of the CM are used by each imaging sensor to make a decision on the target class. Then the single decisions coming

from each sensor are combined, in order to obtain a more reliable estimate of the target class, with respect to the case of a single sensor. The proposed classification algorithm allows us to easily include the classification process in the software simulation of the complex multi-sensor system analyzed.

The overall performance of the integrated system is evaluated in terms of its *Measures of Effectiveness* (MoE), which are the system metrics during the detection, classification, threat level evaluation, and selection of the intervention. The MoE of the system have been evaluated by a Monte Carlo simulation, using the software MatLab[®] and considering a fixed scenario composed of 20 targets, belonging to the four naval classes mentioned above. These metrics have been evaluated considering different suites of imaging sensor active inside the system and considering both the cases where an ideal error free classification process and a non-ideal classification process are performed.

The complete analysis of the performance has been performed only for the case of the IR cameras active on both the land based and the air platform and considering an error free classification process, i.e. $P_{CC} = 1$. Results have shown that the system performance is strongly dependent on the simulation scenario. For the scenario considered in this work, results proved that the notional integrated system has a good capability to intercept the threat targets that cross the monitored region before that they approach the coast. A preliminary analysis of the impact of the classification process on the system performance has been performed, by comparing the metrics during the threat evaluation process when different suites of imaging sensors are active in the system and considering an ideal error free classification process and a non-ideal classification process. More specifically the following cases have been compared:

- the IR cameras on both the platforms are active;
- the spotlight SAR of the air platform is active.

Results have shown that the effect of the classification process on the defined metrics is not very significant, for the particular scenario considered in the simulation. Thus interesting future directions are: the definition of additional

performance metrics and the investigation of different simulation scenarios that allow us to better evaluate the effect of the classification task on the overall performance of the system; the analysis of the case where all the imaging sensors are active inside the system. A further significant future direction is the refinement of the tracking algorithm and the inclusion of the complete tracking architecture in the end to end simulator.

Appendix A

Analytical computation of the confusion matrix

The generic entry of the CM of a sensor is the probability that a target belonging to the class i is misclassified as belonging to class j :

$$c_{ij} = \Pr\{\text{the sensor decides for } H_j \text{ when } H_i \text{ is true}\} \quad (\text{A.1})$$

where H_i represents the hypothesis that the target belongs to class i . The computation of the entries of the CM in the i -th row is derived from the computation of the classification error probability for the i -th class. The error probability is computed in an incremental way by adding the contribution of the generic elemental error event to the overall error probability: these partial contributions to the error probability for the i -th class are assigned to the off diagonal elements c_{ij} of the of the CM. The diagonal elements, representing the conditional correct classification probabilities, can be consequently computed as:

$$c_{ii} = 1 - P_{\text{ERR}|H_i} = 1 - \sum_{i=1, i \neq j}^M c_{ij} \quad (\text{A.2})$$

where M is the number of classes considered. The elemental error event in the classification of an image belonging to a given class is defined through the correlation between the reference images and through their energy differences, compared to the variance of the noise over the single pixel. The error probability can be defined as the average of the conditional error probabilities:

$$P_{ERR} = \sum_{i=1}^M P_{ERR|H_i} \cdot P(H_i) \quad (A.3)$$

Consider a database of M reference images $\{\mathbf{I}_1, \dots, \mathbf{I}_M\}$, one for each class, and a received image \mathbf{I} . These images are represented by matrices whose dimension depends on the sensor resolution, in terms of pixels on the horizontal and vertical planes. In general, these matrices are dependent on the target coordinate along the azimuth and the elevation. In the rest of this appendix this dependence is omitted to simplify the notation. The elements of these matrices are intensities proportional to the optical power received from the target for the video camera and the IR camera, and to the target RCS for the spotlight SAR. In this analysis the following assumption are made:

- The image database is exhaustive, i.e. the possibility that the image of the target under test is not contained in the database is not considered.
- The reference images of each database do not contain any source of noise, but this is added during the analytical computation of the CM.
- The noise added over each image is additive, Gaussian, and independent from pixel to pixel.

Let indicate with Y the observation space and let divide this space in M decision zone $\{Y_1, \dots, Y_M\}$, such that if the image \mathbf{I} belongs to the zone Y_k then the hypothesis H_k is true. The error probability is:

$$P_{ERR} = \sum_{i=1}^M P(H_i) \cdot \sum_{k=1, k \neq i}^M \int_{Y_k} p(\mathbf{I} | H_i) dY \quad (A.4)$$

$$P_{ERR} = \sum_{k=1}^M \int_{Y_k} \left(\sum_{i=1, i \neq k}^M p(\mathbf{I} | H_i) \cdot P(H_i) \right) dY \quad (A.5)$$

where the term $\sum_{k=1, k \neq i}^M \int_{Y_k} p(\mathbf{I} | H_i) dY$ in (A.4) represents the probability that an image \mathbf{I} generated by the i -th class belongs to the decision zone Y_k , thus generating an error in the classification, and the term $\int_{Y_k} \left(\sum_{i=1, i \neq k}^M p(\mathbf{I} | H_i) \cdot P(H_i) \right) dY$ in (A.5)

represents the probability that an image \mathbf{I} belonging to the decision zone Y_k is generated by the i -th class, thus generating an error in the classification.

A given image, \mathbf{I} , belongs to the decision zone Y_k when:

$$\sum_{i=1, i \neq k}^M p(\mathbf{I} | H_i) \cdot P(H_i) < \sum_{i=1, i \neq m}^M p(\mathbf{I} | H_i) \cdot P(H_i) \quad \forall m \neq k \quad (\text{A.6})$$

i.e. when the error probability conditioned to the hypothesis H_k is minimum [47].

Equation (A.6) can be written as follows:

$$\sum_{i=1}^M p(\mathbf{I} | H_i) \cdot P(H_i) - p(\mathbf{I} | H_k) \cdot P(H_k) < \sum_{i=1}^M p(\mathbf{I} | H_i) \cdot P(H_i) - p(\mathbf{I} | H_m) \cdot P(H_m) \quad (\text{A.7})$$

so that the images \mathbf{I} belongs to the decision zone Y_k when:

$$p(\mathbf{I} | H_m) \cdot P(H_m) < p(\mathbf{I} | H_k) \cdot P(H_k) \quad \forall m \neq k \quad (\text{A.8})$$

The set of inequalities in (A.8) defines the boundaries between the decision zones.

Since the reference images have finite energy over their range of definition, i.e. the sensor field of view, the set of the reference images $\{\mathbf{I}_1, \dots, \mathbf{I}_M\}$ can be seen as a vector space where we can define a scalar product, by using the correlation function between a generic couple of elements inside the set. Using the scalar product, we can describe the elements of this vector space by means of their coordinates with respect to an orthonormal base, constructed by a Gram-Schmidt orthonormalization. This representation for the reference images can be used to express the error probability given a certain hypothesis, $P_{\text{ERR}|H_k}$.

In the vector space each image \mathbf{I}_i , for $i=1, \dots, M$, is represented by an M -dimensional vector \mathbf{y}_i , and the energy difference between two images represented by the vectors \mathbf{y}_1 and \mathbf{y}_2 is:

$$\begin{aligned} \Delta E = E_1 - E_2 &= \sum_{k=1}^M (y_{1,k}^2 - y_{2,k}^2) = \sum_{k=1}^M (y_{1,k} + y_{2,k}) \cdot (y_{1,k} - y_{2,k}) = \\ &= (\mathbf{y}_1 + \mathbf{y}_2)^T \cdot (\mathbf{y}_1 - \mathbf{y}_2) \end{aligned} \quad (\text{A.9})$$

where $y_{i,k}$ represents the k -th component of the vector \mathbf{y}_i .

Let indicate with \mathbf{n} the vector representing the noise, assumed to be zero-mean, additive, Gaussian and independent from pixel to pixel with variance σ^2 , and with ζ the elements of the orthonormal Gram-Schmidt base. The statistics of the noise vector \mathbf{n} are related to the sensor signal-to-noise ratio and they do not depend on the class of the image under test.

Assuming that the noise is Gaussian and that the M hypotheses have the same a priori probabilities, the decision criterion of (A.8) can be expressed as:

$$\mathbf{y}^T \cdot \mathbf{y}_k - (1/2) \cdot (\mathbf{y}_k^T \cdot \mathbf{y}_k) \geq \mathbf{y}^T \cdot \mathbf{y}_j - (1/2) \cdot (\mathbf{y}_j^T \cdot \mathbf{y}_j) \quad (\text{A.10})$$

where \mathbf{y} is the vector representing the received image in the vector space. Equation (A.10) can be written as:

$$\left[\mathbf{y}^T - \frac{1}{2}(\mathbf{y}_k^T + \mathbf{y}_j^T) \right] \cdot (\mathbf{y}_k - \mathbf{y}_j) \geq 0 \quad (\text{A.11})$$

since the scalar quantities $\mathbf{y}_k^T \cdot \mathbf{y}_j$ and $\mathbf{y}_j^T \cdot \mathbf{y}_k$ are equal. Then the error event can be characterized as follows:

- The inequality:

$$\left[\mathbf{y}^T - \frac{1}{2}(\mathbf{y}_k^T + \mathbf{y}_j^T) \right] \cdot (\mathbf{y}_k - \mathbf{y}_j) < 0 \quad (\text{A.12})$$

represents the elemental error event in the classification of an image belonging to the k -th class;

- By defining the normalized vector:

$$\mathbf{v}_{jk} = \frac{(\mathbf{y}_k - \mathbf{y}_j)}{\sqrt{E_{jk}}} \quad (\text{A.13})$$

where $E_{jk} = \sum_{i=1}^M (y_{k,i} - y_{j,i})^2$ is the cross energy between an image belonging to the k -th class and another image belonging to the j -th class, the conditional error probability can be expressed as:

$$P_{\text{ERR}|\text{H}_k} = \Pr \left\{ \bigcup_{j=1, j \neq k}^M \left[\left(\mathbf{n} + \frac{1}{2}(\mathbf{y}_k - \mathbf{y}_j) \right)^T \cdot \mathbf{v}_{jk} < 0 \right] \right\} \quad (\text{A.14})$$

- Considering that:

$$\frac{1}{2}(\mathbf{y}_k - \mathbf{y}_j)^T \cdot \mathbf{v}_{jk} = \frac{1}{2}\sqrt{E_{jk}} \quad (\text{A.15})$$

the conditional error probability becomes:

$$P_{\text{ERR}|\text{H}_k} = \Pr \left\{ \bigcup_{j=1, j \neq k}^M \left[\mathbf{n}^T \cdot \mathbf{v}_{jk} < -\frac{1}{2}\sqrt{E_{jk}} \right] \right\} \quad (\text{A.16})$$

and it can be divided in the following contributions:

$$\begin{aligned} P_{\text{ERR}|\text{H}_k} &= \Pr \left\{ \bigcup_{j=1, j \neq k}^M \left(\mathbf{n}^T \cdot \mathbf{v}_{jk} < -\frac{1}{2}\sqrt{E_{jk}} \right) \right\} = \quad (\text{A.17}) \\ &= \Pr \left\{ \bigcup_{j=1, j \neq k}^{M-1} \left(\mathbf{n}^T \cdot \mathbf{v}_{jk} < -\frac{1}{2}\sqrt{E_{jk}} \right) \right\} + \Pr \left\{ \mathbf{n}^T \cdot \mathbf{v}_{Mk} < -\frac{1}{2}\sqrt{E_{Mk}} \right\} \\ &\quad - \Pr \left\{ \left[\bigcup_{j=1, j \neq k}^{M-1} \left(\mathbf{n}^T \cdot \mathbf{v}_{jk} < -\frac{1}{2}\sqrt{E_{jk}} \right) \right] \cap \left[\mathbf{n}^T \cdot \mathbf{v}_{Mk} < -\frac{1}{2}\sqrt{E_{Mk}} \right] \right\} \end{aligned}$$

such that the conditional error probability $P_{\text{ERR}|\text{H}_k}$ can be computed by considering two elements in the union and by reiterating $M-3$ times the operation expressed in (A.17).

The variables $n_{jk} = \mathbf{n}^T \cdot \mathbf{v}_{jk}$ are Gaussian, with zero mean and variance σ^2 . Since the $(M-1)$ normalized vectors \mathbf{v}_{jk} are not orthogonal, the variables n_{jk} are not uncorrelated and independent; for this reason Equation (A.17) is not simple to evaluate. In order to simplify the analysis, the following approximation can be made. Let consider $M = 2$ in Equation (A.17):

$$\begin{aligned}
 P_{\text{ERR}|\mathcal{H}_k} &= \Pr \left\{ \bigcup_{j=1, j \neq k}^2 \left(\mathbf{n}^T \cdot \mathbf{v}_{jk} < -\frac{1}{2} \sqrt{E_{jk}} \right) \right\} = & (A.18) \\
 &= \Pr \left\{ n_{1k} < -\frac{1}{2} \sqrt{E_{1k}} \right\} + \Pr \left\{ n'_{2k} < -\frac{1}{2} \sqrt{E_{2k}} - \rho_{21} \cdot n_{1k} \right\} \\
 &\quad - \Pr \left\{ \left(n_{1k} < -\frac{1}{2} \sqrt{E_{1k}} \right) \cap \left(n'_{2k} < -\frac{1}{2} \sqrt{E_{2k}} - \rho_{21} \cdot n_{1k} \right) \right\}
 \end{aligned}$$

where is $n'_{2k} = n_{2k} - \rho_{21} \cdot n_{1k}$ and ρ_{21} is defined such that n'_{2k} is independent of n_{1k} :

$$\rho_{21} = \frac{\text{Cov}(n_{1k}, n_{2k})}{\text{Var}(n_{1k})} = \frac{\text{Cov}(n_{1k}, n_{2k})}{\sigma^2} \quad (A.19)$$

and:

$$\begin{aligned}
 \text{Var}(n'_{2k}) &= \text{Var}(n_{2k}) - 2\rho_{21} \cdot \text{Cov}(n_{1k}, n_{2k}) + \rho_{21}^2 \cdot \text{Var}(n_{1k}) = & (A.20) \\
 &= \sigma^2 - 2\rho_{21}^2 \sigma^2 + \rho_{21}^2 \sigma^2 = (1 - \rho_{21}^2) \sigma^2
 \end{aligned}$$

Considering that is $\Pr \left\{ n'_{2k} < -\frac{1}{2} \sqrt{E_{2k}} - \rho_{21} \cdot n_{1k} \right\} = \Pr \left\{ n_{2k} < -\frac{1}{2} \sqrt{E_{2k}} \right\}$, an upper

bound for the error probability can be found by considering the following lower bound for the third term in Equation (A.18):

$$\begin{aligned}
 &\Pr \left\{ \left(n_{1k} < -\frac{1}{2} \sqrt{E_{1k}} \right) \cap \left(n'_{2k} < -\frac{1}{2} \sqrt{E_{2k}} - \rho_{21} \cdot n_{1k} \right) \right\} \approx & (A.21) \\
 &\Pr \left\{ \left(n_{1k} < -\frac{1}{2} \sqrt{E_{1k}} \right) \cap \left(n'_{2k} < -\frac{1}{2} \sqrt{E_{2k}} - \rho_{21} \cdot \sqrt{E_{1k}} \right) \right\}
 \end{aligned}$$

This approximation for the conditional error probability in the case of $M=2$ is shown in Figure A.1, where the coloured areas correspond to a wrong decision and the white area correspond to a correct decision in the plane (n_{1k}, n'_{2k}) .

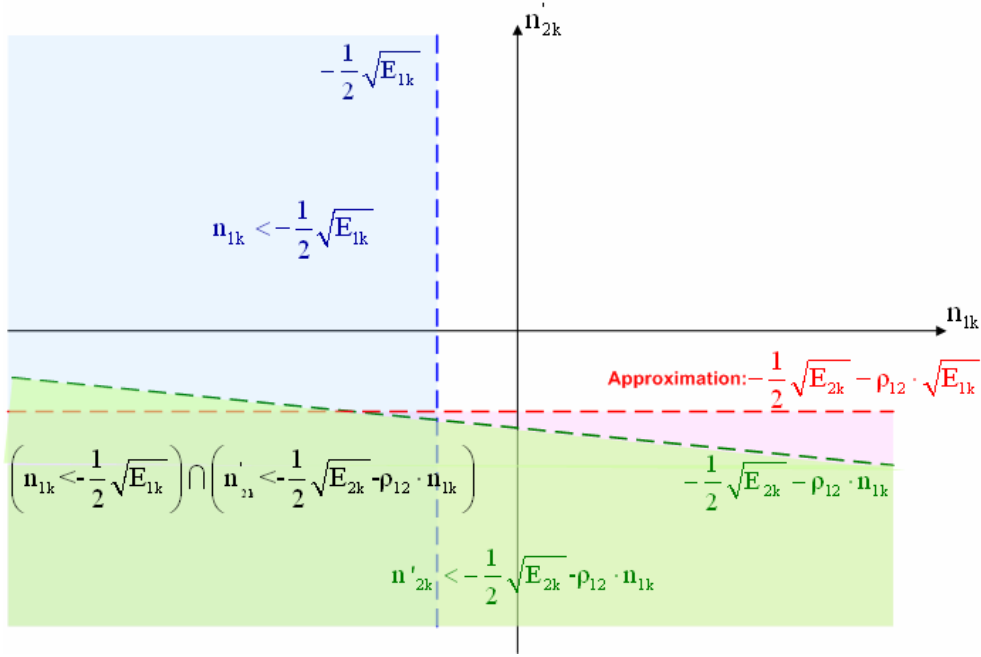


Figure A.1 – Approximation for the conditional error probability

After that this approximation has been introduced, we can define the disjointed elemental error events as follows:

$$\varepsilon_1 = \left(n_{1k} < -\frac{1}{2}\sqrt{E_{1k}} \right) \quad (\text{A.22})$$

$$\varepsilon_2 = \left(n'_{2k} < -\frac{1}{2}\sqrt{E_{2k}} - \rho_{21} \cdot n_{1k} \right) - \left[\left(n_{1k} < -\frac{1}{2}\sqrt{E_{1k}} \right) \cap \left(n'_{2k} < -\frac{1}{2}\sqrt{E_{2k}} - \rho_{21} \cdot \sqrt{E_{1k}} \right) \right] \quad (\text{A.23})$$

The contribution of the j -th elemental error to the conditional error probability $P_{\text{ERR}|\text{H}_k}$ is:

$$p_{jk} = \Pr \left\{ n_{jk} < -\frac{1}{2}\sqrt{E_{jk}} \right\} \quad \text{for } j=1 \text{ and } k=1, \dots, M \quad (\text{A.24})$$

and:

$$\begin{aligned}
 p_{jk} = \Pr(\varepsilon_j) &= \Pr\left\{n_{jk} < -\frac{1}{2}\sqrt{E_{jk}}\right\} - \\
 &\sum_{q=1}^{j-1} \Pr\left\{\varepsilon_q \cap \left(n'_{jk} < -\frac{1}{2}\sqrt{E_{jk}} - \sum_{q=1}^{j-1} \rho_{jq} \sqrt{E_{qk}}\right)\right\} \text{ for } j \geq 2 \text{ and } k=1, \dots, M
 \end{aligned} \tag{A.25}$$

The probabilities p_{jk} represent the entries of the CM for $j, k = 1, \dots, M$ and can be evaluated by means of the disjointed elemental error events. Note that the definition of each disjointed elemental error event ε_j requires the evaluation of the previously evaluated events ε_q , for $q < j$. The expressions reported in (A.24)-(A.25) are valid when is:

$$0 \leq p_{jk} \leq 1 \tag{A.26}$$

For very low values of the SNR, Equation (A.25) can not be applied to evaluate the probabilities p_{jk} , since the sum for $q = 1, \dots, j-1$ tends to become higher than 1. In particular, the SNR for which one diagonal probability in the matrix become equal to zero represents a break down point beyond which the analytical expression can no more be applied. Anyway this break down point occurs for very low values of the SNR, which are outside the range where the real systems operate.

By replacing $j=2$ in (A.25) we obtain $p_{2k} = \Pr(\varepsilon_2)$, since it is

$$\Pr\left\{n'_{2k} < -\frac{1}{2}\sqrt{E_{2k}} - \rho_{21} \cdot n_{1k}\right\} = \Pr\left\{n_{2k} < -\frac{1}{2}\sqrt{E_{2k}}\right\}. \text{ Thus in the case of } M=2,$$

Equation (A.18) becomes:

$$P_{\text{ERR}|\text{H}_k} = \Pr\left\{\bigcup_{j=1, j \neq k}^2 \left(\mathbf{n}^T \cdot \mathbf{v}_{jk} < -\frac{1}{2}\sqrt{E_{jk}}\right)\right\} = \Pr\{\varepsilon_1\} + \Pr\{\varepsilon_2\} \tag{A.27}$$

The use of Equation (A.25) requires the knowledge of the coefficients ρ_{jq} and the

variance of variables $n'_{jk} = n_{jk} - \sum_{q=1}^{j-1} \rho_{jq} n_{qk}$. The coefficients ρ_{jq} are defined such

that the variables n'_{jk} and n'_{qk} are independent and can be computed considering the following condition:

$$\text{Cov}(n'_{jk}, n'_{nk}) = \text{Cov}\left(n_{jk} - \sum_{q=1}^{j-1} \rho_{jq} n'_{qk}, n'_{nk}\right) = 0 \quad \text{for } n = 1, \dots, j-1 \quad (\text{A.28})$$

Since the variable n'_{qk} have been constructed as independent, in the sum only the term for $q = n$ gives a contribution different from zero to the covariance:

$$\text{Cov}\left(n_{jk} - \sum_{q=1}^{j-1} \rho_{jq} n'_{qk}, n'_{nk}\right) = \text{Cov}(n_{jk} - \rho_{jn} n'_{nk}, n'_{nk}) = \text{Cov}(n_{jk} - \rho_{jq} n'_{qk}, n'_{qk}) = 0 \quad (\text{A.29})$$

and:

$$\rho_{jq} = \frac{\text{Cov}(n_{jk}, n'_{qk})}{\text{Var}(n'_{qk})} \quad \text{for } q = 1, \dots, j-1 \quad (\text{A.30})$$

The variance of n'_{jk} is:

$$\text{Var}\left(n_{jk} - \sum_{q=1}^{j-1} \rho_{jq} n'_{qk}\right) = \text{Var}(n_{jk}) - \sum_{q=1}^{j-1} \rho_{jq}^2 \text{Var}(n'_{qk}) \quad (\text{A.31})$$

for $q = 1, \dots, j-1$.

The term $\text{Cov}(n_{jk}, n'_{qk})$ can be computed as a linear combination of the covariance

$\text{Cov}(n_{jk}, n_{qk})$:

$$\text{Cov}(n_{jk}, n'_{qk}) = \sum_{p=1}^q \alpha_p^{qk} \cdot \text{Cov}(n_{jk}, n_{pk}) \quad \text{for } q = 1, \dots, j-1 \quad (\text{A.32})$$

with:

$$\begin{cases} \alpha_q^{qk} = 1 \\ \alpha_p^{qk} = -\left(\rho_{qp} + \sum_{m=p+1}^{q-1} \alpha_m^{qk} \cdot \rho_{mp}\right) \quad \text{for } p = q-1, \dots, 1 \end{cases} \quad (\text{A.33})$$

To clarify the meaning of Expression (A.33), let consider the evaluation of the term

$\text{Cov}(n_{5k}, n'_{4k})$:

$$\begin{aligned}
 \text{Cov}(n_{5k}, n'_{4k}) &= \text{Cov}(n_{5k}, n_{4k} - \rho_{43} n'_{3k} - \rho_{42} n'_{2k} - \rho_{41} n'_{1k}) \\
 &= \text{Cov}(n_{5k}, n_{4k} - \rho_{43} (n_{3k} - \rho_{32} n'_{2k} - \rho_{31} n'_{1k}) - \rho_{42} (n_{2k} - \rho_{21} n'_{1k}) - \rho_{41} n'_{1k}) \\
 &= \text{Cov}(n_{5k}, n_{4k} - \rho_{43} n_{3k} + \rho_{43} \rho_{32} (n_{2k} - \rho_{21} n'_{1k}) + \\
 &\quad + \rho_{43} \rho_{31} n'_{1k} - \rho_{42} n_{2k} - (\rho_{41} - \rho_{42} \rho_{21}) n'_{1k}) = \\
 &= \text{Cov}(n_{5k}, n_{4k} - \rho_{43} n_{3k} - (\rho_{42} - \rho_{43} \rho_{32}) n_{2k} - (\rho_{41} - \rho_{43} \rho_{31} - \rho_{42} \rho_{21} + \rho_{43} \rho_{32} \rho_{21}) n'_{1k})
 \end{aligned} \tag{A.34}$$

where:

$$\begin{aligned}
 \alpha_4^{4k} &= 1 \\
 \alpha_3^{4k} &= -(\rho_{43}) \\
 \alpha_2^{4k} &= -\left(\rho_{42} + \sum_{m=3}^3 \alpha_m^{4k} \cdot \rho_{m2}\right) = -(\rho_{42} - \rho_{43} \rho_{32}) \\
 \alpha_1^{4k} &= -\left(\rho_{41} + \sum_{m=2}^3 \alpha_m^{4k} \cdot \rho_{m1}\right) = -(\rho_{41} - \rho_{43} \rho_{31} - (\rho_{42} - \rho_{43} \rho_{32}) \rho_{21})
 \end{aligned} \tag{A.35}$$

The terms of (A.35) correspond to those of (A.33) when is $q = 4$.

References

- [1] R. M. Adler and J. Fuller, "An integrated framework for assessing and mitigating risks to maritime critical infrastructure", *Proc. of the 2007 IEEE Conference on Technologies for Homeland Security*, Boston, MA, USA, 16-17 May 2007, pp. 252-257.
- [2] C. J. Baker, H. D. Griffiths, and M. Vespe, "Multi-perspective imaging and image interpretation", NATO ASI lectures on Imaging for Detection and Identification, July 2006.
- [3] Y. Bar-Shalom, T. Kirubarajan, and C. Gokberk, "Tracking with classification-aided multiframe data association", *IEEE Transaction on Aerospace and Electronic System*, vol. 41, no. 3, pp. 868-878, July 2005.
- [4] Y. Bar-Shalom and X. Li, *Multitarget-Multisensor Tracking: Principles and Techniques*, YBS Publishing, New York, 1995.
- [5] D. K. Barton, *Modern Radar System Analysis*, Artech House, Norwood, MA, 1988.
- [6] P. Bijl, "Acquisition of sea targets. Part 1: observer performance and "ACQUIRE" model predictions for air-to-surface FLIR imagery", TNO Human Factors Research Institute, TNO-report TM-96-A037, 17 September 1996.
- [7] W. G. Carrara, R. S. Goodman, and R. M. Majewski, *Spotlight SAR Signal Processing Algorithms*, Artech House, Boston, MA, USA, 1995.
- [8] F. R. Castella, "Multisensor, multisite tracking filter", *IEE Proc. of Radar, Sonar and Navigation*, vol. 141, no. 2, pp. 75-82, April 1994.
- [9] Z. Chair and P.K. Varshney, "Optimal data fusion in multiple sensor detection system," *IEEE Transactions Aerospace and Electronic Systems*, Vol. AES-22, pp. 98-101, January 1986.
- [10] H. M. Chen, S. Lee, R. M. Rao, M. A. Slamani, and P. K. Varshney, "Imaging for concealed weapon detection: a tutorial overview of development in imaging sensors and processing", *IEEE Signal Processing Magazine*, vol. 22, no. 2, pp. 52-61, March 2005.
- [11] H. Chen, F. Y. Wang, and D. Zeng, "Intelligence and security informatics for Homeland Security: information, communication, and transportation" *IEEE*

- Transactions on Intelligent Transportation Systems*, vol. 5, no. 4, pp. 329-341, December 2004.
- [12] M. N. Cohen, "An overview of radar-based, automatic, noncooperative recognition techniques", *Proceedings of the IEEE International Conference on System Engineering*, pp. 29-34, August 1991.
- [13] M. Costantini, A. Farina, and F. Zirilli, "The fusion of different resolution SAR images", *Proceedings of the IEEE*, vol. 85, no. 1, pp. 139-146, January 1997.
- [14] F. J. Crawford, "Electro-optical sensors overview", *IEEE Aerospace and Electronic System Magazine*, vol.13, no.10, pp. 17-24, October 1998.
- [15] G. Davidson, S. Symons, and M. Everett, "Sensor fusion system for infra-red and radar", *The IEE Seminar on Signal Processing Solutions for Homeland Security*, 11 October 2005, <http://ieeexplore.ieee.org/xpl/tocresult.jsp?isnumber=32953&isYear=2005>
- [16] S. Deb, K. R. Pattipati, and Y. Bar-Shalom, "A multisensor-multitarget data association algorithm for heterogeneous sensors", *IEEE Transactions On Aerospace and Electronic Systems*, Vol. 29, no. 2, pp. 560-568, April 1993.
- [17] R. Dumont, F. D. Lapierre, J-P. Marcel, and M. Acheroy, "SAFIR, a testbed for maritime simulation", *Proc. of the 3rd International IR Target and Background Modelling and Simulation Workshop (ITBMS)*, Toulouse, France, 25-28 June 2007.
- [18] A. Farina, P. Lombardo, and M. Marsella, "Joint tracking and identification algorithms for multisensor data", *IEE Proceedings on Radar, Sonar and Navigation*, vol. 149, no. 6, pp.271-280, December 2002.
- [19] A. Farina and F. A. Studer, *Radar Data Processing Vol. I – Introduction and Tracking*, Research Studies Press LTD, Letchford, 1985.
- [20] A. Farina and F. A. Studer, *Radar Data Processing Vol. II – Advanced topics and Applications*, Wiley, New York, 1986.
- [21] G. L. Foresti, C. Micheloni, P. Remagnino, and T. Ellis, "Active-video based surveillance systems", *IEEE Signal Processing Magazine*, vol. 22, no. 2, pp. 25-37, March 2005.
- [22] G. Franceschetti and R. Lanari, *Synthetic Aperture Radar Processing*, CRC Press, Boca Raton, FL, USA, 1999.
- [23] D. P. Gaver, P. A. Jacobs, and H. Sato, "Assessing resource requirements for maritime domain awareness and protection (security)", Naval Postgraduate School, Monterey, CA, USA, Technical Report NPS-OR-06-010, September 2006.

- [24] F. Gini, A. Farina, and M. S. Greco, "Radar detection and preclassification based on multiple hypothesis testing", *IEEE Transaction on Aerospace and Electronics Systems*, vol. 40, no. 3, pp. 1046-1059, July 2004.
- [25] S. Giompapa, R. Croci, R. Di Stefano, A. Farina, F. Gini, A. Graziano, and F. Lapiere, "Naval target classification by fusion of IR and EO sensors", *Proc. of SPIE European Symposium on Optics & Photonics in Security & Defence 2007*, Florence, Italy, 17-21 September 2007.
- [26] S. Giompapa, A. Farina, F. Gini, A. Graziano, R. Croci, and R. Di Stefano, "Study of the classification task into an integrated multisensor system for maritime border control", accepted for publication to *IEEE Radar Conference 2008*, Rome, Italy, 26-30 March 2008.
- [27] S. Giompapa, A. Farina, F. Gini, A. Graziano, R. Croci, and R. Di Stefano, "Naval target classification based on confusion matrix", accepted for publication to *IEEE Aerospace Conference 2008*, Big Sky, MT, USA, 1-8 March 2008.
- [28] S. Giompapa, A. Farina, F. Gini, A. Graziano, and R. Di Stefano, "Computer simulation of an integrated multi-sensor system for maritime border control", *Proc. of the IEEE Radar Conference 2007*, Boston, MA, USA, 17-20 April 2007.
- [29] A. Howard and H. Seraji, "Multi-sensor terrain classification for safe spacecraft landing", *IEEE Transaction on Aerospace and Electronic Systems*, vol. 40, no. 4, pp.1122-1131, October 2004.
- [30] H. G. Hughes and C. R. Zeisse., "Infrared propagation modeling beneath marine stratus clouds", *Journal of Atmospheric and Oceanic Technology*, vol.17, pp. 504-511, April 2000.
- [31] IALA Guidelines on AIS as a VTS tool, December 2001, <http://www.iala-aism.org>
- [32] IALA Guidelines on the universal Automatic Identification System (AIS) *Volume 1, Part II, Technical Issues Edition 1.1*, December 2002.
- [33] IALA Guideline No. 1028 on The Automatic Identification (AIS) Volume 1, Part. I, Operational Issues, Edition 1.3, December 2004.
- [34] IALA Recommendation A-124 on Automatic Identification System (AIS) shore station and networking aspected relating to the AIS Service Edition 1.1 December 2003.
- [35] IALA Vessel Traffic Service manual, 2002.
- [36] IMO SN/Circ.227, Guidelines for the installation of a shipborne Automatic Identification System (AIS), 6 January 2003.

- [37] IMO SN/Circ.236, Guidance on the application of AIS binary message, 28 May 2004.
- [38] S. M. Kay, *Fundamental of Statistical Signal Processing, Vol. II, Detection Theory*, Prentice-Hall, Upper Saddle River, NJ, 1998.
- [39] P. E. Kent, "VHF radio transponder for use in vessel traffic services and for ship-to-ship purposes", *IEE Colloquium on Radiocommunication in Transportation*, London, UK, 16 May 1995, pp. 3/1-3/8.
- [40] I. I. Kim , B. McArthur, and E. Korevaar, "Comparison of laser beam propagation at 785 nm and 1550 nm in fog and haze for optical wireless communications", *Proc. SPIE*, vol. 4214, no.2, pp. 26-37, 2000.
- [41] F. D. Lapierre, R. Dumont, A. Borghgraef, J-P. Marcel, and M. Acheroy, "OSMOSIS: an open-source software for modelling and simulation of infrared signatures using general emissivity profiles", *Proc. of the 3rd International IR Target and Background Modelling and Simulation Workshop (ITBMS)*, Toulouse, France, 25-28 June 2007.
- [42] F. D. Lapierre, J-P. Marcel, and M. Acheroy, "Design of an infrared signature simulation software for general emissivity profiles", *Proc. of the 2nd International IR Target and Background Modelling and Simulation Workshop (ITBMS)*, Ettlingen, Germany, 26-29 June 2006.
- [43] D. Li, K. D. Wong, Y. Hen Hu, and A. M. Sayeed, "Detection, classification, and tracking of targets", *IEEE Signal Processing Magazine*, vol.19, no. 2, pp. 17-29, March 2002.
- [44] F. Lombardini, F. Gini, and L. Verrazzani, "Progetto preliminare per SAR multi-beam di seconda generazione (MSAR2G)", Contratto ASI N. I/003/04/0 Output attività WP3200 A-B-C-D-E-F-G – Tecniche ATI, RPT-SMB-0010-UPI-7/A, pp. 39-41, Pisa, 27 October 2004.
- [45] P. Lombardo, M. Greco, A. Farina, F. Gini, and D. Pastina, *Tutorial on radar clutter modeling*, Washington, DC, USA, 5 May 2005.
- [46] R. P. S. Mahler, *Statistical Multisource-Multitarget Information Fusion*, Artech House, Boston, 2007.
- [47] J. L. Melsa and D. L. Cohn, *Decision and Estimation Theory*, McGraw-Hill International Student Edition, 1978.
- [48] PcModWin Manual, Version 4.0, Ontar Corporation, North Andover, MA, USA, June 2001.

- [49] J. A. Ratches., R. H. Vollmerhausen, and R. G. Driggers, "Target acquisition performance modeling of infrared imaging systems: past, present, and future", *IEEE Sensors Journal*, vol. 1, no. 1, pp. 31-40, June 2001.
- [50] M. Reiter and P. Rohatgi, "Homeland Security", *IEEE Internet Computing*, vol.8, no. 6, pp. 16-17, November 2004.
- [51] M. I. Skolnik, *Radar Handbook*, McGraw-Hill, 2nd Edition, New York, 1990.
- [52] M. I. Skolnik, *Introduction to Radar Systems*, McGraw-Hill, 3rd Edition, New York, 2001.
- [53] P. N. Slater, *Remote Sensing, Optics and Optical Systems*, Addison-Wesley Publishing Company, MA, USA, 1980.
- [54] L. Snidaro, R. Niu, G. L. Foresti, and P. K. Varshney, "Quality-based fusion of multiple video sensors for video surveillance", *IEEE Transaction on System, Man, and Cybernetics, Part B: Cybernetics*, vol. 37, no. 4, pp. 1044-1051, August 2007.
- [55] S. J. Symons, R. Philpott, D. Manson, and M. Everett, "MFR-IRST integration in the naval domain", *IEE Colloquium on the Use of Radars with Others Sensing Types*, 6 October 2000, pp.4/1- 4/6.
- [56] J. M. Tien, "Homeland Security services system: critical decision issues", *Proc. of the 2005 International Conference on Services Systems and Services Management (ICSSSM'05)*, Chongqing, P. R. of China, 13-15 June 2005.
- [57] R. H. Vollmerhausen and E. Jacobs, "The targeting task performance (TTP) metric a new model for predicting target acquisition performance", Modeling and Simulation Division Night Vision and Electronic Sensors Directorate U.S. Army CERDEC, Fort Belvoir, VA, Technical Report AMSEL-NV-TR-230, 2004.
- [58] D. R. Wehner, *High Resolution Radar*, 1st edition, Artech House, 1987.
- [59] M. C. Wicks, "Sensors as robots", *Proc. of 2006 International Waveform Diversity and Design Conference*, Hawaii, USA, 22-27 January 2006.
- [60] F. Zhao, J. Shin, and J. Reich, "Information-driven dynamic sensor collaboration", *IEEE Signal Processing Magazine*, vol.19, no.2, pp. 61-72, March 2002.
- [61] <http://geuz.org/gmsh/>
- [62] http://www.imo.org/Safety/mainframe.asp?topic_id=905
- [63] http://www.ssreng.com/vessel_traffic_system.htm

List of Publications

International Conferences

- [IC1] S. Giompapa, A. Farina, F. Gini, A. Graziano, R. Di Stefano, “A model for a human decision-maker in a command and control radar system: surveillance tracking of multiple targets”, *Proceedings of 9th International Conference on Information Fusion*, Florence, Italy, 10-13 July 2006.
- [IC2] S. Giompapa, A. Farina, F. Gini, A. Graziano, R. Di Stefano, “Computer simulation of an integrated multi-sensor system for maritime border control”, *IEEE Radar Conference 2007*, Boston, Massachusetts, USA, 17-20 April 2007.
- [IC3] S. Giompapa, R. Croci, R. Di Stefano, A. Farina, F. Gini, A. Graziano, F. Lapierre, “Naval target classification by fusion of IR and EO sensors”, *SPIE European Symposium on Optics & Photonics in Security & Defence 2007*, Florence, Italy, 17-21 September 2007.
- [IC4] S. Giompapa, A. Farina, F. Gini, A. Graziano, R. Croci, and R. Di Stefano, “Study of the classification task into an integrated multisensor system for maritime border control”, accepted for publication to *IEEE Radar Conference 2008*, Rome, Italy, 26-30 May 2008.

Technical Reports

- [TR1] S. Giompapa, L. Verrazzani, F. Gini, M. S. Greco, “*Modello del comportamento umano in un sistema di comando e controllo: man in the loop*”, Rapporto Tecnico, Università di Pisa, Pisa 04 novembre 2005 (*in Italian*).
- [TR2] S. Giompapa, L. Verrazzani, F. Gini, M. S. Greco, A. Farina, A. Graziano, R. Di Stefano, “*Modello del comportamento umano in un sistema di comando e controllo. Man in the loop: un caso di studio*”, Rapporto Tecnico, Università di Pisa, Pisa, 13 gennaio 2006 (*in Italian*).
- [TR3] S. Giompapa, F. Gini, M. S. Greco, L. Verrazzani, “*Simulazione dell’operatore umano in un sistema integrato di Comando e Controllo: sorveglianza costiera e tracking di bersagli multipli*”, Rapporto Tecnico SESM-FNM, Università di Pisa, Pisa, marzo 2006 (*in Italian*).

- [TR4] S. Giompapa, F. Gini, M. S. Greco, L. Verrazzani, “*Simulazione di un sistema integrato multi-sensore per la sorveglianza costiera*”, Nota Tecnica, Università di Pisa, Pisa, settembre 2006 (*in Italian*).

